ISTANBUL MEDENIYET UNIVERSITY
INSTITUTE OF GRADUATE STUDIES
DEPARTMENTS OF MOLECULAR BIOLOGY AND GENETICS

Double-punch Strategy: Synergistic Impacts of Epidermal Growth Factor and Androgen Receptors Dual Targeting by Osimertinib and Enzalutamide Reversed Epithelial-Mesenchymal Transition and Induced Apoptosis in Glioblastoma Cells

Master's Thesis

Nilay Dinçkurt

January 2026

ISTANBUL MEDENIYET UNIVERSITY
INSTITUTE OF GRADUATE STUDIES
DEPARTMENTS OF MOLECULAR BIOLOGY AND GENETICS

Double-punch Strategy: Synergistic Impacts of Epidermal Growth Factor and Androgen Receptors Dual Targeting by Osimertinib and Enzalutamide Reversed Epithelial-Mesenchymal Transition and Induced Apoptosis in Glioblastoma Cells

Master's Thesis

Nilay Dinçkurt

Supervisor

Prof. Dr. Pınar Obakan Yerlikaya

January 2026

THESIS JURY APPROVAL

This master thesis titled ''Double-punch Strategy: Synergistic Impacts of Epidermal Growth Factor and Androgen Receptors Dual Targeting by Osimertinib and Enzalutamide Reversed Epithelial-Mesenchymal Transition and Induced Apoptosis in Glioblastoma Cells'' written by Nilay Dinçkurt at the Department of Molecular Biology and Genetics was accepted by our jury.

JURY MEMBERS **SIGNATURE**

Supervisor:

Prof. Dr. Pınar Obakan Yerlikaya

İstanbul Medeniyet University

Other Jury Members:

Assoc. Prof. Ayşe Karatuğ Kaçar

Istanbul University

Asst. Prof. Ümmühan Demir

İstanbul Medeniyet University

Date of Defense: 20/01/2026

STATEMENTS

Style and Reference Manual Statement

Having reviewed this thesis written under my supervision, I confirm that it has been written by APA Manual of Styles and consistently used its in text reference format throughout the entire text.

Signature

Prof. Dr. Pınar Obakan Yerlikaya

Declaration of Originality

I hereby declare that all information in this dissertation has been obtained and presented in accordance with academic rules and ethical conduct. I also declare that, as required by these rules and conducts, I have fully cited and references all material and results that are not original to this work.

Signature

Nilay Dinçkurt

ACKNOWLEDGEMENTS

I am deeply indebted to Prof. Dr. Pınar Obakan Yerlikaya, who supported me financially and allowed me to work in her laboratory, first as an intern and later as a master's student. This journey would not have been possible without Esranur Kopal, Ünal Arabaci, Zeynep Demirel and Dr. Zainab Al-Lami, whose harmonious teamwork, moral support, companionship and assistance in conducting experiments made the research both enjoyable and productive. My heartfelt thanks go to Dr. Gülşen Günel and Dr. Derya Akyüz Şengün, who stood by me through all my ups and downs without hesitation, helping shape my education and career. I would like to express my sincere appreciation to Kaan Dinçkurt, Semiha Tozkoparan, Berra Aksu Deniz and Özlem Recimoğlu for all the entertainment, emotional support and countless brainstorming sessions that helped me navigate the challenges of my journey. I am also grateful to my mom for believing in my potential, which sustained me even in moments when I doubted myself. Despite all challenges, I thank myself for not giving up and continuing to pursue my education with perseverance. Special thanks to Asst. Prof. Tanmoy MONDAL at Gothenburg University and Dr. Adrian Biddle at Queen Mary University of London for allowing me to access their laboratories and encouraging me to follow my aspirations.

I would like to thank TÜBİTAK for their financial support throughout master study within the scope of the BİDEB 2210-A scholarship program.

I dedicate my master's thesis to my beloved father, who unwaveringly supported my education as a best friend, mentor and devoted chauffeur. I deeply wish you were here to celebrate my undergraduate and master's graduations with me, as you did for my earlier milestones.

CONTENTS

CONTENTS ..... **ii**
LIST OF SYMBOLS AND UNITS ..... **v**
LIST OF ABBREVIATIONS ..... **vii**
LIST OF FIGURES ..... **xii**
LIST OF TABLES ..... **xiii**
ABSTRACT ..... **xiv**
ÖZET ..... **xvi**
1. INTRODUCTION **1**
1.1 GLIOMA 1
1.2 GLIOBLASTOMA 2
1.2.1. Genetic Alterations in Glioblastoma 3
1.2.2. Epigenetic Alterations in Glioblastoma 7
1.2.3. Transcriptomic Alterations in Glioblastoma 9
1.2.4. Risk Factors of Glioblastoma 10
1.3 DIAGNOSIS AND SCREENING APPROACHES IN GLIOBLASTOMA 12
1.4 THERAPEUTIC STRATEGIES IN THE TREATMENT OF GLIOBLASTOMA 12
1.4.1. Temozolomide in the Treatment of Glioblastoma 15
1.5 THE ROLE AND IMPACT OF EPIDERMAL GROWTH FACTOR RECEPTOR IN GLIOBLASTOMA 16
1.5.1. Osimertinib 24
1.6 THE INFLUENCE OF THE ANDROGEN RECEPTOR IN GLIOBLASTOMA 26
1.6.1. Enzalutamide 30
1.7 THE DUAL TARGETING OF EGFR AND AR IN CANCER THERAPY 31
1.8 EPITHELIAL-MESENCHYMAL TRANSITION 32
1.9 APOPTOSIS 35
2. MATERIALS AND METHODS **39**
2.1 CELL LINES 39
2.2 CELL CULTURE 39

2.2.1. Cell Thawing 39
2.2.2. Cell Freezing 40
2.2.3. Passaging 40
2.3 DRUG PREPARATION 41
2.4 CELL VIABILITY ASSAY 41
2.5 HUMAN ADENOSINE TRIPHOSPHATE (ATP) ELISA ASSAY 42
2.6 TRYPAN BLUE EXCLUSION ASSAY 43
2.7 FLUORESCENCE STAININGS 43
2.8.1. Propidium Iodide (PI) Staining 43
2.8.2. 4',6-Diamidino-2-phenylindole (DAPI) Staining 44
2.8.3. 3,3'-Dihexyloxacarbocynanine Iodide ($DiOC_6$) Staining 44
2.8 CLONOGENIC ASSAY 44
2.9 HANGING DROP 45
2.10 WOUND HEALING ASSAY 45
2.11 FLOW CYTOMETRY 46
2.12 TOTAL PROTEIN ISOLATION 46
2.13 PHOSPHORYLATED PROTEIN ISOLATION 47
2.14 BRADFORD ASSAY 48
2.15 IMMUNOBLOTTING 48
2.16 STATISTICAL ANALYSES 50
3. RESULTS 51
3.1 OSIMERTINIB AND ENZALUTAMIDE COMBINED TREATMENT DRASTICALLY DIMINISHED THE CELL VIABILITY IN LN18 AND U87 CELLS AND DID NOT AFFECT HMC3 CELL VIABILITY IN A DOSE- AND TIME-DEPENDENT MANNER 51
3.2 ATP CONCENTRATION WAS SIGNIFICANTLY DIMINISHED BY THE COMBINED TREATMENT OF OSIMERTINIB AND ENZALUTAMIDE IN GLIOBLASTOMA CELLS 54
3.3 OSIMERTINIB AND ENZALUTAMIDE COMBINATION REDUCED THE SURVIVAL IN BOTH LN18 AND U87 CELL LINES AND THIS EFFECT WAS NOT OBSERVED IN HMC3 IN A DOSE- AND TIME-DEPENDENT MANNER 55
3.4 COMBINED TREATMENT OF OSIMERTINIB AND ENZALUTAMIDE DRAMATICALLY ELEVATED THE NUMBER OF DEAD CELLS IN LN18 AND U87 CELL LINES 56

3.5 DNA FRAGMENTATION WAS AUGMENTED IN LN18 AND U87 CELLS EXPOSED TO OSIMERTINIB AND ENZALUTAMIDE CO-TREATMENT 57

3.6 THE COMBINATION OF OSIMERTINIB AND ENZALUTAMIDE ATTENUATED THE MITOCHONDRIAL MEMBRANE POTENTIAL IN LN18 AND U87 CELLS LINES 58

3.7 THE ABILITY OF COLONY FORMATION OF LN18 AND U87 CELLS WAS DECREASED BY COMBINATION OF OSIMERTINIB AND ENZALUTAMIDE 60

3.8 3D COLONY FORMATION POTENCY OF LN18 AND U87 WERE HALTED BY THE COMBINATION OF OSIMERTINIB AND ENZALUTAMIDE IN GBM CELLS 61

3.9 THE RATE OF WOUND CLOSURE WAS SLOWED DOWN VIA OSIMERTINIB COMBINED WITH ENZALUTAMIDE IN LN18 AND U87 CELLS 62

3.10 THE APOPTOTIC SUBG1 CELL POPULATION WAS INCREASED BY OSIMERTINIB CONCURRENT USAGE WITH ENZALUTAMIDE IN LN18 AND U87 CELL LINES 63

3.11 EGFR SIGNALING DOWNSTREAM TARGETS WERE AFFECTED BY THE COMBINED TREATMENT OF OSI AND ENZ IN LN18 AND U87 64

3.12 AR SIGNALING PARTNERS WERE EVALUATED IN THE PRESENCE OF OSI AND ENZ IN GBM CELLS 65

3.13 THE CELL CYCLE WAS ARRESTED UTILIZING OSIMERTINIB AND ENZALUTAMIDE IN LN18 AND U87 CELLS 66

3.14 EPITHELIAL-MESENCHYMAL TRANSITION MARKERS WERE CHECKED AFTER ADMINISTRATION OF MONOTHERAPY OR COMBINATION OF OSIMERTINIB AND ENZALUTAMIDE 67

3.15 PRO-APOPTOTIC PROTEIN EXPRESSION WERE ELEVATED AND ANTI-APOPTOTIC PROTEIN EXPRESSIONS WERE DECREASED AFTER OSIMERTINIB AND ENZALUTAMIDE COMBINED TREATMENT 67

4. DISCUSSION 69

5. REFERENCES 77

6. SUPPLEMENTARY 95

LIST OF SYMBOLS AND UNITS

%	Percentage
°C	Degree Celsius
µ	Micro
µg	Microgram
µL	Microliter
µM	Micromolar
µm	Micrometer
bp	Base pair
Da	Dalton
dd	Double distilled
g	Gram
Gy	Gray
h	Hour
kb	Kilobase
kDa	KiloDalton
L	Liter
M	Molar
m	Meter
m^2	Square meter
mA	Miliamper
mg	Miligram
min	Minute
mL	Mililiter
mm	Milimetre
mM	Milimolar
MW	Molecular weight
nm	Nanometer
nM	Nanomolar
ns	No significant
pH	Potential of Hydrogen

R^2	R-squared
rpm	Revolutions per minute
RT	Room temperature
SD	Standard deviation
V	Volt
ΔΨM	Mitochondrial membrane potential
κ	Kappa

LIST OF ABBREVIATIONS

5-ALA	5-aminolevulinic acid
AGT	Alkyl guanine transferase
AKT	Protein kinase B
APS	Ammonium persulfate
AR	Androgen receptor
ATCC	American Type Culture Collection
ATM	Ataxia-telangiectasia mutated (ATM)
ATRX	Alpha thalassemia/mental retardation X-linked
BAD	BCL2 associated death protein
BBB	Blood brain barrier
BCNU	Carmustine
BCRP	Breast cancer resistance protein
BSA	Bovine serum albumin
BVZ	Bevacizumab
CCNU	Lomunistine
CDK4	Cyclin-dependent kinase 4
CDK6	Cyclin-dependent kinase 6
CDKN2A	Cyclin-dependent kinase inhibitor 2A
ceRNA	Competitive endogenous RNA
CHEK2	Checkpoint kinase 2
CL GBM	Classical glioblastoma
CNS	Central nervous system
COXII	Cytochrome c oxidase subunit 2
CREB	cAMP response element-binding protein
CRPC	Castration-resistant prostate cancer
ctDNA	Circulating DNA
DAPI	4’,6-Diamidino-2-phenylindole
DESI-MS	Desorption electrospray ionization mass spectroscopy
DHT	Dihydrotestosterone
DISC	Death-inducing signaling complex

$DiOC_6$	3,3'-Dihexyloxacarbocynanine iodide
DMEM	Dulbecco's modified eagles's medium
DMSO	Dimethyl sulfoxide
DNA	Deoxyribonucleic acid
E-cadherin	Epithelial cadherin
ECD	Extracellular domain
ECL	Enhanced chemiluminescence
ECM	Extracellular matrix
EGF	Epidermal growth factor
EGFR	Epidermal growth factor receptor
EGFRvI	Epidermal Growth Factor Receptor variant I
EGFRvII	Epidermal Growth Factor Receptor variant II
EGFRvIII	Epidermal Growth Factor Receptor variant III
EMA	European Medicines Agency
ENZ	Enzalutamide (MDV 3100)
EpCAM	Epithelial cell adhesion molecule
ER	Endoplasmic reticulum
ERK	Extracellular signal-regulated kinase
Ex/em	Excitation/emission
EZH2	Enhancer of zeste homolog 2
FBS	Fetal bovine serum
FDA	Food and Drug Administration
FGFR	Fibroblast growth factor receptor
GBM	Glioblastoma
GICs	Glioma-initiating cells
GLOBOCAN	Global Cancer Observatory
GRB2	Growth factor receptor bound protein 2
HB-EGF	Heparin-binding epidermal growth factor
HDAC	Histone deacetylase
HGG	High-grade glioma
HRP	Horseradish peroxide
ICD	Intracellular domain

IDH	Isocitrate dehydrogenase
IGF-1R	Insulin-like growth factor 1 receptor
JAK	Janus kinase
JNK	Jun N-terminal kinase
KDM	Histone lysine demethylase
Kpuu	Unbound drug accumulation ratio
LGG	Low-grade glioma
lncRNAs	Long non-coding RNAs
mAbs	Monoclonal antibodies
MAPK	Mitogen-activated protein kinase
mCRPC	Metastatic castration-resistant prostate cancer
MDM2	Murine double minute 2
MEK	Mitogen-activated protein kinase kinase
MES GBM	Mesenchymal glioblastoma
MET	Mesenchymal-epithelial transition
MET (HGF)	Mesenchymal-epithelial transition factor receptor
MGMT	O6-methylguanine DNA methyltransferase
mHSPC	Metastatic hormone-sensitive prostate cancer
miRNA	MicroRNA
MNK 1/2	MAPK-interacting kinases
MOMP	Mitochondrial outer membrane permeabilization
M-PER	Mammalian protein extraction reagent
MRI	Magnetic resonance imaging
mRNA	Messenger RNA
MRP	Multidrug resistance proteins
MTT	3-(4,5-Dimethylthiazol-2-yl)-2,5-diphenyltetrazolium bromide
N-cadherin	Neural cadherin
NE GBM	Neural glioblastoma
NF-κB	Nuclear factor kappa B
nmCRPC	Non-metastatic castration-resistant prostate cancer
NOS	Not otherwise specified
NSCLC	Non-small cell lung cancer

One-way ANOVA	One-way analysis of variance
OS	Overall survival
OSI	Osimertinib (AZD 9291)
PARP	Poly (ADP-ribose) polymerase
PBS	Phosphate-buffered saline
PDGFR	Platelet-derived growth factor receptor
Pen/Strep	Penicillin/streptomycin
PET	Positron emission tomography
PFS	Progression-free survival
P-gp	P-glycoprotein
PI	Propidium iodide
PI3K	Phosphatidylinositol 3-kinase
PIP2	Phosphatidylinositol (4,5)-bisphosphate
PIP3	Phosphatidylinositol (3,4,5)-triphosphate
PKC	Protein kinase C
PN GBM	Proneural glioblastoma
PRC2	Polycomb repressor complex 2
PROTAC	Proteolysis-targeting chimera
PSA	Prostate-specific antigen
PSMA	Prostate-specific membrane antigen
PTEN	Phosphatase and tensin homolog
Raf	Rapidly accelerated fibrosarcoma
Ras	Rat sarcoma virus
RB	Retinoblastoma
RNA	Ribonucleic acid
ROS	Reactive oxygen species
RTK	Receptor tyrosine kinase
SDS	Sodium dodecyl sulfate
SDS-PAGE	Sodium dodecyl sulfate polyacrylamide gel electrophoresis
SHC	Src homology 2 domain-containing
Smac	Second mitochondria-derived activator of caspase
SOS	Son of sevenless

STAT3	Signal transducer and activator of transcription 3
TBS	Tris-buffered saline
TBS-T	Tris-buffered saline tween 20
TEMED	N,N,N',N'-Tetramethylethylenediamine
TERT	Telomerase reverse transcriptase
TERTp	Telomerase reverse transcriptase promoter
TES	Testis-derived transcript
TET2	Tet methylcytosine dioxygenase 2
TFs	Transcription factors
TGFR	Transforming growth factor receptor
TGF-α	Transforming growth factor α
TGF-β	Transforming growth factor β
TKIs	Tyrosine kinase inhibitors
TMD	Transmembrane domain
TME	Tumor microenvironment
TMZ	Temozolomide
TNF-α	Tumor necrosis factor-α
TP53	Tumor protein p53
TPSA	Topological polar surface area
Trypsin-EDTA	Trypsin-ethylenediaminetetraacetic acid
Two-way ANOVA	Two-way analysis of variance
VEGF	Vascular endothelial growth factor
VEGFR	Vascular endothelial growth factor receptor
WHO	World Health Organization
Wnt	Wingless-related integration site
wt	Wild-type

LIST OF FIGURES

Figure 1: The representative showing of signaling cascades event through EGFR pathway. **19**
Figure 2: The difference between wild-type EGFR and constitutively active EGFRvIII pathways in GBM progression through downstream of EGFR. **22**
Figure 3: AR signaling through androgen-dependent manner and androgen-independent manner. **27**
Figure 4: Summary of EMT, partial EMT and MET with crucial markers. **35**
Figure 5: Overview of intrinsic and extrinsic apoptotic pathways under physiological conditions. **37**
Figure 6: Co-treatment of OSI and ENZ synergistically decreased the cell viability in LN18 and U87 at 24 h and HMC3 cells remained unaffected.. ..... **54**
Figure 7: The ATP levels decreased following combined treatment of OSI and ENZ in LN18 and U87 cells.. ..... **55**
Figure 8: LN18 and U87 cells showed a reduction in survival following 24 h therapy with the combination of 2.5 μM OSI and 50 μM ENZ while HMC3 was not affected by this administration at any time-point..... **56**
Figure 9: OSI concomitant ENZ usage gave rise to elevated dead cells via PI staining in LN18 and U87 cell lines.. ..... **57**
Figure 10: DAPI staining unmasked DNA fragmentation in GBM cells in response to OSI and/or ENZ, whereas it was not observed with any effect on microglia, HMC3.. ..... **58**
Figure 11: Mitochondrial membrane potential was reduced in LN18 and U87 in the co-treatment of OSI and ENZ for 24 h..... **59**
Figure 12: The 2D colony capacity of GBM cells was diminished in the combination of OSI and ENZ.. ..... **60**
Figure 13: Hanging drop assay unveiled that co-treatment with OSI and ENZ disrupted the spheroid formation and delayed subsequent recovery in 3D cell culture.. ..... **61**
Figure 14: The progression of wound healing declined in LN18 and U87 using OSI and ENZ for 24 hours..... **63**
Figure 15: Apoptotic subG1 accumulation was increased via the combination of OSI and ENZ in LN18 and U87 cells.. ..... **64**
Figure 16: EGFR-related markers were deciphered after administration of OSI and ENZ in LN18 and U87.. ..... **65**
Figure 17: The expression of AR pathway-related markers with OSI, ENZ and its combination were deciphered in LN18 and U87 cell lines.. ..... **66**
Figure 18: The cell cycle was arrested in OSI combined with ENZ in LN18 and U87 cells.. ..... **66**
Figure 19: Epithelial- and mesenchymal-associated markers were investigated in LN18 and U87 in OSI combined with ENZ..... **67**
Figure 20: The combination of OSI and ENZ elevated pro-apoptotic biomarkers while declined anti-apoptotic proteins in GBM cells..... **68**

LIST OF TABLES

Table 1. Types of Gliomas. 1
Supplementary Table 1. The recipe of MTT Reagent 95
Supplementary Table 2. The recipe of 4X BSA 95
Supplementary Table 3. The recipe of M-PER with protease and phosphatase inhibitor cocktails 95
Supplementary Table 4. 10% Sodium dodecyl sulfate (SDS) recipe 95
Supplementary Table 5. 10% Ammonium persulfate (APS) recipe 95
Supplementary Table 6. The recipe of 1.5 M Tris 95
Supplementary Table 7. The recipe of 0.5 M Tris 96
Supplementary Table 8. The recipe of 12% SDS-PAGE (Sodium dodecyl sulfate-polyacrylamide gel electrophoresis) in Merck System 96
Supplementary Table 9. The recipe of 12% SDS-PAGE in Thermo Fisher System 96
Supplementary Table 10. The recipe of 10X Running Buffer 96
Supplementary Table 11. The recipe of 10X Transfer Buffer 97
Supplementary Table 12. The recipe of 1X Transfer Buffer 97
Supplementary Table 13. The recipe for 5% skim milk 97
Supplementary Table 14. The recipe of Coomassie Brillant Blue G-250 97
Supplementary Table 15. The recipe of Destaining Solution 97
Supplementary Table 16. The recipe of 10X TBS 97
Supplementary Table 17. The recipe of TBS-T 98
Supplementary Table 18. The p-Coumaric acid recipe 98
Supplementary Table 19. The Luminol (3-aminopthalhydrazide) recipe 98
Supplementary Table 20. The recipe of 1 M Tris-HCl 98
Supplementary Table 21. The recipe of ECL 98
Supplementary Table 22. The list of chemicals 98
Supplementary Table 23. The list of devices 100

ABSTRACT

Double-punch Strategy: Synergistic Impacts of Epidermal Growth Factor and Androgen Receptors Dual Targeting by Osimertinib and Enzalutamide Reversed Epithelial-Mesenchymal Transition and Induced Apoptosis in Glioblastoma Cells

Dinçkurt, Nilay

Master's Thesis, Department of Molecular Biology and Genetics

Supervisor: Prof. Dr. Pınar Obakan Yerlikaya

January 2026, 123 pages

Glioblastoma (GBM) is a rare but deadly brain tumor within the spectrum of central nervous system (CNS) malignancies. Despite the presence of treatment options, including surgery, radiotherapy and chemotherapy with temozolomide (TMZ), these interventions fail to accomplish clinical improvement in at least half of the patients due to tumor heterogeneity, poor blood brain barrier (BBB) penetration of chemical agents and emergence of drug resistance. Since epidermal growth factor receptor (EGFR) mutations, especially EGFRvIII, occur in more than 50% GBM cases, EGFR targeting by EGFR tyrosine kinase inhibitors (TKIs) is one of the promising treatment strategies. Osimertinib (OSI), a 3rd-generation EGFR TKI, has been proposed to promote apoptosis, trigger cell cycle arrest, and inhibit cell proliferation via selectively targeting EGFRvIII and sparing wild-type (wt) EGFR in GBM. Furthermore, androgen receptor (AR) signaling is overexpressed in GBM in both ligand-dependent and ligand-independent manners to trigger cell proliferation, epithelial-mesenchymal transition (EMT), and evade apoptosis. Targeting of AR by the AR antagonists, particularly 2nd-generation inhibitors, has emerged as a potential treatment approach for GBM. Recent studies showed that the rate of cell proliferation is reduced, and apoptosis is promoted utilizing enzalutamide (ENZ) in GBM. Lately, it has been found that there is a direct interaction between EGFR and AR in GBM, further suggesting dual-targeting strategies. In this study, we hypothesized that dual targeting of EGFR and AR by OSI and ENZ would cause a reduction in cell viability, cell survival and induction of cell cycle arrest, reversed EMT, as well as apoptosis in LN18 and U87 cells without harming non-cancerous cells around the tumor microenvironment (TME), HMC3 cells. We found that OSI and ENZ exerted a synergistic effect on LN18 and U87 to diminish cell viability without affecting

HMC3 cells. This data was corroborated by a reduction in ATP concentrations in GBM cells. Survival assay demonstrated that exposure of OSI and ENZ caused cytotoxicity on LN18 and U87 but not on HMC3 in a dose- and time-dependent manner. With the help of fluorescence staining, combined treatment of OSI and ENZ elevated dead cells, nuclear fragmentation and reduced mitochondrial membrane potential, again specific to GBM cells. Colony formation potency and the ability of spheroid formation were reduced by administering OSI and ENZ in LN18 and U87. Moreover, OSI and ENZ together decreased migration capacity in LN18 and U87, meaning a slow speed of wound healing. Flow cytometry and western blotting results showed an induction in the subG1 population, cleaved caspases and PARP alongside a reduction in full-length caspases and PARP, and Bcl-x_L, indicating induced apoptosis. Immunoblotting results confirmed that EGFR and AR downstream targets were successfully inhibited, leading to cell cycle arrest with a reduction in cyclin D1 expression and reversal of EMT markers in LN18 and U87. To our knowledge, this is the first study to investigate the combination impacts of the 3rd-generation of EGFR TKI and the 2nd-generation AR antagonist on cell cycle, EMT and apoptosis in GBM. Our findings propose that administration of OSI and ENZ target EGFR and AR might represent a new treatment option in GBM.

Keywords: Androgen receptor, apoptosis, enzalutamide, epidermal growth factor receptor, epithelial-mesenchymal transition, glioblastoma, osimertinib

ÖZET

İkili Darbe Stratejisi: Osimertinib ve Enzalutamid ile Epidermal Büyüme Faktörü ve Androjen Reseptörlerinin İkili Hedeflenmesinin Sinerjik Etkisi Glioblastoma Hücrelerinde Epitelyal-Mezenkimal Geçişi Tersine Çevirdi ve Apoptozu İndükledi

Dinçkurt, Nilay

Yüksek Lisans Tezi, Moleküler Biyoloji ve Genetik Bölümü

Danışman: Prof. Dr. Pınar Obakan Yerlikaya

Ocak 2026, 123 sayfa

Glioblastoma (GBM), merkezi sinir sistemi (CNS) malignitelerinin spektrumunda nadir ancak ölümcül bir beyin tümörüdür. Cerrahi, radyoterapi ve temozolomid (TMZ) ile kemoterapi gibi tedavi seçeneklerinin varlığına rağmen bu müdahaleler tümör heterojenikliği, kimyasal ajanların kan beyin bariyerini (BBB) zayıf bir şekilde geçmesi ve ilaç direncinin ortaya çıkması nedeniyle hastaların en az yarısında klinik iyileşme sağlamamaktadır. Epidermal büyüme faktörü reseptörü (EGFR) mutasyonları, özellikler EGFRvIII, GBM vakalarının %50'sinden fazlasında görüldüğünden, EGFR tirozin kinaz inhibitörleri (TKI'lar) ile EGFR'yi hedeflemek umut verici tedavi stratejilerinden biridir. 3. Nesil EGFR TKI olan osimertinib (OSI), GBM'de EGFRvIII'ü seçici olarak hedefleyerek ve yabanıl tip (wt) EGFR'yı koruyarak apoptozu teşvik ettiği, hücre döngüsünü durduğu ve hücre proliferasyonunu inhibe ettiği öne sürülmüştür. Ayrıca, androjen reseptörü (AR) sinyali, hücre proliferasyonunu, epitelyal-mezenkimal geçişi (EMT) tetiklemek ve apoptozu önlemek için GBM'de hem liganda bağımlı hem de liganda bağımlı olmayan şekillerde aşırı ifade edilir. AR antagonistleri, özellikle 2. Nesil inhibitörler tarafından AR'nin hedeflenmesi, GBM için potansiyel bir tedavi yaklaşımı olarak ortaya çıkmıştır. Son çalışmalar, GBM'de enzalutamid (ENZ) kullanılarak hücre proliferasyonunun azaldığı ve apoptozun indüklendiğini göstermiştir. Son zamanlarda, GBM'de EGFR ve AR arasında doğrudan bir etkileşim olduğu bulunmuştur, bu da ikili hedefleme stratejilerini daha da desteklemiştir. Bu çalışmada, OSI ve ENZ tarafından EGFR ve AR'nin çift hedeflenmesi, tümör mikroçevredeki (TME) sağlıklı hücrelere, HMC3 hücrelerine, zarar vermeden LN18 ve U87 hücrelerinde hücre canlılığı, hücre sağkalımı ve hücre döngüsü durmasının indüksiyonunda azalma, EMT'nin tersine dönmesi ve apoptoza neden olacağı hipotezini kurduk. OSI ve

ENZ'nin HMC3 hücrelerini etkilemeden LN18 ve U87 üzerinde hücre canlılığını azaltan sinerjik bir etki yarattığını ortaya koyduk. Bu veri, GBM hücrelerinde ATP konsantrasyonlarının azalmasıyla doğrulandı. Trypan mavisi ile canlılık tayini, OSI ve ENZ'ye maruz kalmanın, doz ve zamana bağlı bir şekilde LN18 ve U87 üzerinde sitotoksisiteye neden olduğunu, ancak HMC3 üzerinde böyle bir etki yaratmadığını gösterdi. Floresan boyama yardımıyla, OSI ve ENZ'nin kombine tedavisinin, yine GBM hücrelerine özgü olarak ölü hücreleri, nükleer fragmantasyonu arttırdığı ve mitokondriyal membran potansiyelini azalttığı gözlemlendi. Koloni oluşum potansiyeli ve sferoid oluşum yeteneği, LN18 ve U87'de OSI ve ENZ uygulanarak azaltıldı. Ayrıca, OSI ve ENZ birlikte LN18 ve U87'de göç kapasitesini azalttı, bu da yara iyileşmesinin yavaşladığını ortaya koymaktadır. Akış sitometrisinde subG1 popülasyonunda bir indüksiyonun yanı sıra western blotting sonuçlarında kesilmiş kaspazlar ve PARP'da protein ifadesinin artmasıyla birlikte kesilmemiş kaspazlar ve PARP ile Bcl-x_L'de protein ifadesinin azaldığı görülmüştür, bu da indüklenmiş apoptozu göstermektedir. İmmunoblotting sonuçları, EGFR ve AR sinyal yolaklarının alt hedeflerinin başarılı bir şekilde inhibe edildiğini doğruladı ve bu da LN18 ve U87'de siklin D1 ekspresyonunda azalma ve EMT belirteçlerinin tersine dönmesi ile hücre döngüsünün durmasına yol açtığını ortaya koydu. Bildiğimiz kadarıyla, bu çalışma, 3. Nesil EGFR TKI ve 2. Nesil AR antagonistinin GBM'de hücre döngüsü, EMT ve apoptoz üzerindeki kombinasyon etkilerini araştıran ilk çalışmadır. Bulgularımız, OSI ve ENZ hedef EGFR ve AR'nin uygulanmasının GBM'de yeni bir tedavi seçeneği olabileceğini göstermektedir.

Anahtar kelimeler: Androjen reseptörü, apoptoz, enzalutamid, epidermal büyüme faktörü reseptörü, epitelyal-mezenkimal geçiş, glioblastoma, osimertinib

1. INTRODUCTION

1.1 GLIOMA

Tumors in the brain and spinal cord are called brain and CNS tumors and are seen in children as well as adults. Brain and other CNS tumors have tremendous effects on mortality even though they are rare (Ostrom et al., 2021). According to the Global Cancer Observatory (GLOBOCAN), 321,731 patients were diagnosed with brain and other CNS cancer and 248,500 of them passed away in 2022 worldwide. New cases were 6,511, and 6,051 people died due to brain and CNS tumors in 2022 in Turkey (Ferlay J. et al., 2024). Glioma is a primary brain tumor and has been classified based on the cellular origin, including oligodendroglioma, oligoastrocytoma and astrocytoma (Hanif et al., 2017). According to the guideline of the World Health Organization (WHO), gliomas are sorted into grades (Grade I, II, III and IV) rather than stages with respect to histopathology (Verhaak, 2016). The higher grade it is classified the more aggressiveness and potential of growth it is related to and observed. Grade I and II are defined as low-grade glioma (LGG) whilst high-grade glioma (HGG) represents Grade III and IV. In addition to grade classification, glioma is also derived from different origins such as oligodendroglioma, oligoastrocytoma and astrocytoma. Oligodendroglioma and oligoastrocytoma are observed in grade II and III, whereas astrocytoma ranges from grade I to IV as depicted in Table 1 (Arcella et al., 2020). Among these, GBM is the most aggressive tumor originating from astrocytoma and defined as grade IV in the brain (Hanif et al., 2017).

Table 1. Types of Gliomas.

	Origin of Glioma		
Grades	Oligodendroglioma	Oligoastrocytoma	Astrocytoma
Grade I			Pilocytic astrocytoma
Grade II	Oligodendroglioma	Oligoastrocytoma	Diffuse astrocytoma
Grade III	Anaplastic oligodendroglioma	Anaplastic oligoastrocytoma	Anaplastic astrocytoma
Grade IV			Glioblastoma

1.2 GLIOBLASTOMA

GBM, also known as astrocytoma grade IV, is a cold tumor characterized by notoriously aggressive and invasive behavior with a high density of intra- and inter-tumor heterogeneity (Zhou et al., 2023; Huang et al., 2024). It has a notable proclivity to infiltrate the surrounding brain tissue, regarded as the deadliest form of brain tumor (D'Alessio et al., 2019; Lan et al., 2024). Although GBM has an incidence of 4.17 per 100,000 individuals, it is an ineluctably relapse primary intra-axial brain tumor with a poor prognosis, and the overall life span is restricted to approximately 15 months (Oronsky et al., 2021; Lan et al., 2024).

Necrosis, microvascular proliferation, nuclear atypia, hypercellularity and cellular pleomorphism are marked as common morphological features of GBM (D'Alessio et al., 2019; Lan et al., 2024). The commonly detected area of GBM is the cerebral hemispheres. Approximately 95% of cases stems from the supratentorial location whilst the remaining brings about in the cerebellum, spinal cord and brainstem (Nakada et al., 2011). Macroscopically, GBM is a heterogeneous tumor composed of necrosis, multifocal hemorrhage and cystic and gelatinous regions. Some zones are observed as soft and yellow due to tissue necrosis whereas others appear as white and firm. The tumor is unremarkably depicted by a single, slightly enormous lesion stemming from the white matter. From the perspective of histology, GBM resembles anaplastic astrocytoma due to prevalent mitotic activity, multinucleate cells and multifocal necrosis. Moreover, one of the features of GBM is vascular endothelial cell proliferation with glomeruloid structure (Hanif et al., 2017). GBM encompasses several scarce variants, including gliosarcoma, giant-cell GBM, small-cell GBM, GBM with oligodendroglial traits and epithelioid GBM. Gliosarcoma exhibits malignant astrocytic characteristics alongside sarcoma-like mesenchymal metaplasia elements. Small-cell GBM is related to EGFR amplification while giant-cell GBM contains excessively pleomorphic giant cells. GBM with oligodendroglial properties is relevant to a better prognosis than classic GBM. Epithelial GBM, the most recently identified variant, is characterized by salient epithelioid morphology and BRAF V600E mutation in the cells (Lan et al., 2024).

In 2016, WHO revised and redefined the CNS 4 tumors, and the classification of GBM according to histopathologic traits was redesignated (Lan et al., 2024). This updated classification is divided into two chief types: primary and secondary GBM (Ohgaki & Kleihues, 2013). Even though these two classes are mainly indistinguishable from each other and have nearly the same response to traditional therapy, they are separated according to genetic and epigenetic profiles. Thereby, the targeted therapy response might be distinct (D'Alessio et al., 2019). The primary GBM is isocitrate dehydrogenase (*IDH*) wt GBM and arises *de novo* without either clinical or histological pioneer lesion (Ohgaki & Kleihues, 2013; Hanif et al., 2017). It is predominantly seen in elderly patients (older than 50 years old) with a more aggressive course and represents relatively 90% of GBM cases. On the other hand, the secondary GBM is *IDH* mutant type and takes place by slow progression from preexisting low-grade diffuse astrocytoma or anaplastic astrocytoma. This subtype represents nearly 10% of patients younger than 50 years of age with usually a more favorable prognosis (Ohgaki & Kleihues, 2013; Lan et al., 2024). There is also a group for GBM classification defined as GBM not otherwise specified (NOS). This term is used for the GBM cohort whose *IDH* situation for diagnosis has not been identified yet (Khandwala et al., 2021).

1.2.1. Genetic Alterations in Glioblastoma

Advances in genomic technologies have contributed to the understanding of the GBM heterogeneity for categorization as well as the identification of the biomarker changes and mechanisms driving GBM. Thereby, these advancements contribute to ameliorate diagnostic approaches and the development of the targeted therapeutic approaches (Arcella et al., 2020; Grochans et al., 2022). The most frequently observed mutations in GBM happen in genes such as *TERT* (telomerase reverse transcriptase), *EGFR*, *ATRX* (alpha thalassemia/mental retardation X-linked), *TP53* (tumor protein p53) and *PTEN* (phosphatase and tensin homolog). EGFR amplification, PTEN mutation and TERT promoter mutations are typical features of *IDH* wt GBM while TP53 mutation and ATRX mutations are usually observed in *IDH* mutant-type GBM (Lan et al., 2024). Mutations in *TP53* cause inactivation of p53, guardian of the genome, leading to evading cell death, enhancing proliferation, increasing invasiveness, metastasis and

demonstrating resistance to chemotherapeutic agents in GBM. *PTEN* is a tumor suppressor gene located on chromosome 10q23. Loss of PTEN expression is related to poor prognosis of GBM and worse overall survival (OS) on account of impairing the regulation of cell growth, survival and proliferation. EGFR amplification is associated with the constitutive activation of EGFR, so it brings about the activation of downstream tyrosine kinases (Grochans et al., 2022). *ATRX* is a gene responsible for protein encoding related to chromatin remodeling to allow histone variant H3.3 to be involved in heterochromatin, and ATRX mutations cause resistance to chemotherapy (Y. Zhao et al., 2024). Additionally, *MGMT* [O^6-methylguanine DNA (Deoxyribonucleic acid) methyltransferase] is a gene that has a role in DNA repair by removing alkyl groups from the O^6 position of guanine. Overexpression of MGMT gives rise to resistance to alkylating agents utilized for therapeutic regimens and treatment failure (Hegi et al., 2005). BRAF is a protein involved in the Ras (Rat sarcoma virus)-Raf (rapidly accelerated fibrosarcoma)-MAPK (mitogen-activated protein kinase) signaling pathway and participates in cell growth. Mutation of BRAF activity leads to uncontrolled cell proliferation. In addition, the V600E mutation, where valine is substituted for glutamate at position 600, contributes to persistently activated Serine/Threonine kinase BRAF (Grochans et al., 2022). The nucleoprotein complexes at the end of chromosomes are called telomeres and their role is to shorten at each cell cycle to finally lead to cell death or senescence. Telomerase is an enzyme that plays a role in sustaining telomere length and evading cell death, so that it gives rise to infinite cell growth for cancer. *TERTp* (Telomerase reverse transcriptase promoter) mutations were detected among GBM patients with an 80% occurring rate regardless of being wt and a mutation in *IDH* (Olympios et al., 2021). Loss of heterozygosity on chromosome 22q has an impact among Grade II and IV originating from astrocytes. *CHEK2* (checkpoint kinase 2) is one of the tumor suppressor genes located on chromosome 22q12.1 and has a role in DNA damage response. It is activated by ATM (Ataxia-telangiectasia mutated) and then phosphorylates TP53, BRCA1 and phosphatases, Cdc25A and Cdc25C, giving rise to cell cycle arrest and DNA repair-related pathways activation. A mutation in *CHEK2* is one of the prevalent features to detect GBM genomic profiles (Sallinen et al., 2005). *CDKN2A* (cyclin-dependent kinase inhibitor 2A) is a gene responsible for encoding tumor suppressor

proteins such as p16 and p14 and mediates cell cycle arrest interacting with *MDM2* (murine double minute 2) and apoptosis pathway. Homozygous deletion in *CDKN2A* in *IDH* mutant GBM causes tumorigenic burden and poor prognosis (Lu et al., 2020). Upregulation of *MDM2* negatively regulates and leads to driver oncogenic events, which contribute to p53 inactivation (Pellot Ortiz et al., 2023; Han et al., 2024).
Besides uncovering genetic mutations in GBM, it also has introduced the major signaling pathways supporting tumorigenesis, evading senescence and progression of GBM. There are 3 continuously altered core signaling molecules which are retinoblastoma (RB), receptor tyrosine kinase (RTK) and p53.

1.2.1.1. Retinoblastoma (RB): The dysregulation of the RB signaling is commonly found in secondary GBM tumors and causes tumorigenesis. RB is altered in almost 78% of GBM (Hanif et al., 2017). Under normal circumstances, the complex of CDK4 (cyclin-dependent kinase 4)/Cyclin D1 aids RB protein phosphorylation to hinder cell cycle from G1 phase to S phase by connecting with the transcription factor, E2F. RB signaling might crosstalk with the p53 signaling via CDKN2A, which encodes Ink4a and Arf proteins. However, the inhibition of the RB signaling is impaired in GBM on account of the amplification of CDK4/6 (cyclin-dependent kinase 6) and inactivation of CDKN2A/2B and RB1 in GBM. Hence, it eventually prompts dysregulation of cell cycle checkpoint function and then loss of control over cell proliferation (Lan et al., 2024).

1.2.1.2. Receptor Tyrosine Kinase (RTK) Pathways: RTKs are transmembrane proteins with an extracellular ligand-binding domain (Tilak et al., 2021). They act as cell surface receptors for hormones, cytokines, growth factors and neurotrophic factors. Under normal physiological conditions, RTKs have control over survival, growth, cell cycle progression, migration and differentiation via activation of two major signaling pathways, Ras/MAPK/ERK (extracellular signal-regulated kinase) and Ras/PI3K (phosphatidylinositol 3-kinase)/AKT (protein kinase B) (Pearson & Regad, 2017). However, cascades of RTK signaling are mostly and persistently changed signaling pathways in GBM with an 88% ratio, peculiarly in primary GBM tumors (Hanif et al., 2017; Lan et al., 2024). Aberrant activation of RTK family members, including EGFR, PDGFR (platelet-derived growth factor receptor), TGFR (transforming growth factor receptor), FGFR (fibroblast growth factor receptor), MET (mesenchymal-epithelial transition factor receptor), VEGFR (vascular endothelial growth factor receptor) and IGF-1R (insulin-like growth factor 1 receptor), shows an oncogenic phenotype in the modulation of cell proliferation, angiogenesis, survival and differentiation (Pearson & Regad, 2017; Tilak et al., 2021). This oncogenic phenotype might be occurred by overexpression/amplification of the RTK, chromosomal translocation for increased kinase activity, inducing overproduction of growth factors by the tumor, fusion of kinase domains with irrelevant proteins, and having mutations in ligand-binding/kinase domains (Tilak et al., 2021).

1.2.1.3. TP53 Signaling: *TP53* is a transcription factor gene encoding a well-known tumor suppressor protein, p53. p53 contributes to cancer prevention by regulating cellular events such as proliferation, migration, invasion, evasion of cell death and cancer cell stemness. The p53/MDM2/CDKN2A signaling pathway is disrupted in 94% of GBM cell lines. A mutation in *TP53* causes inactivation itself and loss its tumor suppressive features for the prevention of tumorigenesis. This mutation is seen among the one-third of *IDH* wt GBM and the second-third *IDH* mutant GBM. Amplification of MDM2 is responsible for blocking p53 by degrading p53 to trigger tumor formation. MDM2 overexpression is generally mutually exclusive with mutation in p53 and is predominantly observed in primary GBM, which is deprived of p53 mutation. Homozygous deletion in CDKN2A gives rise to the inactivation of the p53 signaling pathway and then less overall life span of GBM individuals. CDKN2A mutation is seen in primary GBM at 58% while detected in secondary GBM with a 16-47% ratio (Lan et al., 2024).

1.2.2. Epigenetic Alterations in Glioblastoma

Epigenetic modifications, including histone modifications, DNA methylation and chromatin remodeling, have been extensively investigated and recognized as critical contributors to GBM tumorigenesis and drug resistance. These modifications might hold potential as biomarkers and therapeutic targets (Q. Wu et al., 2021; Lan et al., 2024). Hitherto, numerous studies about epigenetic alterations in GBM have focused on DNA methylation, such as hypermethylation, gene-specific hypomethylation and genome-wide hypomethylation. MGMT is the best-studied example of DNA methylation, and the methylation status of *MGMT* determines the response to TMZ, an alkylating chemotherapy agent. An unmethylated *MGMT* promoter brings about a worse response to TMZ leading to drug resistance in GBM patients. Hypermethylation of *IDH1* mutation leads to silence of the α-KG-dependent DNA modifying enzyme, TET2 (Tet methylcytosine dioxygenase 2). In GBM, CpG promoter hypermethylation happens in genes having different roles relevant to angiogenesis, invasion, drug resistance, tumorigenesis, cell cycle control (*CDK2A-p16INK4a* and *CDK2B-p15INK4b*), hampering of apoptosis (*CDH1*, *DAPK1* and *TIMP3*), DNA repair (*MLH1*) and tumor suppression (*RB1*, *BLU*, *EMP3*, *RASSF1A* and *VHL*. A pile of

novel silencing via hypermethylation has been revealed including polycomb repressor complex 2 (PRC2) target genes, the cell motility regulator testis-derived transcript (*TES*) and a myelin-relevant gene playing a role in cell-cell interaction and proliferation. The most hypomethylation has been detected occurring in tandem repeat satellite 2 (Sat2) found in the juxtacentromeric region of chromosomes 1-9-16 as well as in D4Z4 found in the subtelomeric areas of chromosomes 4q35 and 10q26. Furthermore, hypomethylation in Sat2 in GBM is associated with copy number changes in the vicinity of euchromatic sequences, especially adjacent to the pericentromeric region of chromosome 1. Hence, it suggests that hypomethylation of repeated sequences in GBM is prone to copy number changes and chromosomal breakage (A. Liu et al., 2016).

Histone modifications, including methylation, acetylation, ubiquitylation and phosphorylation, change gene expression without affecting the sequences of DNA. Aberrant histone modifications cause the transcription of genes which drive GBM progression leading to drug resistance. To illustrate, the enhancer of zeste homolog 2 (EZH2), a histone methyltransferase in PRC2, is related to GBM progression. High expression of *EZH2* upregulates c-MYC and enhances phosphorylation of signal transducer and activator of transcription 3 (STAT3), giving rise to GBM tumor formation and reducing OS in GBM. It has been inspected that histone lysine demethylase (KDM) genes are also responsible for dysregulation of apoptosis, senescence and cell proliferation. For instance, lysine demethylase 1A (KDM1A) and KDM2B have a susceptibility to the stemness phenotype in GBM. Meanwhile, upregulation of both KDM5A and H3K4 demethylase in GBM propagates the TMZ resistance (Q. Wu et al., 2021). Moreover, a couple of histone deacetylase (HDAC) expressions, particularly class II and IV, are found to be changed in GBM leading to diminishing messenger ribonucleic acid (mRNA) expressions (Liu et al., 2016).

Chromatin remodeling has been linked to drug resistance in GBM as if DNA methylation and histone modifications do (Q. Wu et al., 2021). As an illustration, poly (ADP-ribose) polymerase 1 (PARP1) is a major enzyme participated in chromatin remodeling through histone modification and inhibition of the complex of ISWI (Romani et al., 2018). PARP1 gives rise to enhanced radioresistant and cell survival, and DNA damage response expressions are increased in GBM samples (Lee et al.,

2017). In addition to PARP1, the catalytic subunit of the human SWI/SNF chromatin remodeling complex, called BRG1 (Brahma-related gene 1), has a significant role in sustaining glioma-initiating cells (GICs) in their stem-like state. BRG1 negatively regulates TXNIP, a redox regulator and a negative glycolysis regulator, through a STAT3-dependent pathway leading to drug resistance of GICs in GBM (Ganguly et al., 2018).

The long non-coding RNAs (lncRNAs) affect gene expression by cross-talking with epigenetic mechanisms in physiological and pathological conditions. For example, metastasis-associated lung adenocarcinoma transcript 1 (MALAT1) is shown as an overexpressed oncogenic lncRNA which brings about tumor formation, proliferation and stemness via regulating miR-129, non-canonical wingless-related integration site (Wnt) pathway and sex-determining region Y-box 2 (SOX2) in GBM. The upregulation of H19, another lncRNA, has been correlated with neurosphere formation, angiogenesis, stemness, invasion and TMZ resistance in GBM (Q. Wu et al., 2021).

1.2.3. Transcriptomic Alterations in Glioblastoma

GBM has been stratified into distinct subtypes with respect to transcription profiles elucidated by high-throughput transcriptome profiling and computational analysis (Lan et al., 2024). It allows the targeted therapy to be tailored to the transcriptomic features of subclasses. In 2006, Phillips and colleagues delineated that there are 3 subtypes of GBM, proliferative (Prolif), proneural (PN) and mesenchymal (MES), based on 35 characteristic genes and 76 astrocytoma gene expression profiles (Phillips et al., 2006). However, in 2010, it was revised and revealed four distinct subtypes of GBM, PN, MES, classical (CL) and neural (NE), through 200 gene expression profiles assayed across 3 different sequencing platforms (Affymetrix HuEx array and Affymetrix U133A array and Agilent 244k array) (Verhaak et al., 2010). As of 2017, Wang and colleagues resolved this debate by publishing data that identified three subtypes of GBM, PN, CL and MES while the NE phenotype is excluded from the subtype and tackled as non-tumor specific detected by contaminating normal tissue from tumor periphery in the brain (Q. Wang et al., 2017). This proposal was also fortified by standardized normal distribution convolutional deep neural networks

(SND-CDNN) in 2022 (Mao et al., 2022). This classification generates a framework for personalized therapeutic strategy, improving outcomes in GBM management.

CL GBM has been associated with high *EGFR* expression and *CDKN2A* deletion, alongside activation of Notch and Sonic Hedgehog pathway-related factors. The characteristic traits of CL GBM might be relevant to mouse astrocytes. This subtype might not have cancer stemness features while PN and MES subtypes do. In CL GBM, genes related to alternative RNA splicing are overexpressed (Xu et al., 2024). Additionally, it has also been noticed amplification of chromosome 7 and loss of chromosome 10 (Jovčevska, 2018).

Three crucial traits of the PN GBM are *PDGFR* alterations, point mutations in *IDH1* and *TP53*, and loss of heterozygosity. Upregulation of *PATZ1* and *DRP5* stimulates the maintenance of the PN stemness. The activation of Notch1 poses to the survival of PN GBM through the nuclear factor kappa B (NF-κB) signaling pathway. The main biomarkers of the PN subtype are *OLIG2*, *DCX*, *DLL3*, *TCF4*, *SOX*, *NKX2-2* and *ASCL1*. It has been suggested that the PN GBM subtype may be associated with vascular pathology, as evidenced by the correlation between higher brain volume in infiltrative peripheral edema with the PN GBM subtype (Xu et al., 2024).

The most common features of the MES subtypes are loss of *NF1*, activation of NF-κB and AKT signaling pathways. The enhanced heterogeneous and drug-resistant tumor cells and infiltrating immune cells are vital hallmarks of the MES GBM class. It has also been found that enhanced endoplasmic reticulum (ER) stress is associated with MES GBM. The MES class possesses the highest content of immune cells. The biomarkers, *TGFBR2*, *GIT2*, *RAP1B*, *RUNX1* and *PPARG*, have an interaction with protein factors in competitive endogenous RNA (ceRNA) regulated manner in the MES GBM (Xu et al., 2024).

1.2.4. Risk Factors of Glioblastoma

Age is one of the risk factors for developing diseases such as cancer. Numerous studies unveiled that the older people get (especially more than 65 years old), the more chances they are likely to have GBM (peaking at between 75 and 84 years old). In addition, the older patients diagnosed with GBM the less life expectancies unfortunately they have (Tamimi & Juweid, 2017). Moreover, in the literature, it is

indicated that there is a higher case of GBM in men than in females. Another risk factor for GBM is socioeconomic status. The case of GBM is higher for high-income groups than for low-income groups but the mortality in countries with higher socioeconomic status is lower than with lower socioeconomic status because of better access to healthcare (Grochans et al., 2022). A meta-analysis manifested that non-Hispanic white people are listed as having the highest incidence of GBM and the poorest survival rate among all racial groups followed by blacks. Following, Hispanic whites are ranked as third. Asians or Pacific Islanders have less incidence of GBM and a higher life span than other races or ethnicities (Patel et al., 2019). The relationship between nicotine consumption and GBM development has not been cleared very well owing to sparse clinical outcomes. However, there are a few studies that say nicotine might promote angiogenesis, invasion, migration and evade apoptosis as well as developing chemotherapy drug resistance (McConnell et al., 2019). There is an ongoing debate about the impact of alcohol intake on GBM development. Some articles mentioned hazardous effects of alcohol in GBM progressing because of producing reactive oxygen species (ROS) and acetaldehyde (Grochans et al., 2022). Conversely, the latest studies have divulged that different alcohol involving beverages hampered cell proliferation and risk of GBM (Cote et al., 2021; Sheikh et al., 2021). According to allergy-related germline polymorphism analysis, the people who don't have atopy and allergies show more tendency risk of GBM (Tamimi & Juweid, 2017). The results from people who are in the farming industry indicated that pesticides elevated the risk of GBM (Gatto et al., 2021). Furthermore, the GBM cells exposed to pesticides composed of fungicide metiram, deltamethrin and herbicide glyphosate dramatically displayed multidrug resistance to anti-cancer drugs (Doğanlar et al., 2020). The rare hereditary disorders, Turcot syndrome, Li-Fraumeni syndrome and Neurofibromatosis 1, are susceptible to increase of GBM incidence (Smith et al., 2024).

1.3 DIAGNOSIS AND SCREENING APPROACHES IN GLIOBLASTOMA

Contrast-enhanced magnetic resonance imaging (MRI) is considered the gold standard for non-invasive imaging technology for GBM. Positron emission tomography (PET) is recommended for specific imaging. There is a promising approach, immuno-targeted imaging, which contributes to combining target-specific antibodies with the tumor cell surface target utilizing PET and immunohistochemistry referred to as virtual biopsy. For further diagnostic strategies, histological examinations are required and performed via tumor resection by a fine-needle aspiration biopsy. The liquid biopsy is tackled as an alternative non-invasive examination after the discovery of circulating biomarkers. Biomarkers such as microRNA (miRNA), exosomes, proteins and circulating DNA (ctDNA) can be examined in cerebrospinal fluid, serum and/or plasma. Also, with the help of liquid biopsy, tumor cells that have spread into the body fluids can be detected. Furthermore, to assess the prognosis and the invasiveness of GBM, the mutation status of biomarkers is analyzed. The most checked biomarkers are *IDH1/2*, *ATRX*, *TERT*, *MGMT*, *BRAF* V600E, *TP53*, *EGFR*, Ki-67, *PTEN* and chromosome 1p and 19p codeletion (J. Li et al., 2022).

1.4 THERAPEUTIC STRATEGIES IN THE TREATMENT OF GLIOBLASTOMA

Despite plenty of efforts to find novel therapeutic strategies such as laser interstitial thermal therapy, stem cell-based therapy and alternating electric field therapy, there are still widely accepted three conventional treatment options due to the uncertain outcomes of the long-term effects of novel treatment options. The first standard treatment option for GBM is surgical resection. Maximal safe surgery is performed for situations which aren't suited for total elimination, such as invasive and/or metastatic GBM. Surgical options are categorized based on the extent of tumor resection such as biopsy, partial resection, subtotal resection and gross total resection (J. Li et al., 2022). To augment the contrast during surgery, patients receive oncological fluorescence 5-ALA (5-aminolevulinic acid) before the surgical removal of GBM (nearly 24 h) so that

it enhances the effectiveness and safety of the surgery. Throughout the operation, the areas surrounded by neoplastic infiltrate begin to glow after enlightening the surgical area with pink or red light (Czarnywojtek et al., 2023). More than one surgical resection might be performed depending on emerging requirements whereas the outcome remains poor. Postoperative complications in GBM patients are likely to suffer from seizures and central neurological deficits. The well-known side effects are headache, stupor, unconsciousness owing to intracranial hypertension and nausea (J. Li et al., 2022). Despite surgical advancements, the life span does not extend and is restricted to 15 months. One of the negative outcomes might be related to the tumor size, bigger than 5-6 cm, which crosses the midline. The GBM in the brainstem or diencephalon has worse prognosis compared to tumors in the cerebrum and cerebellar (Davis, 2016).

Radiotherapy is suggested within 4-6 weeks to target microscopic tumor lesions after waiting for the healing of the craniotomy wound (Davis, 2016; J. Li et al., 2022). Radiotherapy can be used in various forms, for instance X-ray photons, protons or gamma photons, whereas all of them haven't become validated for the standard of care yet. 3D conformal radiotherapy, which utilizes X-ray photons, is applied to patients who get chemoradiation therapy to directly target the tumor from different angles. Delivering the recommended dose to the tumor area benefits from the CT and MRI images. Radiotherapy is generally distributed over six weeks in 2 gray (Gy) fractions for a suitable total dosage of 40 to 60 Gy. Targeting tumors and providing approximately 1-2 cm margin in the vicinity of the periphery are done by particular formed beams from the radiotherapy device containing complex multi-leaf collimators. X-ray treatment allows low linear energy that brings about direct and indirect biological harm. Nearly one-third of the treatment impact comes from direct damage to DNA while roughly two-thirds of are stems from indirect biological damage, such as the ionization of water to generate free radicals that wreak havoc on DNA (W. Wu et al., 2021). For patients over 70 years of age and those in poor general health, accelerated hypo-fractionated radiotherapy is applied (Li et al., 2022). Concurrent chemoradiation therapy has been recommended to expand the life span of patients since 2005. Even though the combination of radiotherapy and chemotherapy is a better option than radiotherapy alone, overall life expectancy is still restricted (14.6

months and 12.1 months respectively) (Davis, 2016). Unfortunately, tumor recurrence remains inevitable owing to tumor cell intrinsic or TME-mediated resistance to radiotherapy.

In addition to radiotherapy, chemotherapy is tackled as standard postoperative care (Li et al., 2022). There are 5 FDA (Food and Drug Administration)-approved drugs for GBM therapy: intravenous carmustine (BCNU; bis-chloroethylnitrosourea), carmustine wafer implants, lomunistine (CCNU; chloroethylcyclohexylnitrosourea), bevacizumab (BVZ) and TMZ. Outside of TMZ, other ones are recommended for treating recurrent tumors and symptoms. Intravenous BCNU obtained FDA approval for GBM cure in 1977 (Fisher & Adamson, 2021). Carmustine is a nitrogen mustard compound and a non-specific alkylating agent which gives rise to crosslinking of DNA and RNA (Fisher & Adamson, 2021; W. Wu et al., 2021). Furthermore, BCNU binds to and adjusts glutathione reductase that brings about apoptosis in tumor cells. The dosage of 150 to 200 mg/m^2 is decided to be given to the patients once every six weeks. Unfortunately, there are some side effects, pulmonary toxicity, ocular toxicity and bone marrow suppression. Due to the detrimental effects of BCNU and deciphering other chemotherapeutic reagents, intravenous BCNU is applied less and recommended for only recurrent GBM (Fisher & Adamson, 2021). Carmustine wafer implants were developed and approved by the FDA for GBM relapse in 1996 and newly diagnosed GBM in 2003 (Fisher & Adamson, 2021). These implants are biodegradable discs which are intraoperatively applied to tumor resection cavities to allow a slow release of the drug over 2 weeks. In addition, in order to increase the efficacy of treatment, carmustine is co-administered with alkyl guanine transferase (AGT) inhibitors not to be reversed carmustine effect by AGT (W. Wu et al., 2021). Common side effects are cerebral edema, intracranial infection due to assuming wafers as a foreign substance in the body and abnormal wound healing complications (Fisher & Adamson, 2021; W. Wu et al., 2021). Moreover, carmustine wafers are overpriced and are not easy to cope with the agent by operating room staff. 19 studies on 795 patients exposed to carmustine wafer have revealed a complication rate of 42.7%, and not to suggest these implants anymore (Fisher & Adamson, 2021). CCNU is another alkylating reagent which leads to crosslinking of DNA and RNA to promote apoptosis in tumor cells. This agent is given orally once every 6 weeks and crosses BBB due to small size and

high lipophilicity. Hematologic toxicity is one of the frequent common toxicities observed in GBM patients. BCNU and CCNU used to be tackled as standard of care prior to the early 21st century but now they are recommended for recurrent GBM (Fisher & Adamson, 2021; W. Wu et al., 2021). BVZ is a humanized monoclonal antibody which was approved by the FDA for recurrent GBM in 2009. This targeted antibody binds and impedes vascular endothelial growth factor (VEGF), which boosts neovascularity. In GBM, BVZ hinders VEGF to avoid tumor angiogenesis, so slowing down the spread of tumors. Even though BVZ is well-tolerated, some side effects are shown such as wound healing, cerebral bleeding, hypertension, proteinuria, gastrointestinal perforation and thromboembolic events (Fisher & Adamson, 2021). BVZ doesn't improve OS for individuals with newly diagnosed GBM, but it is utilized to treat recurrent GBM (W. Wu et al., 2021).

1.4.1. Temozolomide in the Treatment of Glioblastoma

TMZ, marketed under the brand names Temodar or Temodal, is the solely FDA-approved drug to be administered to individuals with newly diagnosed GBM since 2005 (N. Singh et al., 2020). It is an imidazotetrazine lipophilic drug that penetrates the BBB quickly disrupts DNA replication and promotes modification and cross-linking of DNA causing to apoptosis (Singh et al., 2020; Li et al., 2022). This alkylating agent exhibits a high penetration ability in the tissues and shows a peak plasma concentration after 20 min following administration orally, meaning that it has rapid absorption (Ortiz et al., 2021). This prodrug is steady at acidic pH and basically causes DNA damage. Negatively charged DNA is tackled as a nucleophile and the methyl group from the methyldiazonium ion is delivered to DNA, bringing about mismatched base pairing and eventually cytotoxicity. TMZ agent has an impact on DNA at specific locations, methylating DNA at the N7 position of guanine, O^3 position of adenine and O^6 position of guanine. Alkylating of O^6 area on guanine attempts to the formation of O^6 methylguanine and the insertion of thymine instead of cytosine. These mutations promote the generation of single- and double-stranded DNA breaks causing to cell cycle arrest (G2/M) and programmed cell death (N. Singh et al., 2020). TMZ combined with radiotherapy is suggested to augment the OS and quality of life as well as TMZ alone therapy (JIAPAER et al., 2018). In contrast to other drugs

mentioned before, TMZ doesn't have side effects like myelosuppression or respiratory changes because of cytochrome P450 enzymes, and the kidneys aren't included in its metabolism (Ortiz et al., 2021). However, TMZ still displayed some adverse effects such as lymphocytopenia, anorexia, thrombocytopenia, vomiting, neutropenia, leukopenia, lung infection, anemia, urinary frequency and pro-inflammatory effect (Bae et al., 2014; J. Hu et al., 2021; Y. Zhou et al., 2024). Moreover, it has been shown that the administration of TMZ leads to drug resistance. These main contributors are MGMT, base excision repair, autophagy, mismatch repair, persistence of cancer stem cells (Ortiz et al., 2021; Li et al., 2022). Even though GBM pathology remains a prominent focus of research, little step has been taken owing to the challenges such as the penetrance of BBB and genetic heterogeneity. Therefore, these problems lead to reducing or nullifying the effectiveness of therapeutic strategies. Consequently, there is an urgent requirement to develop effective GBM treatment options (C. Chen et al., 2021).

1.5 THE ROLE AND IMPACT OF EPIDERMAL GROWTH FACTOR RECEPTOR IN GLIOBLASTOMA

Several members of the RTKs family are a group of membrane-bound receptors which lie at the center of sophisticated interconnecting signaling pathways and take part in cell proliferation, differentiation, survival, metabolism, migration, apoptosis and cell cycle under normal and pathological conditions (Lemmon & Schlessinger, 2010; Sudhesh Dev et al., 2021). They transduce signals to mediate cell-to-cell communication via tyrosine phosphorylation on intracellular substrate proteins (Sudhesh Dev et al., 2021). There are 58 RTKs, which are subdivided into 20 subfamilies. All RTKs are structurally comprised of similar components, a single transmembrane helix and a cytoplasmic region composed of a protein tyrosine kinase domain with an additional carboxy terminus and juxtamembrane regulatory regions. Regardless of whether the inactive state is monomeric or oligomeric, the receptor is required to have the bound ligand to mediate a particular relationship among individual receptor molecules in an active dimer or oligomer. Activity or regulation of RTKs can be unhinged by genetic alterations or anomalies, and these mutations in RTKs have

been linked to persistent activity and diseases, including diabetes, inflammation, arteriosclerosis, angiogenesis and cancer (Lemmon & Schlessinger, 2010). Generally, the deviant behavior of RTKs in cancer can be classified into four main categories: overexpression, activation of autocrine, chromosomal translocations and gaining-of-function mutations (Kennedy et al., 2016).

The ErbB (erb-b2 receptor tyrosine kinase) or HER (human epidermal growth factor receptor) family is subgrouped into 4 members: EGFR (ErbB1 or HER1), ErbB2 (Neu or HER2), ErbB3 (HER3) and ErbB4 (HER4) (Pan & Magge, 2020). This family is found in nearly every cell type, except for hematopoietic cells, and plays pivotal roles in embryonal development, homeostasis and pathophysiological conditions, especially in cancer (Kennedy et al., 2016; Wee & Wang, 2017). Under pathophysiological conditions, ErbB family instigates cell proliferation, cell motility, adhesion, metastasis, angiogenesis and inhibition of apoptosis (Wee & Wang, 2017). Of these, EGFR has become the limelight of research on the ErbB family in cancer because of ectopic expression of EGFR ligands, mutation and overexpression of the receptor, and controlling the many signaling pathways, such as ERK/MAPK, PI3K/AKT, SRC, PLC-γ1/PKC (protein kinase C), Jun N-terminal kinase (JNK) and JAK (Janus kinase)/STAT (Kennedy et al., 2016; Wee & Wang, 2017). These pathways crosstalk with each other and have roles in cell growth, differentiation, migration and the prevention of programmed cell death (Wee & Wang, 2017). EGFR has known 7 different ligands: epidermal growth factor (EGF), epiregulin, amphiregulin, betacellulin, heparin-binding EGF (HB-EGF) and transforming growth factor α (TGF-α) (An et al., 2018). Even though each ligand activates the EGFR via dimerization of EGFR, transphosphorylation of dimerized receptors and then activation of tyrosine kinase, each ligand might give rise to different signaling patterns, leading to differential biological outcomes (Gomez et al., 2013; Wee & Wang, 2017). Activation by ligand binding triggers homo- or heterodimerization of the receptors, cytoplasmic autophosphorylation of downstream of MAPK, PI3K and STAT3 pathways, regulating cell survival, angiogenesis and migration. Constitutively active oncogenic mutations in the EGFR bring about uncontrolled cell proliferation (Ezzati et al., 2024).

EGFR is a transmembrane receptor and is synthesized as a 1,210-residue precursor, which is cleaved at the N-terminal to the mature 1,186-residue protein, 170 kDa in

mass (Wee & Wang, 2017; Pan & Magge, 2020; Ezzati et al., 2024). *EGFR* spans 110 kb of DNA, comprising 28 exons with three different domains: extracellular domain (ECD), transmembrane domain (TMD) and intracellular domain (ICD). Extracellular region of EGFR is divided into four subdomains: domain I (amino acids 1-133; exons 1-4), domain II (amino acids 134-312; exons 5-7), domain III (amino acids 313-445; exons 8-12) and domain IV (amino acids 446-621; exons 13-16). TMD is made of 23 amino acids, from isoleucine 622 to methionine 644. Moreover, ICD is comprised of 542 amino acids long, including the juxtamembrane region (approximately 40 amino acids), tyrosine kinase domain (amino acids 690-953; exons 18-24) and C-terminal tail (amino acids 954-1136; exons 25-28) (Wee & Wang, 2017). EGFR remains as an inactive monomer till ligand binding triggers ECD-mediated dimerization. Those dimerized receptors undergo transphosphorylation, activating the tyrosine kinase domain to alter the inner state of the cell (Gomez et al., 2013; Pan & Magge, 2020; Ezzati et al., 2024). This activation drives time-dependent biological events, including downregulation of a great deal of miRNAs and upregulation of synthesized mRNAs (Uribe et al., 2021).

EGFR signaling can be categorized according to the localization of EGFR: signaling from the plasma membrane and from the non-plasma membrane compartments. Plasma membrane-related signaling includes RAS/MAPK/ERK pathway, PI3K/AKT pathway, JAK/STAT pathway and PKC pathway, whilst non-plasma membrane signaling takes place through Histone H4 and STAT proteins and cytochrome c oxidase subunit 2 (COXII) (An et al., 2018). Driving RAF-MEK (mitogen-activated protein kinase kinase)-ERK MAPK signaling cascades via activation of RAS is one of the most fundamental signaling pathways in modulating the physiological response of EGFR (Wee & Wang, 2017; An et al., 2018). Mechanistically, Src homology 2 domain-containing (SHC) is phosphorylated itself and then binds to growth factor receptor-bound protein 2 (GRB2). Linking two adaptor proteins to each other leads to the engagement of son of sevenless (SOS) to activate RAS and its downstream kinases, respectively (Wee & Wang, 2017). ERK 1/2 has vital roles in mediating cell proliferation, metabolism and survival and functioning in the tumor-suppressing signaling cascade (An et al., 2018). PI3K-AKT-mTOR, having a role in metabolism, cell survival, motility and proliferation, is another signaling cascade activated by the

EGFR pathway, but EGFR is deprived of a motif for directly binding to PI3K (Wee & Wang, 2017; Uribe et al., 2021). Phosphatidylinositol (4,5)-bisphosphate (PIP2) is phosphorylated by PI3K to create phosphatidylinositol (3,4,5)-triphosphate (PIP3). PIP3 subsequently recruits AKT serine/threonine kinase to the plasma membrane (Uribe et al., 2021). A variety of AKT substrates influence cell survival, proliferation and metabolism, including Beclin-1, caspase 9, BCL2-associated death protein (BAD) and cAMP response element-binding protein (CREB). JAK becomes activated through cytokine binding, and then STAT is phosphorylated for dimerization and translocation to the nucleus, as STAT can be directly activated by phosphorylation via EGFR. Nuclear STAT proteins have the capacity either to activate or block transcription of genes related to migration, stemness and inflammation-associated tumorigenesis (Figure 1) (An et al., 2018).

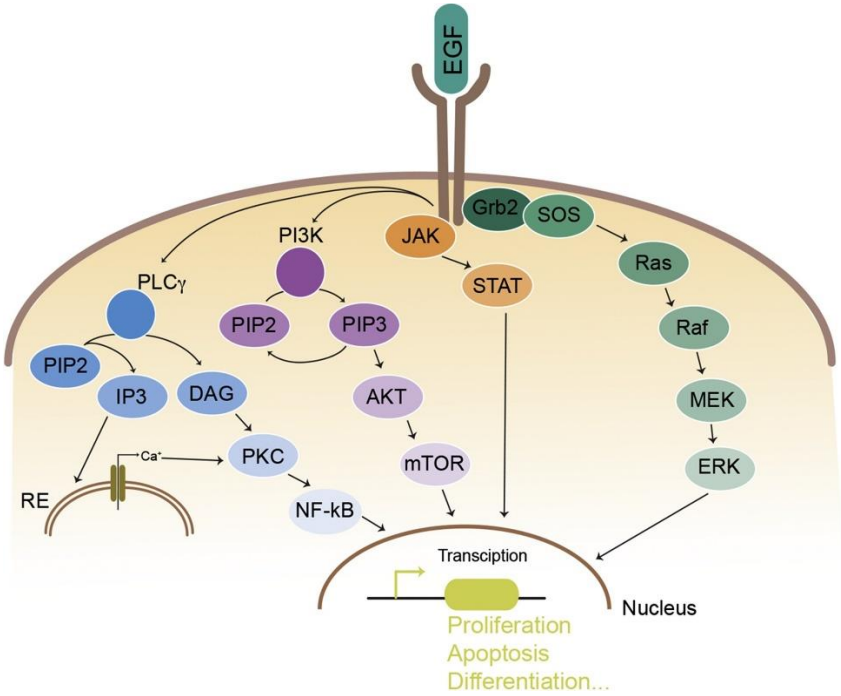


Figure 1: The representative showing of signaling cascades event through EGFR pathway (Barberán & Cebrià, 2019)**.**

Upregulation and/or dysregulation of EGFR signaling is mainly detected in various cancers, such as non-small cell lung cancer (NSCLC), head and neck cancer, colorectal cancer, pancreatic cancer, breast cancer and GBM (Gomez et al., 2013; Wee & Wang,

2017). The aberrant activity of EGFR promotes uncontrolled cell proliferation and evades programmed cell death primarily through overactivated downstream signaling pathways, RAS-RAF-MAPK and AKT-PI3K-mTOR (Wee & Wang, 2017). Under baseline physiological conditions, EGFR molecules are found at $4x10^4$ up to $1x10^5$ per cell. On the other hand, under tumorigenic conditions, cancer cells can express drastically enhanced levels, ranging from $5x10^5$ to $2x10^6$ EGFR molecules/cell. (Gomez et al., 2013). The most detected EGFR mutations are in NSCLC because in 2004, the first identification of point mutations was made in NSCLC (An et al., 2018; Uribe et al., 2021). In addition to EGFR in NSCLC, for a decade, EGFR in GBM has also been a standout studied area because mutations in EGFR are commonly detected in GBM, arising from amplification or rearrangement of the *EGFR* gene (H. Xu et al., 2017; Uribe et al., 2021). *EGFR* is amplified to extremely elevated levels, exceeding 20 copies per cell (Gomez et al., 2013). Overexpression and/or mutations in EGFR endow some traits of cancer, such as cell survival, invasion, cell proliferation, chronic cell cycle progression (particularly via the complex of CDK4/6-cyclin D1), migration, angiogenesis, opposing apoptosis and EMT (Wee & Wang, 2017; H. Xu et al., 2017; Khabibov et al., 2022). The mutant version of EGFR tries to mimic the wt of EGFR activated by a ligand. Even though these mutated EGFRs seem to be enzymatically active, the phosphorylation status is considerably lower than wt EGFR. This suggests that low and insistent kinase activity provokes non-canonical biochemical machinery. Furthermore, these mutations usually escape negative regulatory processes such as receptor endocytosis and degradation, facilitating them to evade cellular mechanisms which normally restrict receptor signaling (Uribe et al., 2021). Roughly 57% of GBM has EGFR variants, including mutations, selective splicing, rearrangements and amplifications (X. Liu et al., 2019). Generally, EGFR mutations are detected within the ECD in GBM, whereas are still scarcely found in ICD. The most frequently observed GBM-related variants are EGFR variant III (EGFRvIII), EGFR variant II (EGFRvII), EGFR variant IV (EGFRvIV), EGFRx and missense mutations. These variants dimerize with EGFR receptors or other ErbB family receptors, HER2. It enhances heterogeneity in GBM, so comprehending their structure is fundamental to strategically targeting them (Ezzati et al., 2024).

EGFRvIII (also known as EGFRΔIII, de2-7EGFR or Δ2-7 EGFR) is the most notable mutant form of EGFR in GBM, which is exclusively detected in cancer cells but not in normal cells (Lemmon & Schlessinger, 2010; Gomez et al., 2013; H. Xu et al., 2017). Roughly 50-60% of GBM cases with amplified wt EGFR also express EGFRvIII (H. Xu et al., 2017; Rabah et al., 2023). EGFRvIII is generated by an in-frame deletion of 801 base pairs (bp) in the DNA sequence, which is responsible for encoding ECD, and it corresponds to the deletion of exons 2 through 7 (lacking residues 6-273) (H. Xu et al., 2017; Pan & Magge, 2020). Since the deletion removes the ligand-binding domain (all of domain I and most of domain II), it gives constitutively ligand-independent activity because of loss of residues 6-273 generating a junction site with a novel glycine residue between amino acids 5 and 274 (Lemmon & Schlessinger, 2010; Arcella et al., 2020; Chagoya et al., 2020; Pan & Magge, 2020). Although there is constitutive tyrosine kinase activity in EGFRvIII, this activity is low-level owing to impaired endocytosis and degradation (Lemmon & Schlessinger, 2010; An et al., 2018). However, this constitutive low-level kinase activity is adequate to affect cancer with enhanced signaling for growth because it has been revealed that EGFRvIII co-expressed with wt EGFR to augment signaling (Wee & Wang, 2017; An et al., 2018). EGFRvIII enables transduction of signals by canonical EGFR pathways maintained by RAS/MAPK, PI3K/AKT and JAK/STAT (An et al., 2018). However, there are still a couple of differences between wt EGFR and EGFRvIII receptors to be considered. To illustrate, wt EGFR has lower PI3K activity than EGFRvIII, whilst in contrast to wt EGFR, EGFRvIII doesn't seem to activate the STAT3 pathway through direct phosphorylation (Figure 2) (Rabah et al., 2023). EGFRvIII activity gives rise to elevated tumor progression, invasion, stemness, evading apoptosis by increased Bcl2 family members, metabolism, angiogenesis, survival, migration and chronic cell cycle proliferation (Wee & Wang, 2017; H. Xu et al., 2017). Since EGFRvIII is specific to cancer, it makes it a highly attractive candidate to seek therapy intervention in GBM (An et al., 2018).

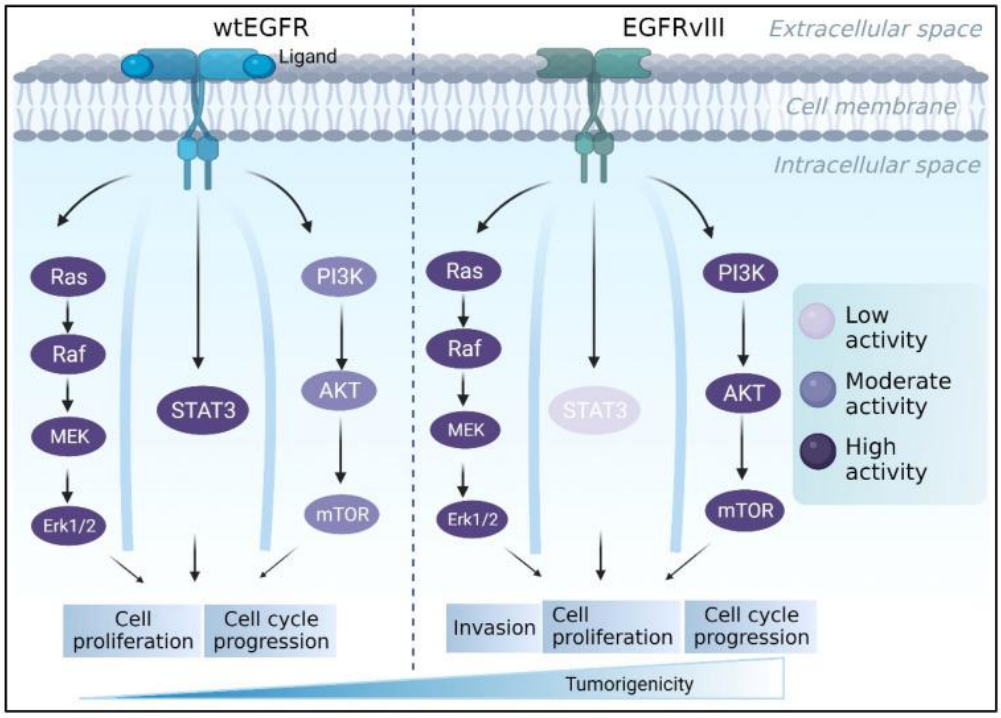


Figure 2: The difference between wild-type EGFR and constitutively active EGFRvIII pathways in GBM progression through downstream of EGFR (Rabah et al., 2023)**.**

Overactivation of EGFR has a pivotal role in cell signaling in several types of cancers. Therefore, EGFR and its downstream signaling have become one of the rational therapeutic approaches in cancer treatment. Small-molecule TKIs and monoclonal antibodies (mAbs) are two valuable approaches as anti-EGFR therapies (Ayati et al., 2020). TKIs are much more convenient than mAbs in anti-EGFR treatments due to oral administration instead of intravenous delivery, lower cardiotoxicity, enhanced BBB penetrance and multiple cellular targets (Iancu et al., 2022). Mechanistically, TKIs contribute to the prevention signal transduction by mimicking ATP so that it binds to the kinase pocket of the receptor to eliminate ATP (Wee & Wang, 2017). In the context of GBM, EGFR TKIs are designed to decrease cell proliferation, trigger apoptosis, impede invasion and hamper angiogenesis (Ezzati et al., 2024). Even though there are many approved kinase inhibitors for different types of cancer, there is still no approved TKI in GBM treatment (Frumento et al., 2024). TKIs are broadly sorted into three generations. 1st-generation EGFR TKIs, gefitinib, erlotinib and lapatinib, are synthesized to reversibly hinder the ATP/substrate-binding pocket of EGFR in the tyrosine kinase domain via orthosteric sites (An et al., 2018). These inhibitors were prepared to target specific mutations in exon 21 (L858R point mutation) and in-frame

deletions in exon 19. Over time, resistance emerged owing to the secondary gatekeeper mutation T790M in NSCLC, which elevates and recovers the affinity of L858R for ATP (Pan & Magge, 2020). Besides mutations, 1st-generation EGFR TKIs showed limited treatment efficiency in clinical trials (X. Liu et al., 2019). Even though these inhibitors are effective and then developed resistance, GBM does not have mutations in exons 19 and 21, so there is a chance that these inhibitors may not have an impact on GBM therapeutic strategies. 2nd-generation EGFR inhibitors, which are afatinib and dacomitinib, are synthesized to irreversibly bind to the tyrosine kinase domain of EGFR and the rest of the ErbB family (An et al., 2018). Although 2nd-generation TKIs demonstrated efficacy against L858R and T790M mutations, these TKIs led to unacceptable low maximum tolerated dose and then finally dose-limiting toxicities, including skin rash, gastrointestinal, diarrhea and mucositis (An et al., 2018; Ayati et al., 2020; Pan & Magge, 2020). Developing resistance to the T790M mutation and poor selectivity between mutant EGFR and wt EGFR led to the generation of a 3rd-generation EGFR inhibitor (Cross et al., 2014). Both 1st- and 2nd-generation EGFR inhibitors failed to improve OS in clinical trials for the cure of GBM with respect to tolerability (X. Liu et al., 2019). Thereby, it has emerged to investigate whether 3rd-generation EGFR inhibitors are efficient or not. This gatekeeper mutation augments the competition between reversible EGFR TKIs and ATP by exerting impacts on both steric impediment and elevated ATP affinity to mutant EGFR, so this led to diminished efficiency of 1st- and 2nd-generation EGFR TKIs (He et al., 2021). 3rd-generation irreversible EGFR TKIs, which are rociletinib, furmonertinib, lazertinib and OSI, are more effective than 1st- and 2nd-generation EGFR inhibitors to overcome the acquired resistance mediated via gatekeeper mutation in NSCLC and brain metastasis (An et al., 2018; He et al., 2021; Cheng et al., 2024). Most of the 3rd-generation EGFR TKIs built on an aminopyrimidine scaffold form a covalent bond with the active thiol group of Cys797 through their electrophilic acrylamide Michael acceptors. These inhibitors act as selective and irreversible inhibitors to target the T790M mutation over wt EGFR (Ayati et al., 2020). To illustrate, one of the advantages of 3rd-generation EGFR inhibitors for GBM is that they have more capacity to penetrate and cross the BBB than first- and second-generation EGFR inhibitors, making the treatment more efficient for GBM by decreased toxicity (Feng et al., 2025). They are improved to

target specific mutations and spare the wt EGFR, so they minimize the off-target effects (Pan & Magge, 2020). Since they are mutant selective and cross the BBB with a better penetration ratio than 1st- and 2nd-generation EGFR inhibitors, they are used at a low dosage which increases the safety and tolerability of usage in the treatment of GBM (Feng et al., 2025). Furthermore, 3rd-generation EGFR TKIs showed better OS and progression-free survival (PFS) than 1st- and 2nd-generation EGFR inhibitors in GBM (Frumento et al., 2024). Among the 3rd-generation EGFR TKIs, their efficacy in GBM is determined by their penetration rate of the BBB. Many experiments revealed that OSI is the most promising candidate in GBM treatment because treatment efficiency in brain tumors basically depends on the capacity of the chemicals to cross the BBB, and P-glycoprotein (P-gp) and breast cancer resistance protein (BCRP) transporters manage to allow blocking the passage of molecules through the BBB. Compared to other 3rd-generation EGFR inhibitors, OSI exhibited the lowest efflux ratio and the weakest transporter substrate, showing high efficacy and mild adverse effects (Ayati et al., 2020; Colclough et al., 2021). Although the T790M mutation is seldom found in GBM, OSI efficiently enables crossing the BBB, making it a promising therapeutic candidate to hamper EGFR overactivity in GBM (An et al., 2018).

1.5.1. Osimertinib

OSI (N-2-{2dimethylaminoethyl-methylamino}-4methoxy-5-{[4-(1-methylindol-3-yl)pyrimidin-2yl]amino}phenyl)prop-2-enamide), also known as AZD9291 and marketed as Tagrisso, is a small molecule which is developed by AstraZeneca Pharmaceuticals. This agent is approved by the FDA and European Medicines Agency (EMA) as a gold standard and first-line therapy for NSCLC patients to hamper mutated T790M EGFR in NSCLC (Dong et al., 2018; Kast et al., 2021; Frumento et al., 2024). Molecular weight of OSI is 499.619 Da, and the mean half-life of OSI is 48.3 hours according to the AURA study (Dong et al., 2018; Grande et al., 2019). OSI is orally taken and is a selective 3rd-generation irreversible EGFR inhibitor that covalently binds to Cys797 on the EGFR kinase domain with T790M to maintain its anti-cancer impact on NSCLC. Also, OSI can hinder the kinase activity of wt EGFR with weaker binding than mutant EGFR (X. Liu et al., 2019). By irreversibly blocking the kinase

pocket, OSI overcomes the increased ATP affinity exerted by T790M and demonstrated approximately 200 times greater potency against T790M and L858R EGFR mutants than wt EGFR (He et al., 2021). It has also been divulged that OSI has fundamental robust clinical activity in CNS metastasis with a higher penetration rate in NSCLC (Frumento et al., 2024). Drug repositioning is one of the preferred approaches to seeking novel available therapeutic strategies for unmet clinical demands (Chen et al., 2021). OSI was proposed to be utilized in GBM treatment for EGFRvIII mutation due to successfully crossing the BBB compared to other EGFR TKIs. Results revealed that OSI impeded EGFRvIII with higher potency via blocking growth in GBM (Kast et al., 2021; Frumento et al., 2024). OSI triggered cell cycle arrest, inhibition of colony formation, migration and invasion *in vivo* and *in vitro* GBM models (Frumento et al., 2024). It is also known that EGFR TKIs are substrates for BBB efflux transporters, which affect the distribution of agents in the brain at equilibrium. In addition, BBB is comprised of endothelial cells which are rich in efflux transporters such as P-gp, BCRP and multidrug resistance proteins (MRP) to contribute to pumping molecules from the brain into the blood. Comparative studies of 16 reversible and irreversible EGFR TKIs revealed that OSI is the most prominent candidate as a therapeutic strategy for GBM. OSI is the weakest substrate of BBB efflux transporters among the other EGFR inhibitors. However, only the detection of the transport efflux ratio does not imply successful brain penetrance, so results are required to be strengthened with the Kpuu (unbound drug accumulation ratio) value, which is a key parameter to determine permeability. They also calculated the Kpuu value, and they observed that OSI has the highest score of Kpuu value for achieving significant BBB penetrance *in vivo*. With the help of desorption electrospray ionization mass spectroscopy (DESI-MS), the results of mouse brain models demonstrated that OSI readily and successfully distributes across tumor tissue and healthy brain (Colclough et al., 2021). There are several factors which elevate crossing the BBB successfully, such as molecular weight below 400-600 Da, being lipophilic and low topological polar surface area (TPSA) (<90 $Å^2$) (Kralj et al., 2023). MW of OSI is 499.619 Da, OSI is lipophilic and showed 87.55 $Å^2$ for low polarity (Bellettato & Scarpa, 2018; Dong et al., 2018; Varrone et al., 2020; Kralj et al., 2023; Attwa et al.,

2025). These traits for BBB penetrance, combined with efficacy and safety, make OSI a good intervention candidate for GBM.

1.6 THE INFLUENCE OF THE ANDROGEN RECEPTOR IN GLIOBLASTOMA

AR, located on the long arm of the X chromosome, is a type of nuclear receptor NR3C4 (nuclear receptor subfamily 3, group C, member 4) and acts as a ligand-dependent transcription factor (Davey & Grossmann, 2016; Kolyvas et al., 2022; Simińska et al., 2022; Fariña-Jerónimo et al., 2024). This gene is comprised of >90 kb pairs and 8 transcripts. The encoded AR protein is found in two isoforms, with MW of roughly 110 kDa and 87 kDa, respectively (Simińska et al., 2022). Structurally, AR consists of three major functional domains: the N-terminal transcriptional regulation domain, the DNA-binding domain and the ligand-binding domain. Among these, the DNA-binding domain, which is composed of two zinc finger motifs, is the most highly conserved, whereas the N-terminal transcriptional regulation domain is the most variable region. These zinc fingers contribute to the direct DNA binding of AR to the promoter of AR-regulated genes, thereby activating the N-terminal and ligand-binding domains to repress or trigger the transcription of these genes. This steroid hormone-activated transcription factor resides in the cytoplasm in an inactive form, binding to heat shock proteins (Michmerhuizen et al., 2020; Zalcman et al., 2021). It is activated by the binding of androgens, primarily dihydrotestosterone (DHT) and testosterone (Fariña-Jerónimo et al., 2024). Also, there are other androgens, including androstenedione, androstenediol and dehydroepiandrosterone, which are less potent than DHT and testosterone. Circulating androgens are expressed at different levels with respect to gender, with higher concentrations observed in males compared to females (Kolyvas et al., 2022). Once AR is released from its chaperone, it translocates to the nucleus, dimerizes and binds to the androgen response elements, allowing the specific activation of the AR in the promoter and promoting the transcription of target genes termed androgen-responsive genes (Davey & Grossmann, 2016; Zalcman et al., 2021; Kolyvas et al., 2022; Fariña-Jerónimo et al., 2024). This results in the transcription initiation, cell survival, proliferation and negative feedback to inactive AR

transcription (Kolyvas et al., 2022). Furthermore, there is an inverse relationship between AR and prostate-specific membrane antigen (PSMA), which is a transmembrane glycoprotein (Batra et al., 2019). Downregulation of PSMA is related to resistance to PSMA-based imaging and therapy while AR expression is upregulated (Sommer et al., 2022).

In addition to a ligand-dependent manner, AR can also be activated via a ligand-independent manner with EGF, IGF-1, cytokines and cAMP-dependent PKA through ERK, PI3K-AKT, mTOR and Wnt-β-catenin signaling pathways (Recchia et al., 2009; Kolyvas et al., 2022). Overall, AR has been involved in various biological actions, including crucial roles in the development and maintenance of cardiovascular, immune, reproductive, musculoskeletal, hemopoietic and neural systems as well as driving cancer such as prostate, liver, kidney, bladder, breast, lung and GBM (Davey & Grossmann, 2016; Michmerhuizen et al., 2020). These AR-dependent pathways stimulate cell growth, proliferation, migration, apoptosis, metastasis, DNA damage repair and cell cycle (Michmerhuizen et al., 2020; Zalcman et al., 2021).

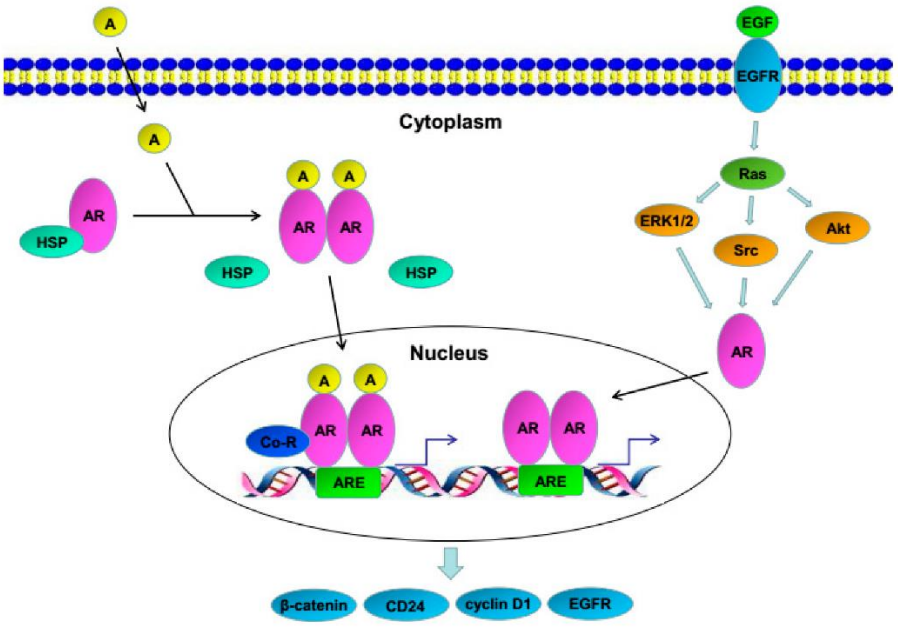


Figure 3: AR signaling through androgen-dependent manner and androgen-independent manner (P. Li et al., 2017).

Approximately a decade ago, it was discovered that the role of AR in GBM (Fariña-Jerónimo et al., 2024). Considering the low level of circulating androgens in the brain

compared to prostate cancer, it is proposed that cell proliferation occurs through AR, being activated in an androgen-independent manner in GBM (Zalcman et al., 2021). Furthermore, higher AR expression is found in GBM than in the normal brain, and there is a relationship between elevated AR expression and increased grade, leading to GBM proliferation, migration and invasion. *In vitro* and *in vivo* studies demonstrated that silencing of *AR* or inhibiting AR resulted in programmed cell death. However, epidemiological data revealed that GBM case is higher in men than in women, which is supported by higher circulating androgen levels in men than in women. Thereby, the higher androgen level in GBM TME, the worse its behavior, making AR activation in an androgen-dependent signaling. Considering the low expression of androgen in the brain, AR activation in GBM is most likely driven in an androgen-independent manner. Importantly, AR activity should be emphasized, rather than AR expression (Fariña-Jerónimo et al., 2024).

Since AR has been extensively studied in prostate cancer, several therapeutic options have been generated to inhibit AR activity, including androgen deprivation therapy (ADT), AR degraders and AR antagonists (J. Huang et al., 2022; Bolek et al., 2024). Even though ADT is a cornerstone treatment approach for prostate cancer, there are severe adverse effects of this treatment, such as bone loss, testosterone depletion, depression, hot flashes, anxiety and sleep disturbance (Gudenkauf et al., 2024). AR degraders, also known as proteolysis-targeting chimeras (PROTACs), promote degradation of AR via the ubiquitin-proteasome pathway (Q.-H. Chen et al., 2024). However, clinical use of AR degraders also showed adverse effects such as elevated blood creatinine, loss of appetite, fatigue, diarrhea and nausea (Petrylak et al., 2024). Furthermore, AR antagonists have been developed to cure prostate cancer and are categorized into 2 groups: 1st- and 2nd-generation AR antagonists. With the help of these chemical agents, AR signaling is blocked by sequestration of itself, thereby preventing nuclear translocation and signaling to AR target genes (Rice et al., 2019). The first-generation AR antagonists -flutamide, nilutamide and bicalutamide- are designed to impede the binding of DHT and testosterone to AR, interrupting androgen-dependent signaling responsible for tumor growth (F. Huang et al., 2025). However, these compounds did not completely block AR activity due to partial agonist activity in cells with high levels of AR (Campodonico et al., 2024). Moreover, first-generation

ones frequently develop drug resistance, which arises from AR amplification, expression of AR splice variants and point mutations, which are ligand-independent signaling (Rice et al., 2019). To overcome these problems, 2nd-generation AR antagonists -apalutamide, darolutamide and ENZ- are being developed. These ones hamper androgen binding to AR by inhibiting nuclear translocation of activated AR and by hindering AR-DNA interactions, ultimately inducing apoptosis (Rice et al., 2019; Danielli et al., 2025). The connection between AR and DNA is blocked even if the AR translocates into the nucleus, silencing the transcription of genes associated with cell proliferation and survival (Danielli et al., 2025). Consequently, inhibition of AR leads to hampering the signaling of cellular proliferation and differentiation of the prostate (Campodonico et al., 2024). In contrast to 1st-generation antagonists, this generation retains antagonistic properties even in the presence of overexpressed AR, so basically, effectiveness and potency have been improved with 2nd-generation AR antagonists that remain the standard of care for castration-resistant prostate cancer (CRPC). Additionally, they elevated the specificity toward AR over other steroidal receptors, resulting in higher affinity than the 1st-generation ones and reduced risk of androgen withdrawal phenomena. This generation also prolongs the lifespan, metastasis-free OS and declined circulating and intratumoral androgen concentrations as well as serum prostate-specific antigen (PSA) levels (Rice et al., 2019). Among them, ENZ is the first 2nd-generation and most widely utilized 2nd-generation AR antagonist for prostate cancer treatment (Campodonico et al., 2024). Based on the results from AFFIRM, PREVAIL, PROSPER and ARCHES clinical trials, ENZ is the only 2nd-generation AR antagonist approved for metastatic CRPC (mCRPC), non-metastatic CRPC (nmCRPC) and metastatic hormone-sensitive prostate cancer (mHSPC). In addition, ENZ significantly elevated the OS of the patient diagnosed with prostate cancer by reducing mortality and postponing the initiation of chemotherapy (Scher et al., 2012; Beer et al., 2014; Armstrong et al., 2019; Sternberg et al., 2020). On the other hand, apalutamide and darolutamide are currently utilized for patients diagnosed with nmCRPC and mHSPC, not mCRPC (Bolek et al., 2024; Rifaldi et al., 2025). ENZ and apalutamide are not influenced by mild or moderate renal impairment, but darolutamide is. Darolutamide is specifically designed to diminish the risk of penetration of the CNS, causing seizures (Zurth et al., 2019). ENZ has the highest

capacity of penetration of the BBB among 2nd-generation AR antagonists, resulting in seizures. However, it's shown that the reported incidence is low, <1% (Campodonico et al., 2024). Since ENZ has the capacity to cross the BBB, it has been proposed that ENZ could be a therapeutic candidate for GBM treatment to block the overexpression of AR (N. Zhao et al., 2021).

1.6.1. Enzalutamide

ENZ, also known as MDV3100 and XTANDI, is the first FDA-approved 2nd-generation AR antagonist for prostate cancer treatment, authorized in 2012 (Rice et al., 2019). This agent is structurally relevant to bicalutamide, whereas it has 5- to 8-fold higher binding affinity for AR than bicalutamide, merely slightly lower affinity than DHT (Rice et al., 2019; Bolek et al., 2024). ENZ is a diarylthiohydantoin compound that also functions as a pure AR antagonist, hampering growth and promoting apoptosis. This agent impedes the competitive binding of androgen to the AR, the nuclear translocation of AR and DNA binding of androgen response elements and co-activator recruitment (Bolek et al., 2024). This compound is readily absorbed and can be orally administered with or without food (Gibbons et al., 2015). The half-life of ENZ is 5.8 days, and the molecular weight of ENZ is 464.44 Da (Gibbons et al., 2015; Dhillon et al., 2024). ENZ is a small molecule, and its solubility isn't influenced by pH over the physiological range. ENZ displays restricted aqueous solubility and isn't a substrate for P-gp (Rifaldi et al., 2025). ENZ is also known for binding weakly to GABAA receptors, which may induce seizure risk (Bolek et al., 2024). Although there is a chance of induction of seizures due to crossing the BBB, the rate is low, and it's thought that ENZ could be a potential therapy approach for GBM (N. Zhao et al., 2021; Campodonico et al., 2024). The reasons why ENZ is a good candidate are favorable MW, not being a substrate of P-gp, being lipophilic and low TPSA (76.44 Å) (Dhillon et al., 2024). It's shown that *in vitro* and *in vivo* studies ENZ declined cell proliferation, suppressed glioma stem cells, triggered apoptosis and cell cycle arrest in both TMZ-resistant and TMZ-sensitive GBM cell lines (Zalcman et al., 2018; N. Zhao et al., 2021; Chang et al., 2022). Recent investigations into crossing the BBB with ENZ and its impact on signaling pathways further support its promise as a GBM treatment candidate.

1.7 THE DUAL TARGETING OF EGFR AND AR IN CANCER THERAPY

Studies have unveiled that crosstalk between growth factor receptors and nuclear hormone receptors brings about the activation of nuclear receptor-mediated transcription (IZUMI et al., 2012). In normal prostate epithelial cells, EGFR is downregulated by androgens, but this regulation is lost in prostate cancer. The disruption of EGFR regulation changed signaling, leading to the transition of prostate cancer from an androgen-dependent to an androgen-independent state. Notably, regulation of uncontrolled growth without androgen stimulation is mediated through the interaction between EGFR and AR (Y. Hu et al., 2009). Thereby, it has been found that, in prostate cancer, *EGFR* and *ERBB2* expressions are upregulated by AR signaling, while activation of EGFR and ErbB2 maintains AR functions, promoting AR transactivation (Zheng et al., 2011; IZUMI et al., 2012). Furthermore, EGFR expression can be increased by androgens, contributing to activation of AKT and ERK. The recurrence of prostate cancer following hormone treatment is thought to be derived from amplification of AR signaling via EGFR signaling, indicating the existence of a positive regulation loop between EGFR and AR in prostate cancer (HSIEH et al., 2013). In prostate cancer, a co-immunoprecipitation experiment showed that EGF ligand contributes to AR transactivation through MAPK to TIF2/GRIP1 and PI3K/AKT to elevate expression of some transcriptional co-factors (Gregory et al., 2004; Zheng et al., 2011). This EGFR-AR crosstalk has also been investigated in breast cancer and bladder cancer (Zheng et al., 2011). In bladder cancer, in the presence of AR and under castration androgen level, cell proliferation, invasion and migration have been detected through EGFR signaling, MAPK and PI3K/AKT. These findings highlight the potential of combinational therapeutic approaches against crosstalk between EGFR and AR to obstruct growth and stimulate apoptosis in cancer (Y. Hu et al., 2009; IZUMI et al., 2012; HSIEH et al., 2013). Approximately a decade ago, the crosstalk between EGFR and AR was also discovered in GBM. Thereby, as a new therapeutic approach for EGFR and AR, it has been focused on targeting EGFR and AR in GBM, correlating with RNA sequencing of The Cancer Genome Atlas (TCGA) (Zalcman et al., 2021; Dewdney et al., 2023; Fariña-Jerónimo et al., 2024). In GBM,

AR activation is also androgen-independent manner through EGFR signaling. Expression of AR varies across the tumor regions, showing higher protein expressions in the tumor periphery and peritumoral areas as well as stronger protein localization in CD133+ cells, suggesting a potential role in glioma stem cells (Dewdney et al., 2023). To find alternative treatment options for TMZ-sensitive and TMZ-resistant GBM cell lines, instead of TMZ treatment, co-treatment of erlotinib and ENZ or cetuximab and ENZ was evaluated and did not yield an effective impact on cancer. However, a combination of ENZ and afatinib was administered in EGFR and EGFRvIII-overexpressing cells and showed synergistic and additive effects. It was noted that EGFR or EGFRvIII upregulation stimulates overexpression of AR and nuclear translocation in GBM (Zalcman et al., 2021). However, due to the lethal dosage of afatinib, it did not proceed to a clinical trial. As an emerging treatment direction in GBM, targeting the EGFR and AR axis requires exploration in detail with more effective combination strategies and safer doses.

1.8 EPITHELIAL-MESENCHYMAL TRANSITION

EMT is a dynamic cellular process which is vital for embryogenesis, wound healing and malignant progression. Under physiological conditions, cells which form epithelial sheets in several distinct tissues of the body exhibit apical-basal polarity and are held together laterally via tight junctions, gap junctions, desmosomes and adherens junctions, which are made by cell surface epithelial cadherin (E-cadherin). This structural organization is significant for maintaining the integrity of epithelia. In the early stages of cancer, cells typically exhibit epithelial-like features and then gradually obtain mesenchymal characteristics. Throughout EMT, expressions of E-cadherin and specific cytokeratins are downregulated, leading to the detachment of epithelial cells from one another and from the basement membrane, as well as the loss of the typical morphology of epithelial cells. Once epithelial cells lose their cobblestone morphology, extracellular matrix (ECM) is reorganized and a new reversible cellular program is activated to trigger mesenchymal fate, appearing as a spindle-shaped morphology. Markers related to mesenchymal state are expressed, such as neural cadherin (N-cadherin), fibronectin, vimentin, β1 and β3 integrins. EMT is maintained

by a network of EMT-inducing transcription factors (TFs), which cooperate in several combinations to activate the expression of genes that are relevant to mesenchymal fate and suppress the expression of genes governing the epithelial phenotype. These TFs are SNAIL, SLUG, ZEB, ZEB2, TWIST1 and TWIST2. This mesenchymal state can also revert to the epithelial state through a reverse process referred as mesenchymal-epithelial transition (MET). EMT cellular process is divided into three distinct types: type I EMT, associated with embryonic development, such as activation of neural crest and formation of mesoderm during gastrulation; type II EMT, involved in wound healing and tissue regeneration; type III, which takes place throughout carcinoma progression (Dongre & Weinberg, 2019).

In the context of cancer progression, EMT, which is orchestrated by EMT TFs, is a key process that causes invasion, metastasis, resistance to various therapeutic regimens, evasion of apoptosis, ECM degradation and acquisition of stem cell-like characteristics (Dongre & Weinberg, 2019; Xia, 2026). Accordingly, EMT-related markers can be utilized as crucial histopathological indicators of high-grade malignancy. In cancer, EMT activation scarcely occurs autonomously. Signaling from tumor-associated reactive stroma has a role in cancer, such as stimulating EMT TFs. Tumor-associated fibroblasts and macrophages within the stroma lead to paracrine and juxtacrine signaling to trigger EMT in several types of adjacent tumor cells. Cancer cells express EMT-associated markers and sustain the activities of many components of the stroma to form TME together. In addition, cells that undergo EMT also have ability to control anti-tumor immunity. Mesenchymal cells exhibit augmented resistance to eradication by adaptive immune cells, which are generally present in tumor-associated stroma. Interestingly, invading cells are frequently found in clusters rather than as single cells. It has been revealed that these clusters are promoted by E-cadherin expressions, which paradoxically contradict the canonical EMT program, which involves repression of E-cadherin. Some reports demonstrated that normal and cancer epithelial cells, which activate EMT, rarely achieve a fully mesenchymal state. Instead, these clusters undergo partial EMT, characterized by a mixture of partially epithelial and partially mesenchymal state (Dongre & Weinberg, 2019). For a long time, it was considered that EMT is a strictly bidirectional cellular process. However, nowadays it has been envisaged that an intermediate phase called partial EMT. This

phase is identified as an incomplete loss of epithelial markers and an incomplete gain of mesenchymal markers. Partial EMT also shows intro-tumoral heterogeneity and epithelial-mesenchymal plasticity, coexisting with both fully epithelial and mesenchymal states (Figure 4). In skin and mammary primary cancer cells, early, intermediate and late partial EMT states can be determined by surface proteins, CD106, CD61 and CD51 (Aggarwal et al., 2021). Also, to distinguish between fully EMT and partial EMT, CD44 and epithelial cell adhesion molecule (EpCAM) can be determined, $CD44^{high}EpCAM^{high}$ indicating partial EMT and $CD44^{high}EpCAM^{low}$ corresponding to full EMT (Yamamoto et al., 2017). The crosstalk between partial EMT and acidic TME gives rise to the activation of paracrine signaling that induces tumor progression. Partial EMT is regulated through ECM-associated factors, fibronectin, collagen and laminins (Aggarwal et al., 2021). Partial EMT has been observed in lung, breast, colorectal, pancreatic cancers, oral squamous cell carcinoma and NSCLC as well as GBM (Aggarwal et al., 2021; Mondal et al., 2025). Transforming growth factor β (TGF-β) is the key factor that leads to the induction of EMT across various types of tissues. TGF-β binds to complexes of TGF-β receptor type I (TGF-βRI) and TGF-β receptor type II (TGF-βRII), contributing to SMAD2 and SMAD3 phosphorylation to form complexes with SMAD4. Similarly, activation of SMAD1 and SMAD5 leads to a complex with SMAD5. When formed, these SMAD complexes translocate to the nucleus, functioning as TFs to regulate expression of genes responsible for mesenchymal state, motility, cell proliferation, invasion, angiogenesis, programmed cell death and senescence. These signaling pathways interact with multiple signaling pathways such as ERK, PI3K-AKT, p38 MAPK and RHO-like GTPases, reinforcing EMT activation. Within the context of neoplasia, TGF-β induces the acquisition of a mesenchymal state and triggers invasion and metastasis. The TGF-β signaling pathway contributes to EMT activation in many ways. SMAD complexes induced by TGF-β transcriptionally activate mesenchymal-related genes, such as fibronectin and vimentin and upregulate EMT TFs that suppress E-cadherin. EMT TFs further overexpress expression of the TGF-β ligands, contributing to autocrine signaling that facilitates a positive feedback loop. Basically, once they are activated, they help cells to sustain the expression of the EMT process. Moreover, once mitogenic growth factors bind to mitogenic growth factor receptors

and induce dimerization of receptors, followed by activation of tyrosine kinases, these steps contribute to the activation of ERK, PI3K-AKT, JNK and p38 MAPK signaling cascades, triggering EMT-associated cell proliferation, migration and motility (Dongre & Weinberg, 2019).

EMT confers plasticity, tumor initiation, metastasis and resistance to treatment, making it a fundamental mechanism in the disease pathophysiology. E-cadherin expressions are detectable in normal brain tissue, LGG and HGG, reflecting a unique EMT pattern distinct from epithelial cancers. Unlike epithelial cancers, GBM doesn't exhibit prominent epithelial markers, such as E-cadherin, and it showed a more plastic and heterogeneous phenotype, which contributes to the transition to a mesenchymal-like state (Xia, 2026).

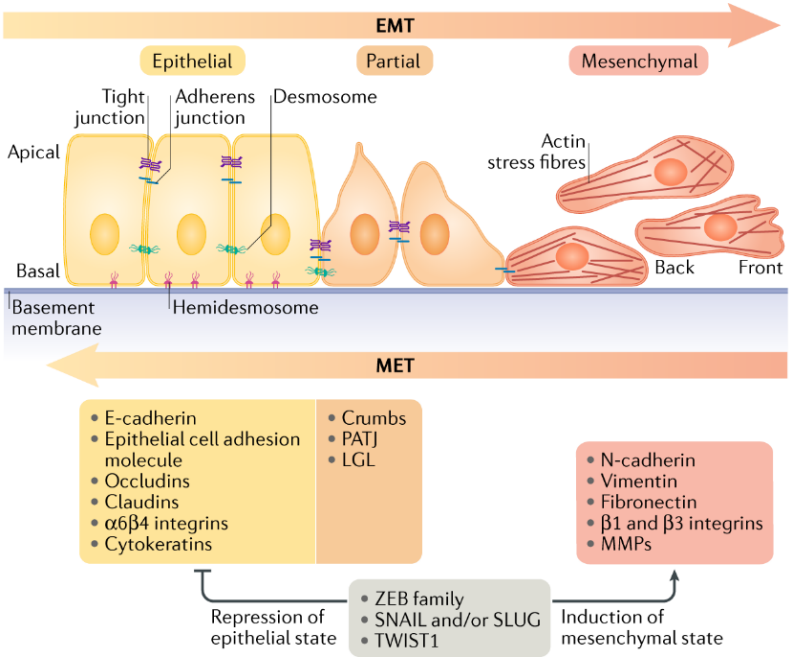


Figure 4: Summary of EMT, partial EMT and MET with crucial markers (Dongre & Weinberg, 2019).

1.9 APOPTOSIS

Apoptosis is a meticulously fundamental programmed cell death that governs the balance between cell survival and death (Valdés-Rives et al., 2017; Mustafa et al., 2024). Apoptosis is a key mechanism that facilitates the development of embryonic, maintains tissue homeostasis and contributes to immunological functioning (Mustafa et al., 2024). Morphologically, apoptosis is distinguished by cell shrinkage and

chromatin condensation, followed by the formation of small membrane-bound apoptotic bodies that are subsequently phagocytosed and removed by immune cells, such as macrophages, resulting in no inflammation and tissue damage (Park et al., 2023; Eskander et al., 2025). Cells initiate the activation of apoptosis because they become irreparably damaged and cannot recover from repair. This apoptosis mechanism is primarily maintained by proteases of the caspase family (Valdés-Rives et al., 2017; Mustafa et al., 2024). The caspase family is subdivided into two classes: initiator (caspase-8 and caspase-9) and executioner (caspase-3, caspase-6 and caspase-7). Caspases are found in an inactive form, and once they are activated, they participate in intrinsic and extrinsic signaling pathways, which finally converge on executing the programmed cell death. Depending on the stimulus that allows activation of apoptosis, the intrinsic or extrinsic signaling pathway is induced (Mustafa et al., 2024).

The intrinsic (mitochondrial) pathway occurs within the mitochondria and can be promoted by intracellular stressors such as oxidative stress, hypoxia, viral infections, DNA damage, toxins, and DNA and/or mitochondrial damage, leading to mitochondrial outer membrane permeabilization (MOMP) (Valdés-Rives et al., 2017; Park et al., 2023; Gao et al., 2024; Eskander et al., 2025). Intrinsic pathway is controlled by the Bcl-2 family, which includes pro-apoptotic proteins (Bax, Bok & Bak), anti-apoptotic proteins (Bcl-2, Mcl-1 &Bcl-x_L) and BH3-only proteins (Bid, Bik, Bad & Bim) (Park et al., 2023; Eskander et al., 2025). Upon exposure to cytotoxic stimuli, the activation of pro-apoptotic BH3-only proteins hampers anti-apoptotic proteins, promoting the release of cytochrome c and second mitochondria-derived activator of caspase (Smac) from mitochondria into the cytosol via Bax and Bak proteins (Valdés-Rives et al., 2017; Park et al., 2023). Released cytochrome c forms a complex with apoptotic protease activating factor-1 (APAF1) called apoptosome, which activates initiator caspase, pro-caspase-9 (Valdés-Rives et al., 2017; Gao et al., 2024). This cleaved caspase-9 brings about activation of executioner caspases, which are caspase-3 and caspase-7, in turn having an impact on apoptosis through cleavage of enzymes, which are critical in DNA repair, such as PARP, triggering the apoptosis (Figure 5) (Valdés-Rives et al., 2017; Malone et al., 2025).

The extrinsic pathway is stimulated from outside the cell by extracellular ligands, such as tumor necrosis factor (TNF)-α and Fas ligand (FasL), activating cell surface death

receptors - TNF and Fas receptors. After binding to the death receptors, it contributes to the generation of the death-inducing signaling complex (DISC), giving rise to recruitment of initiator caspases, including pro-caspase-8 and caspase-10 (Valdés-Rives et al., 2017; Park et al., 2023). Activation of initiator caspases cleaves and activates executioner caspases, caspase-3, caspase-6 and caspase-7, to carry out proteolytic cleavage and then induce apoptosis (Figure 5) (Park et al., 2023; Gao et al., 2024).

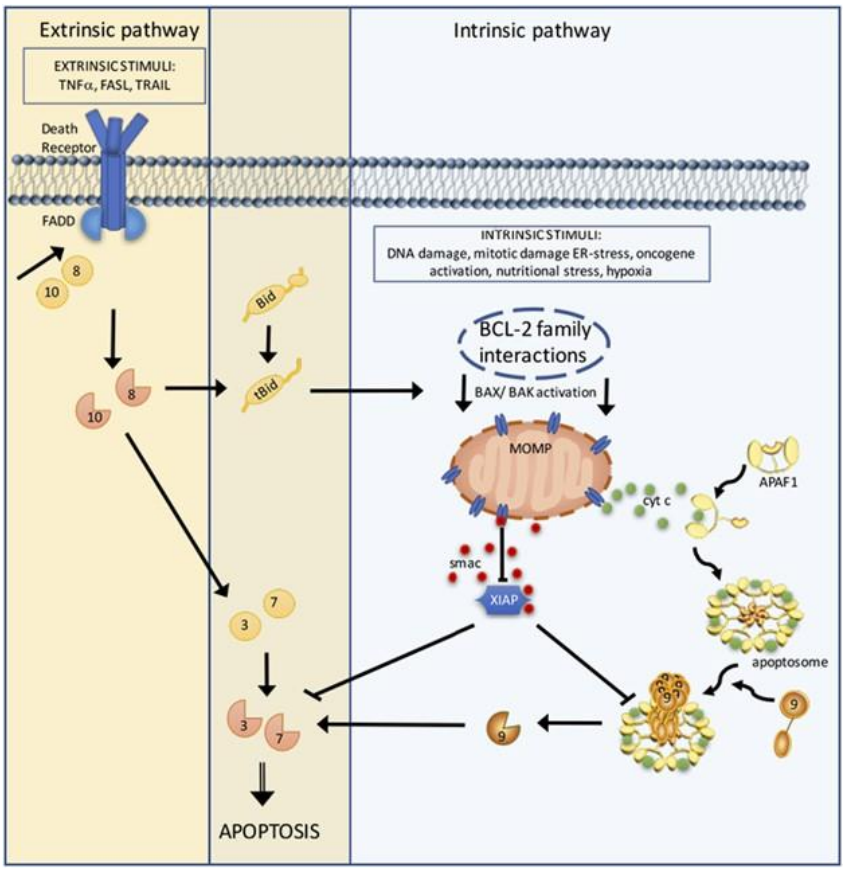


Figure 5: Overview of intrinsic and extrinsic apoptotic pathways under physiological conditions (Kalkavan & Green, 2018)**.**

Deregulation of apoptosis gives rise to developing disorders such as hepatic, renal, cardiovascular, neurological conditions, as well as cancer, which leads to evading apoptosis (Vitale et al., 2023; Malone et al., 2025). The dysregulation of PI3K-AKT pathway contributes crucial chances to mitochondrial apoptotic members in many cancers, resulting in resistance to apoptotic stimuli (Malone et al., 2025). It has been published that PI3K-AKT pathway is deregulated in roughly 80% of GBM incidence,

primarily due to overexpression of EGFRvIII and loss of PTEN (Valdés-Rives et al., 2017). It has been reported that when PTEN is re-introduced, it contributes to reduction in cell viability and proliferation in many cell lines of GBM. BAD protein, BH3-only protein, is phosphorylated and inhibited by AKT, releasing Bcl-2 and Bcl-x_L to hinder apoptosis. In addition, pro-caspase-9 is phosphorylated and impeded by AKT. The interaction between astrocyte and GBM through gap junctions enhances NF-κB, MAPK and JAK-STAT signaling, leading to reduced Bax while elevating expression of Bcl-2. It has been found that overexpression of EGFRvIII has been associated with augmented expression of anti-apoptotic proteins (Malone et al., 2025). Furthermore, downregulation of cleaved caspase-8 correlates with aggressive phenotype and worse OS. Low levels of activated caspase-8 and FADD are detected in GBM compared to heathy brain, resulting in increased cell proliferation and inhibited apoptosis (Malone et al., 2025). Overall, GBM exhibits deregulation in apoptosis which causes resistance to anti-tumor agents and radiotherapy that maintains apoptosis. Therefore, it is required to search novel effective treatments for GBM against pro-survival mechanism (Valdés-Rives et al., 2017).

In this study, it was aimed to investigate the dual inhibition of EGFR and AR via OSI and ENZ in LN18 and U87 as well as human microglial cell line, HMC3 through cell cycle arrest, EMT and apoptosis. This combination could be treatment approach for GBM.

2. MATERIALS AND METHODS

2.1 CELL LINES

Two adherent GBM cell lines, LN18 and U87 were provided from the American Type Culture Collection (ATCC, USA) (https://www.atcc.org/). HMC3, healthy cell line, was received as a generous gift from Assoc. Prof. Dr. Timuçin Avşar's laboratory (Bahçeşehir University, Turkey) LN18 cells (ATCC number: CRL-2610) are one of the poorly differentiated cell lines derived from right temporal lobe glioma and have a p53 mutation and wt PTEN. They are negative for glial fibrillary acidic proteins while they show deletions in *p16* and *p14ARF* tumor suppressor genes. U87 cells (ATCC number: HTB-14) are characterized as aggressive, adherent cells that are PTEN-mutated and express wt *TP53*. This cell line is hypoploid, possessing a chromosome number of 44. HMC3 cell line (ATCC number: CRL3304) is a microglial cell and immortalized.

2.2 CELL CULTURE

2.2.1. Cell Thawing

2 mL cryovial tubes (Biosigma, Italy) containing GBM cell lines, HMC3, LN18 and U87, were taken out from the -80°C freezer (Haier, Qingdao, China). The frozen cells preserved in the freezing medium consisting of 90% Fetal Bovine Serum (FBS) (Gibco, USA) and 10% Dimethyl sulfoxide (DMSO) (Riedel-De-Haën, Germany) were partially thawed by a warm hand when 1 mL of DMEM (Gibco, USA) with 10% FBS and 1% Penicillin/Streptomycin (Pen/Strep) (10,000 units/mL penicillin and 10,000 µg/mL streptomycin) (Gibco, USA) was added into cryovial tube. The mixture of cells, complete DMEM and freezing medium were put in a 15 mL conical tube (Jet Biofil, China) and centrifuged at 2,500 rpm for 5 minutes (Centrifuge Z 206 A) (Hermle, Germany). The supernatant was carefully eliminated, and the pellet was resuspended in 1 mL DMEM supplemented with 10% FBS and 1% Pen/Strep (10,000 units/mL penicillin and 10,000 µg/mL streptomycin) (Gibco, USA). 3 mL complete DMEM and 1 mL cell suspension were spilt into the T25 culture flask (Jet Biofil,

China). Cells were checked under the inverted microscope (ECLIPSE TS100) (Nikon, Japan) and incubated in an incubator (BINDER, Germany) maintained at 37°C with 5% CO_2.

2.2.2. Cell Freezing

Approximately $4.5x10^5$ cells/cryovial was centrifuged in a 15 mL conical tube (Jet Biofil, China) at 2,500 rpm for 5 minutes (Centrifuge Z 206 A) (Hermle, Germany) for freezing. Thereafter centrifugation, the supernatant was discarded, and the cell pellet was pipetted with a freezing medium composed of 90% FBS (Gibco, USA) and 10% DMSO (Riedel-De-Haën, Germany) within the same conical tube. This mixture was transferred directly to the 2 mL cryovial (Biosigma, Italy) and kept at -80°C freezer (Haier, Qingdao, China) as a stock.

2.2.3. Passaging

HMC3 cell line and GBM cells underwent passage when the confluency reached 80% or higher. The existing medium in the T25 flask (Jet Biofil, China) was removed, and the flask was rinsed with 1X PBS (EcoTech, Turkey) once (2- or 3-times if required). Once the PBS was got rid of, 1 mL 1X 0.25% trypsin-EDTA (ethylenediaminetetraacetic acid) (Gibco, USA) was added to the flasks and allowed to detach the cells from the flasks for 2-4 min in the incubator. When the time was up, the cells were observed under the inverted light microscope (ECLIPSE TS100) (Nikon, Japan) to determine whether the cells were dissociated from the flask surface. If detachment wasn't achieved adequately, the mechanical disaggregation was performed gently. Afterwards, trypsin activation was ceased by complete DMEM in a 1:1 ratio. All cell suspension was taken and transferred to the 15 mL conical tube (Jet Biofil, China) for centrifugation at 2,500 rpm for 5 min (Centrifuge Z 206 A) (Hermle, Germany). Complete DMEM was added to the flask to cover the surface of the flask for adherent cells. The supernatant was discarded, and the pellet was resuspended in DMEM by pipetting according to the amount of pellet. 10 µL of cell suspension was taken from the 15 mL conical tube and placed onto the hemocytometer (Isolab, Germany) to count the number of cells under the inverted microscope (ECLIPSE TS100) (Nikon, Japan). At least three sets were counted under the inverted microscope

to obtain an average number of cells. According to the requirements of experiments, freezing and main stock, cells were calculated and seeded into T25 flasks, plates, Petri dishes and cryovials.

2.3 DRUG PREPARATION

1 mg of OSI (AZD 9291) (MW: 499.6) (Cayman Chemical, USA) was dissolved in sterile 400.32 µL DMSO (Riedel-De-Haën, Germany) to make a final stock concentration of 5 mM.

25 mg of ENZ (MDV 3100) (MW: 464.4) (Cayman Chemical, USA) was dissolved in sterile 5382 µL DMSO (Riedel-De-Haën, Germany) to acquire 10 mM final stock concentration.

2.4 CELL VIABILITY ASSAY

LN18, U87 and HMC3 cells were passaged and counted using a Neubauer hemocytometer (Isolab, Germany). Based on the counting, $7.5x10^3$ cells/well for 12 & 24 h, $5x10^3$ cells/well for 48 h and $3x10^3$ cells/well for 72 h were seeded from LN18 cell line respectively into a 96-well plate (Jet Biofil, China) while for U87 cell line $5x10^3$ cells/well for 12 & 24 h, $2.5x10^3$ cells/well for 48 h and $1.5x10^3$ cells/well for 72 h were seeded into a 96-well plate for cell viability assay. A total of $7.5x10^3$ HMC3 cells were seeded per 96-well plates for 12- and 24-hour time points. $3.5x10^3$ cells/well were counted for 48 h while for 72 h, $2.5x10^3$ HMC3 cells per well were seeded in 96-well plates. After 24 h incubation in the humidified incubator, cells were administered with OSI (Cayman Chemical, USA) and/or ENZ (Cayman Chemical, USA) with respect to different desired concentrations. After 12, 24, 48 and 72 h incubations 10 µL MTT (3-(4,5-Dimethylthiazol-2-yl)-2,5-Diphenyltetrazolium Bromide) reagent (BioBasic, Canada) was added to each well and the plate was incubated for 4-6 h in the incubator at 37°C with 5% CO_2 for formazan crystal formation. At the end of the incubation, the medium was cautiously discarded, leaving the formazan crystal intact, and 100 µL DMSO (Riedel-De-Haën, Germany) was given to each well for

solubilization of insoluble formazan crystals. The 96-well plate was incubated in the dark for 15 min, and then the density was gauged at 570 nm under favour of a spectrophotometer (Multiskan FC 357) (Thermo Fisher, USA).

2.5 HUMAN ADENOSINE TRIPHOSPHATE (ATP) ELISA ASSAY

For LN18 and U87 cell lines, $2.5x10^6$ and $2x10^6$ cells, respectively, were seeded into 6-well plates (Jet Biofil, China). After 24 h, GBM were exposed to desired doses of OSI and ENZ. Following 24 h of treatment, the 6-well plates were kept at -80°C with 1 mL of 1X PBS per well until the human ATP ELISA Kit (BT-Lab, China) was utilized. Prior to the assay, all reagents and samples were equilibrated to RT. Cellular disruption was done through freeze-thaw cycles, at least 3 times, to release the inside components. After thawing, the resulting lysates were transferred to 1.5 mL microcentrifuge tubes (Isolab, Germany) and centrifuged at 2,500 rpm for 20 min (Centrifuge 5424 R) (Eppendorf, Germany). After centrifuging, the supernatant without sediment was transferred into new 1.5 mL microcentrifuge tubes. One microcentrifuge tube was prepared with 120 µL of the standard (6400 nmol/L) and 120 µL of standard diluent for making a 3200 nmol/L standard stock solution. By the help of serial dilution, standard points were generated as 1600 nmol/L, 800 nmol/L, 400 nmol/L, 200 nmol/L and 0 nmol/L, which is zero standard (blank). Two repeats were done for each condition. 50 µL of each standard point was added per well according to their conditions, while 40 µL of each sample and 10 µL anti-ATP antibody (only into sample wells) were added per well for samples. Subsequently, 50 µL of streptavidin-HRP was added to the sample and standard point wells, except blank wells. The plate was covered with aluminum foil and incubated at 37°C for 1 h. Liquid from the wells was removed onto a paper towel, and the plate was rinsed five times with 300 µL of 1X wash buffer, allowing one minute per wash. Then, 50 µL of Solution A and 50 µL of Solution B were added into each well, and the plate was covered with aluminum foil for incubation at 37°C for 10 min. Following 10 min incubation, the reaction was ceased by adding 50 µL Stop Solution into each well, observing the change in color from blue to yellow immediately. After adding the stop solution into each well, 10 min later, read the samples at 450 nanometer (nm) using a

microplate reader (Multiskan FC 357) (Thermo Fisher, USA). Data analysis was done via MyAssays software.

2.6 TRYPAN BLUE EXCLUSION ASSAY

$4.5x10^4$ LN18 cells/well and $5.5x10^4$ HMC3 cells/well were seeded in 6-well plates while $2.5x10^4$ U87 cells/well were seeded in 6-well plates. After 24 h incubation, the cells were treated with OSI or/and ENZ. Following incubation periods of 24, 48 and 72 h, the medium from wells was collected into 1.5 mL microcentrifuge tubes (Isolab, Germany) and centrifuged at 13,200 rpm for 1 min (Centrifuge 5424 R) (Eppendorf, Germany). The supernatant was eliminated whilst the remaining cells were rinsed with 750 µL 1X PBS (EcoTech, Turkey) and centrifuged at 13,200 rpm for 1 min. The cells were trypsinized with 0.5 mL trypsin-EDTA (0.25%) (Gibco, USA), and trypsin activity was ceased by 0.5 mL complete DMEM while the supernatant was removed. The detached cells were collected and centrifuged at 13,200 rpm for 1 min, and then the supernatant was eradicated. The pellet was resuspended in a complete medium mixed with 0.4% trypan blue solution (EcoTech, Turkey) (1:1 ratio). 10 µL cell suspension per condition was put in a Neubauer hemocytometer (Isolab, Germany) and counted under the inverted light microscope (ECLIPSE TS100) (Nikon, Japan).

2.7 FLUORESCENCE STAININGS

2.8.1. Propidium Iodide (PI) Staining

HMC3, LN18 and U87 cells were respectively seeded at the density of $7.5x10^3$, $7.5x10^3$ and $3x10^3$ in each well of a 96-well plate (Jet Biofil, China). Following 24 h, they were administered by OSI and/or ENZ. After 24 h treatment incubation, the medium with drugs was removed, and a medium including 1 mg/mL PI dye (Sigma-Aldrich, USA) (PI: medium ratio was 1 µL:1000 µL) was given to each well as 100 µL. The cells were incubated in the incubator at 37°C for 15 min. After incubation was completed, they were examined under the fluorescence microscope (Carl Zeiss Microscopy, Axio Observer 5 Colibri 7, Germany) with respect to excitation/emission (ex/em): 535/617 nm. The number of dead cells was counted, and the graph was made

via GraphPad Prism software version 8.0 for Windows (GraphPad Software, Boston, Massachusetts, USA, www.graphpad.com).

2.8.2. 4',6-Diamidino-2-phenylindole (DAPI) Staining

$3x10^3$ cells/well, $7.5x10^3$ and $7.5x10^3$ cells/well were seeded for U87, LN18 and HMC3 respectively into 96-well plates (Jet Biofil, China), and then the cells were exposed to the required dosages of OSI and ENZ for 24 h. After the treatment period, the medium was removed, and a mixture of 5 mg/mL DAPI stain (Thermo Fisher, USA) supplemented with DMEM (ratio was 1 µL DAPI: 1000 µL complete medium) was added to each well. They were left for incubation in the incubator for 15 min and then were examined under the fluorescence microscope (Carl Zeiss Microscopy, Axio Observer 5 Colibri 7, Germany) (ex/em: 359/461 nm).

2.8.3. 3,3'-Dihexyloxacarbocynanine Iodide ($DiOC_6$) Staining

The cells were counted and seeded at a density of $7.5x10^3$ for HMC3 cells, $3x10^3$ cells for U87, and $7.5x10^3$ cells for LN18 into each well of a 96-well plate (Jet Biofil, China). Following 24 h, they were exposed to OSI and/or ENZ for 24 h treatment. After completion of 24 h treatment, the drug-containing medium was got rid of, and the cells were dyed with 4 nM $DiOC_6$ (Thermo Fisher, USA) prepared in complete medium (1:1000 ratio) to incubate in the incubator for 15 min. After the incubation step, they were investigated by the help of a fluorescence microscope (Carl Zeiss Microscopy, Axio Observer 5 Colibri 7, Germany) at ex/em: 482/504 wavelength.

2.8 CLONOGENIC ASSAY

A density of $1.5x10^4$ cells/well for LN18 and $2.5x10^3$ cells/well for U87 was seeded into 6-well plates. Following 24 h incubation, the cells were exposed to drugs which were OSI and ENZ. After 24 h of treatment, the medium was discarded, and GBM cells were rinsed with 1X PBS. A fresh complete DMEM was added to each well and the cells were left for proliferation and colony formation over nearly 7-10 days. Moreover, the medium was refreshed every 3-4 days when needed. The experiment came to an end when the control condition reached the desired confluency, 95%. At the end of the experiment, the media was discarded, and the cells were rinsed with 1

mL ice-cold 1X PBS twice. After the rinsing step, 1 mL of methanol (Sigma-Aldrich, USA): acetic acid (Bio-Rad, USA) in a 3:1 ratio was given to cells for fixation for 45 min at room temperature (RT) on the shaker. After that, the fixed cells were dyed with 750 µL of 0.5% crystal violet (Merck, USA) for 2 h at RT on the shaker. After the staining process, the dye was removed, and the 6-well plate was washed with ddH_2O and left to dry. The image of each well was captured to analyze via ImageJ for number of colonies.

2.9 HANGING DROP

Cell suspensions consisting of $2x10^4$ cells per drop for LN18 and $1.2x10^4$ cells per drop for U87 were prepared with the desired concentrations of OSI and ENZ in 0.2 mL PCR tubes (Isolab, Germany). The treated cells were seeded as 20 µL/drop on the lid of 60 mm Petri dishes (Jet Biofil, China) whilst 2 mL of 1X PBS (EcoTech, Turkey) was poured at the bottom of 60 mm Petri dishes to make and sustain the environment's moisture. The cover was flipped over gently to allow the drops to hang. The drops were examined for 24, 48, and 72 h under the inverted light microscope (H600L, Nikon, Japan), and images were taken. With the help of ImageJ and GraphPad software, the diameters of the spheres were calculated, and their graphs were plotted.

2.10 WOUND HEALING ASSAY

U87 and LN18 cells were seeded (Jet Biofil, China) at a density of $1.6x10^5$ and $2x10^5$ per well of a 6-well plate and incubated in the incubator for 24 h. Afterwards, a straight line was scratched by the help of a 1 mL pipette tip (CAPP, Germany) into every well. The medium was discarded, and the cells were rinsed with 1 mL of 1X PBS to get rid of floating cells due to scratching. The desired concentrations of drugs were given to the cells, and a photo of each well at the pointed same area was taken under the microscope for 0, 24 and 48 h to observe wound healing at the scale of 200 µm (Carl Zeiss Microscopy, Axio, Observer 5 Colibri 7, Germany).

2.11 FLOW CYTOMETRY

$2.5x10^6$ and $2x10^6$ were seeded into 6-well plates (Jet Biofil, China) for LN18 and U87 respectively. Following 24 hours, cells were treated with desired dosages of OSI and ENZ and incubated for an additional 24 h in the incubator. Subsequently, the medium of treated cells was transferred to 1.5 mL microcentrifuge tubes (Isolab, Germany) and centrifuged for 1 min at 13,200 rpm (Centrifuge 5424 R) (Eppendorf, Germany) while 750 µL 1X PBS (EcoTech, Turkey) was trickled into every well. After centrifugation, the supernatant was disposed of from the tube and 1X PBS was inserted into the microcentrifuge tubes for centrifugation for 1 min at 13,200 rpm. The supernatant was discarded when 1X 0.25% 500 µL trypsin-EDTA (Gibco, USA) was spilt into each well for detachment, and trypsin activation was halted by 500 µL complete medium. The medium from wells was placed into microcentrifuge tubes to centrifuge for 1 min at 13,200 rpm. The wells were inspected to see if any adherent cells were remaining. The supernatants were carefully and utterly removed, and then 1 mL of ice-cold sterile 70% ethyl alcohol (Isolab, Germany) was gradually added dropwise to each pellet to fix with gentle agitation. After resuspension, the cells were stored at +4°C (Flavel, Turkey) for a maximum of 6 months. Prior to analysis utilizing the BD Accuri C6 flow cytometer device (BD Biosciences, USA), the cells were centrifuged for 1 min at 13,200 rpm to cleanse from ethanol. 1 mL of ice-cold 1X PBS was poured into each microcentrifuge tube for resuspension and centrifugation for 1 min at 13,200 rpm. The supernatant was eliminated and the combination of 300 µL ice-cold 1X PBS, 3 µL PI and 1 µL RNase A (EcoTech, Turkey) was mixed into every tube for resuspension for 15 min incubation in the dark before being read at a flow cytometer instrument. The results were analyzed by C6 Plus Analysis Software and graphs were done using GraphPad Prism.

2.12 TOTAL PROTEIN ISOLATION

$4.5x10^6$ cells were seeded into 60 mm Petri dishes (Jet Biofil, China) as an estimated roughly 80% confluency. They were treated with OSI and/or ENZ with respect to

required dosages when reaching confluency and were incubated in the incubator at 37°C with 5% CO_2 for 24 h. Following treatment, the medium containing drugs was collected into 1.5 mL microcentrifuge tubes (Isolab, Germany) (excluding control condition) and centrifuged at 13,200 rpm for 1 min (Centrifuge 5424 R) (Eppendorf, Germany). The supernatant was removed whilst 1 mL ice-cold 1X PBS (EcoTech, Turkey) was spilt onto 60 mm Petri dishes (for all conditions) and Petri dishes were scrapped under favour of the back of a pipette tip (CAPP, Germany). The scrapped medium was collected and centrifuged at 13,200 rpm for 1 min (Centrifuge, 5424 R) (Eppendorf, Germany), and the supernatant was removed. These scraping and collecting steps were done twice for all conditions. According to the amount of the pellet formation, Mammalian Protein Extraction Reagent (M-PER) (Thermo Fisher, USA) containing a protease inhibitor cocktail (Roche, Switzerland) was added into microcentrifuge tubes for resuspension of pellet and incubated for 20 min at RT on the shaker (SKO180S) (DLAB, Malaysia). Following incubation, the microcentrifuge tubes were placed into the cold centrifuge (Centrifuge 5418 R) (Eppendorf, Germany) at +4°C for 15 minutes. At the end of the cold centrifuge step, the supernatants were transferred to new sterile microcentrifuge tubes to store them at -20°C.

2.13 PHOSPHORYLATED PROTEIN ISOLATION

A total of $4.5x10^6$ cells/60 mm Petri dish (Jet Biofil, China) was seeded. Following 24 hours of incubation, LN18 and U87 cells were administered by OSI and ENZ according to predetermined concentrations. Following 24 h drug exposure, all Petri dishes were kept on ice to prevent degradation and loss of phosphorylated proteins during the entire procedure. The culture medium (excluding control conditions) was stockpiled into 1.5 mL microcentrifuge tubes (Isolab, Germany) and centrifuged at 13,200 rpm for 1 min (Centrifuge 5418 R) (Eppendorf, Germany) at +4°C. The supernatant was eliminated and then 1 mL ice-cold 1X PBS (EcoTech, Turkey) was added into the Petri dishes including all conditions. The adherent cells were detached utilizing the back of a pipette tip (CAPP, Germany). The medium was collected and then centrifuged at 13,200 rpm for 1 min (Centrifuge 5418 R) (Eppendorf, Germany) at +4°C. The supernatant was discarded, and this washing step was done two times.

With respect to the amount of the pellet, M-PER (Thermo Fisher, USA) including a protease inhibitor cocktail (Roche, Switzerland) and phosphatase inhibitor cocktail (Thermo Fisher, USA) was added into each microcentrifuge tube and pipetted. The cell suspension was incubated for 20 min on ice on the shaker (SKO180S) (DLAB, Malaysia). After incubation, the lysates were put into the cold centrifuge (Centrifuge 5418 R) (Eppendorf, Germany) at +4°C for 15 min. The next step was that the resulting supernatants were carefully transferred into the new microcentrifuge tubes for storing them at -20°C.

2.14 BRADFORD ASSAY

100 µL Bradford reagent (Sigma-Aldrich, USA) was added into a 96-well plate (Jet Biofil, China) when 1X Bovine Serum Albumin (BSA) (Sigma-Aldrich, USA) standard was poured into the plate in volumes of 0, 2, 4, 6 & 8 µL/well and 1 µL protein samples which were isolated according to conditions were added into the 96-well plate. Two repeats were done for 1X BSA & protein samples, and the plate was incubated in the dark for 15 min at RT. Subsequently, absorbances of protein samples were examined at 595 nm utilizing a spectrophotometer (Multiskan FC 357) (Thermo Fisher, USA). With the help of absorbances of BSA standards, the graph was drawn in Excel with an R^2 value, and the amounts of each protein sample were measured.

2.15 IMMUNOBLOTTING

A handmade 12% Tris-glycine gel was prepared according to the recipe given in Supplementary Table 8-9 for Thermo Fisher or Merck system. 30 µg of proteins were prepared into 0.2 mL PCR tubes (Isolab, Germany) according to Bradford assay with 4X Laemmli buffer (EcoTech, Turkey) for running and were heated for 5 min at 95°C in the heat blocker (Thermo Fisher, USA) for denaturation. The proteins were loaded into the wells, and the running protocol was initialized at 50 V and continued with 70 V when reaching the beginning of separating gel and eventually set to 90 V in the middle of separating gel to terminate the process at the end of separating gel according to protein marker (Abbkine, USA). After completion of the running procedure, the gel

and filter papers were put into 1X transfer buffer while 0.45 μm polyvinyl fluoride (PVDF) membrane (GVS, Italy) was activated by methanol (Sigma-Aldrich, USA) for 1 min, ddH_2O for 5 min and eventually 1X transfer buffer for 10 min. 4 filter papers were put onto the semi-dry Biometra Fastblot instrument (Analytik Jena, Germany), and then the smooth side of the activated membrane was placed facing upwards. Subsequently, the gel was put onto the smooth side of the activated membrane, and the sandwich was completed with the other 4 filter papers onto the gel. 200 mA was stably set for semi-dry transfer, and 15 or 20 min were adjusted for <100 kDa (kiloDalton) or >100 kDa of proteins respectively. After achieving the transfer step, the gel was dyed with Coomassie brilliant blue G-250 (Merck, USA) for evidence of completion of running while the membrane was put into 5% skim milk (BioShop, Canada) for 1 h incubation at RT on the shaker (DLAB, Malaysia). Coomassie blue was discarded and the destaining solution was poured into the gel to acquire more apparent wells for 30 min incubation at RT on the shaker. After the blocking method, the membrane was incubated into a 50 mL conical tube (Jet Biofil, China) including primary antibody p-AKT (Ser473) (1:1000) (CST, USA), AKT (St. John's Laboratory, UK), p-ERK 1/2 (Thr202/Tyr204) (1:500) (CST, USA), ERK 1/2 (1:500) (St. John's Laboratory, UK), p-AR (Ser380) (1:250) (Santa Cruz, USA), AR (1:500) (CST, USA), PSMA (1:500) (Elabscience USA), Cyclin D1 (1:500) (GeneTex, USA), Cyclin E2 (CST, USA), E-cadherin (1:1000) (CST, USA), N-cadherin (1:1000) (CST, USA), Caspase 3 (1:1500) (Novus, USA), Caspase 9 (1:1000) (GeneTex, USA) PARP (1:1000) (CST, USA), Bcl-xL (1:1000) (GeneTex, USA), GAPDH (2:5000) (Boster, USA), β-actin (1:1000) (CST, USA) on the roller (DLAB, Malaysia) overnight at +4°C. After primary antibody incubation, the membrane was rinsed with 1X tris-buffered saline tween-20 (TBS-T) three times for 5 min onto the shaker and incubated into horseradish peroxide (HRP)-conjugated anti-rabbit (1:1000) (CST, USA), anti-rabbit (1:1000) (Boster, USA) or anti-mouse (1:1000) (Boster, USA) secondary antibody in 50 mL conical tube on the roller overnight at +4°C. Following incubation, the membrane was washed with 1X TBS-T three times and 1X tris-buffered saline (TBS) once for 5 min on the shaker at RT. To assess bands and expression of proteins by HRP-conjugation, the enhanced chemiluminescence (ECL) solution was prepared as solutions A and B given in Supplementary Table 21 in 15 mL conical tubes. ECL

solutions were mixed, and the membrane was put into the ECL solution for 1 minute in the dark. Afterwards, the membrane was inserted into the C300 gel imaging system (Azure Biosystems, USA) to be analyzed in multiple different periods. The band thickness was gauged using ImageJ and normalization was done in Excel.

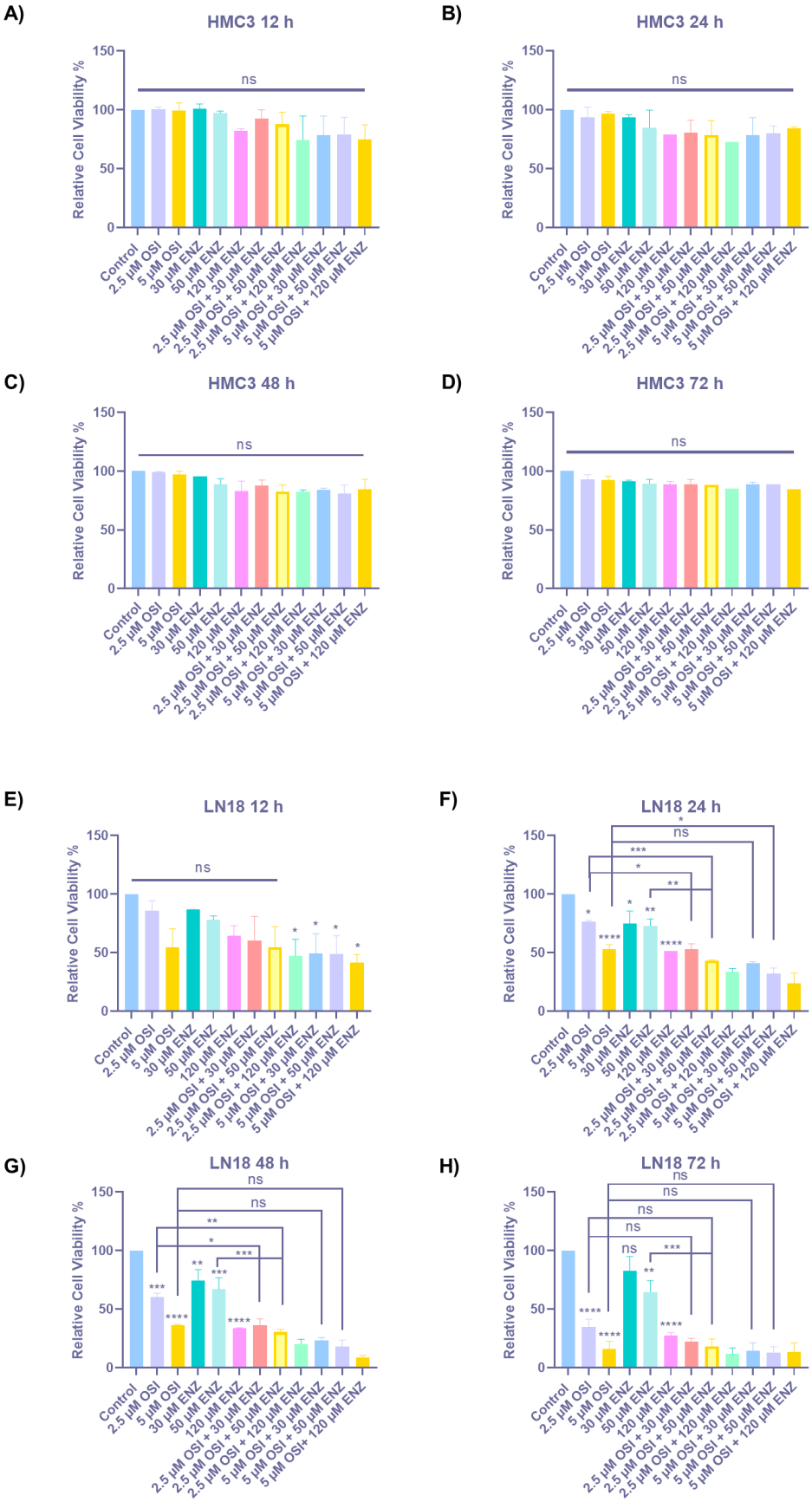
2.16 STATISTICAL ANALYSES

GraphPad Prism 8 software (https://www.graphpad.com) was utilized for analyzing all the experiments to show their statistical significance. One-way- and two-way ANOVA tests were used to analyze the whole data with the mean ± standard deviation (SD) to demonstrate the margin of error. The statistical significance concept was tackled if the p value is *p<0.05, **p<0.01, ***p<0.001, and ****p<0.0001. ImageJ software was utilized for $DiOC_6$ staining, colony formation, hanging drop, wound healing and immunoblotting analysis. Flow cytometry results were examined by BD Accuri C6 Software. ATP ELISA analysis was performed by MyAssays software (https://www.myassays.com/). Each experiment was replicated at least three times.

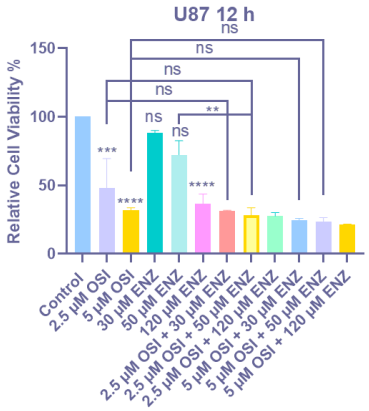
3. RESULTS

3.1 OSIMERTINIB AND ENZALUTAMIDE COMBINED TREATMENT DRASTICALLY DIMINISHED THE CELL VIABILITY IN LN18 AND U87 CELLS AND DID NOT AFFECT HMC3 CELL VIABILITY IN A DOSE- AND TIME-DEPENDENT MANNER

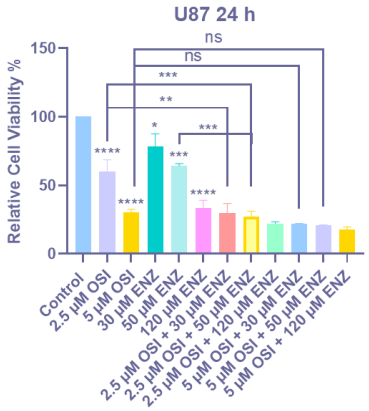
MTT cell viability was assessed in a dose- and time-dependent manner (12, 24, 48 and 72 hours) to unveil and evaluate the impacts of OSI and/or ENZ on healthy cell populations, HMC3, and GBM cells, LN18 and U87. As illustrated in Figure 6 A-L, 2.5 μM and 5 μM OSI were applied whilst 30 μM, 50 μM and 120 μM ENZ were utilized for healthy human microglial and GBM cells, both as monotherapies and in combination. At 12 hours of treatment, HMC3 was not affected while in LN18 the combination and in U87 alone treatments showed reduced cell viability but not shown in combined treatments (Figure 6 A-E and I). For 24 h treatment, it has not been observed cytotoxicity of drugs in HMC3. In contrast, in LN18 and U87 the alone and co-treatment of 2.5 μM OSI and 50 μM ENZ successfully showed a marked reduction in the cell viability below 50% (Figure 6 B-F-J). The combined treatment exerted a synergistic effect (ZIP, Loewe, HAS and BLISS scores are higher than 10) on GBM cells for 24 h treatment analyzed via SynergyFinder (https://synergyfinder.org) (Figure 6 M and N). 48- and 72-hour administrations of drugs demonstrated that the microglia cell line continued to display no signs of cytotoxicity in response to both alone and co-treatments (Figure 6 C and D) while for 48 and 72 hours LN18 and U87 exhibited that either alone treatment showed significant cell reduction with high cytotoxicity or no significant cell reduction in combined therapies (Figure 6 G-H-K-L). Taken together, MTT and SynergyFinder results interpret that utilizing 2.5 μM OSI and 50 μM ENZ together for 24 h was tackled as a suitable dosage combination in LN18 and U87 while sparing HMC3 cells.


A)
HMC3 12 h
B)
HMC3 24 h
C)
HMC3 48 h
D)
HMC3 72 h
E)
LN18 12 h
F)
LN18 24 h
G)
LN18 48 h
H)
LN18 72 h
Relative Cell Viability %
150
100
50
0
ns
Control
2.5 µM OSI
5 µM OSI
30 µM ENZ
50 µM ENZ
120 µM ENZ
2.5 µM OSI + 30 µM ENZ
2.5 µM OSI + 50 µM ENZ
2.5 µM OSI + 120 µM ENZ
5 µM OSI + 30 µM ENZ
5 µM OSI + 50 µM ENZ
5 µM OSI + 120 µM ENZ

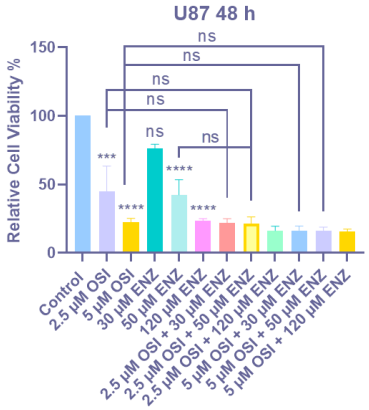
I)



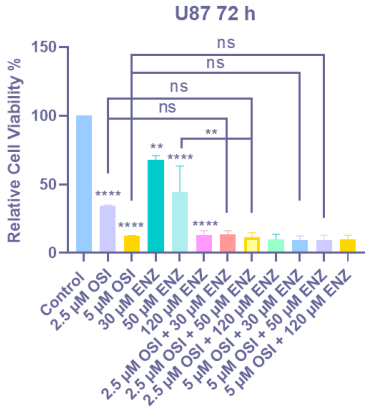
J)



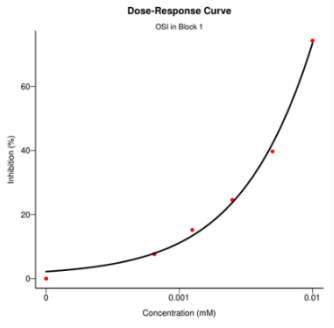
K)

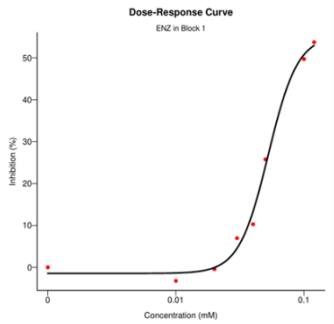


L)



M)





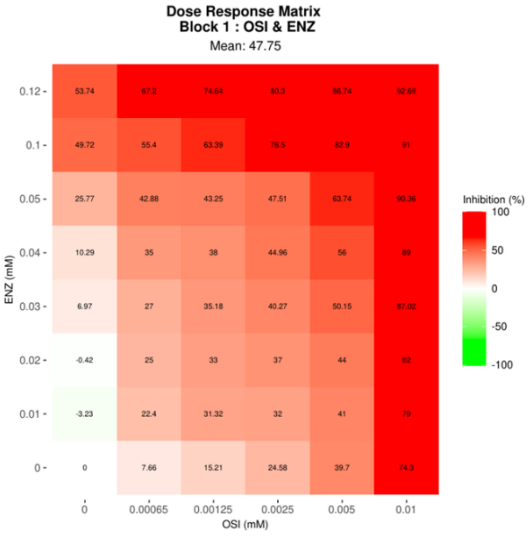


Table 1: Drug Combiantion Meta Data

Block ID	$Drug_1$	$Drug_2$	$Conc\ Unit_1$	$Conc\ Unit_2$
1	OSI	ENZ	mM	mM

Table 2: Synergy Score Summary Table

Block ID	ZIP	Loewe	HSA	Bliss
1	10.4	10.95	16.73	10.69

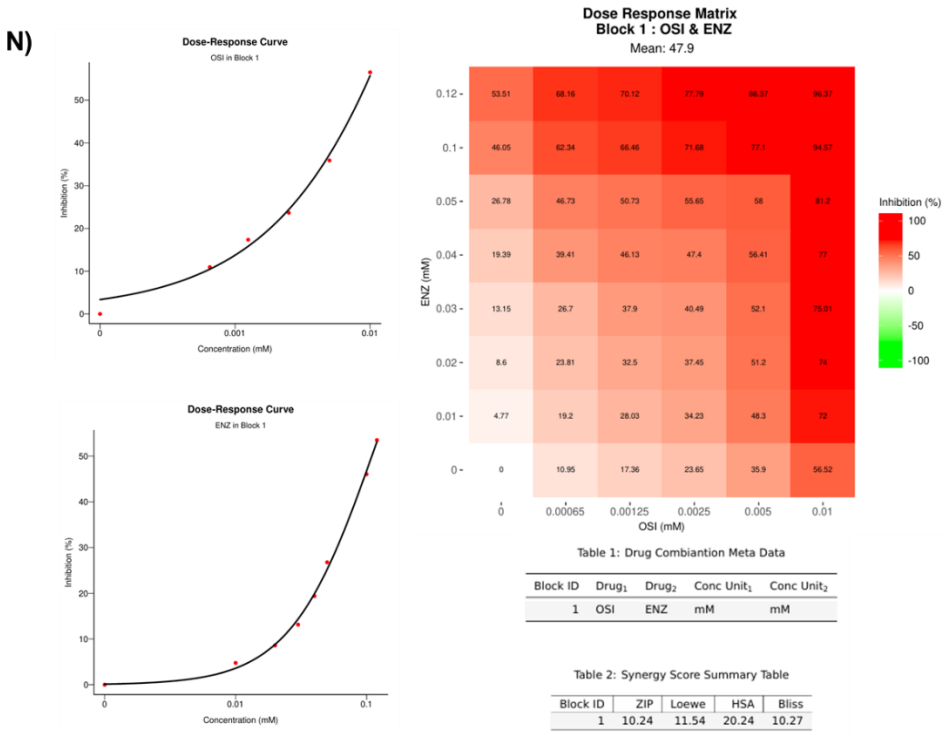


Figure 6: Co-treatment of OSI and ENZ synergistically decreased the cell viability in LN18 and U87 at 24 h and HMC3 cells remained unaffected. A-L. HMC3, LN18 and U87 cells were administered with different dosages of OSI and ENZ in a time-dependent manner (12-, 24, 48- and 72-h time points for cell viability assay. **M-N.** Broad doses of OSI (0.65, 1.25, 2.5, 5 and 10 µM) and ENZ (10, 20, 30, 40, 50, 100 and 120 µM) were utilized to LN18 and U87 for 24 h to decipher the score of drug interactions. 2.5 µM OSI and 50 µM ENZ combination for 24 h showed a synergistic effect in LN18 and U87 cell lines. At least triplicates were conducted, and the results serve the mean ± SD. Statistical significance: ns: no significant, *p<0.05, **p<0.01, ***p<0.001, and ****p<0.0001.

3.2 ATP CONCENTRATION WAS SIGNIFICANTLY DIMINISHED BY THE COMBINED THERAPY OF OSIMERTINIB AND ENZALUTAMIDE IN GLIOBLASTOMA CELLS

To further support the MTT results, a human ATP ELISA Kit was used for LN18 and U87. The synthesis of ATP is considered a fundamental indicator of mitochondrial function. With the help of this kit, compared to the control condition, monotherapy with OSI and ENZ significantly diminished the concentration of ATP in both LN18 and U87 cell lines following 24 h of treatment. Moreover, the combination of 2.5 µM OSI and 50 µM ENZ caused the most significant reduction in ATP levels among all conditions in both GBM cell lines (Figure 7).

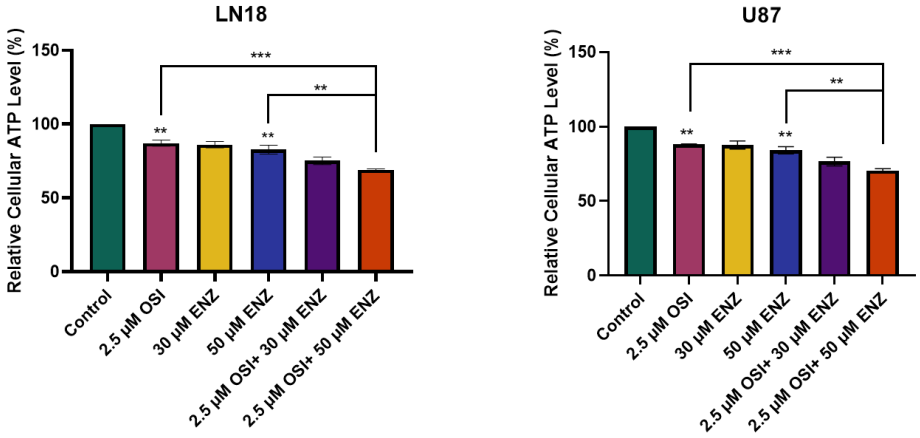


Figure 7: The ATP levels decreased following combined treatment of OSI and ENZ in LN18 and U87 cells. The ATP concentrations were quantified using a human ATP ELISA kit after 24 h administration of OSI and ENZ in GBM cell lines. At least three independent experiments were conducted, and the results are represented as the mean ±SD. Statistical significance: $^{**}p<0.01$, and $^{***}p<0.001$.

3.3 OSIMERTINIB AND ENZALUTAMIDE COMBINATION REDUCED THE SURVIVAL IN BOTH LN18 AND U87 CELL LINES IN A DOSE- AND TIME-DEPENDENT MANNER

To validate the results from the MTT cell viability assay, a survival assay was carried out to examine the survival potency depending on a time interval (0, 24, 48 and 72 hours) with different doses (30 µM and 50 µM of ENZ) combined with 2.5 µM of OSI in HMC3, LN18 and U87. Non-viable cells and viable cells can be distinguished in this assay when dead ones were seen as blue dots because of the uptake of the dye through compromised membranes while living ones appeared as light dots because of excluding Trypan blue through their selective permeable plasma membranes. Living cells were counted at every time-point and their graphs were drawn. It culminated that HMC3 cell lines were not influenced in both monotherapy and co-treatment and still survived across all time points. However, cell survival dramatically declined by 2.5 µM OSI combined with 50 µM ENZ in GBM cell lines compared to the alone treatment (2.5 µM OSI and 50 µM ENZ) for 24 hours intervention. By 48 h treatment, GBM cell lines tried to recover from drug-induced cytotoxicity. Thereby, 2.5 µM OSI concurrent usage with 50 µM ENZ for 24 h was selected as the next step dose (Figure 8).

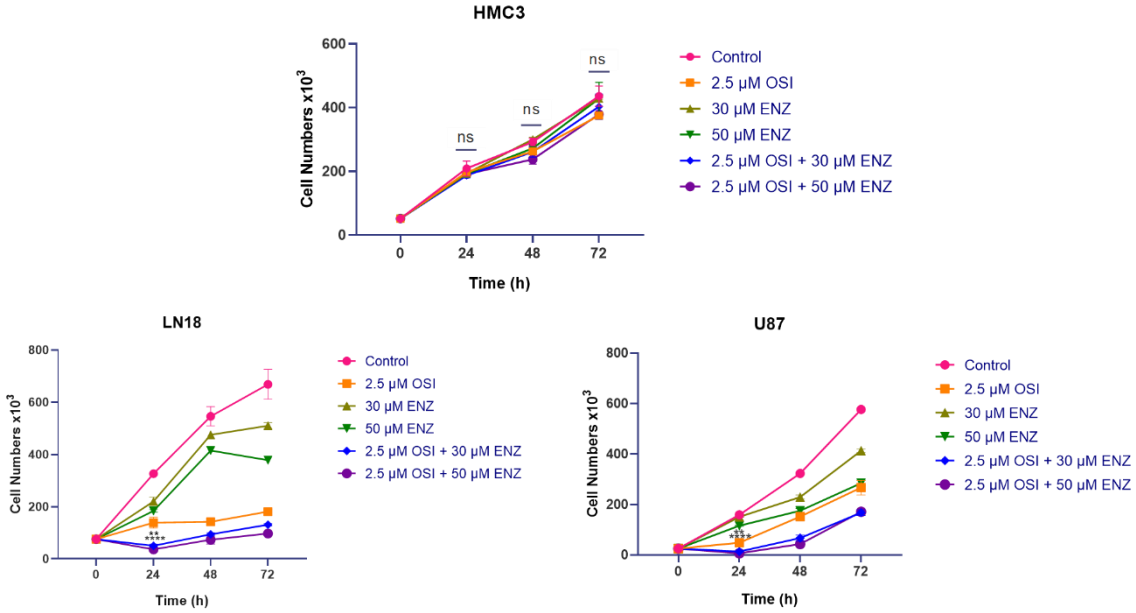


Figure 8: LN18 and U87 cells showed a reduction in survival following 24 h therapy with the combination of 2.5 µM OSI and 50 µM ENZ while HMC3 was not affected by this administration at any time-point. The survival assay was done in HMC3, LN18 and U87 cell lines in a dose- and time-dependent manner (0, 24, 48 and 72 h). A decline in survival was observed in 2.5 µM OSI, 50 µM ENZ and their combination in LN18 and U87 but had no effect in microglia cells, HMC3 (** denotes comparison between 2.5 µM OSI and 2.5 µM OSI + 50 µM ENZ while **** indicates comparison between 50 µM ENZ and 2.5 µM OSI + 50 µM ENZ). Data are presented as mean ±SD of 3 replicates. Statistical significance: ns: no significant, $^{**}p<0.01$, and $^{****}p<0.0001$.

3.4 COMBINED TREATMENT OF OSIMERTINIB AND ENZALUTAMIDE DRAMATICALLY ELEVATED THE NUMBER OF DEAD CELLS IN LN18 AND U87 CELL LINES

PI staining was employed to detect dead cells under the fluorescence microscope after exposing drugs, OSI and/or ENZ in HMC3, LN18 and U87 cells for 24 h. The results demonstrated that HMC3 had either too few or no PI-positive (dead) cells among all conditions. However, in LN18 and U87 cells upon treatment with 2.5 µM OSI, 50 µM and then their combination elevated dead cells respectively. PI-positive cells were counted, and the data were graphically represented utilizing GraphPad (Figure 9 A-B).

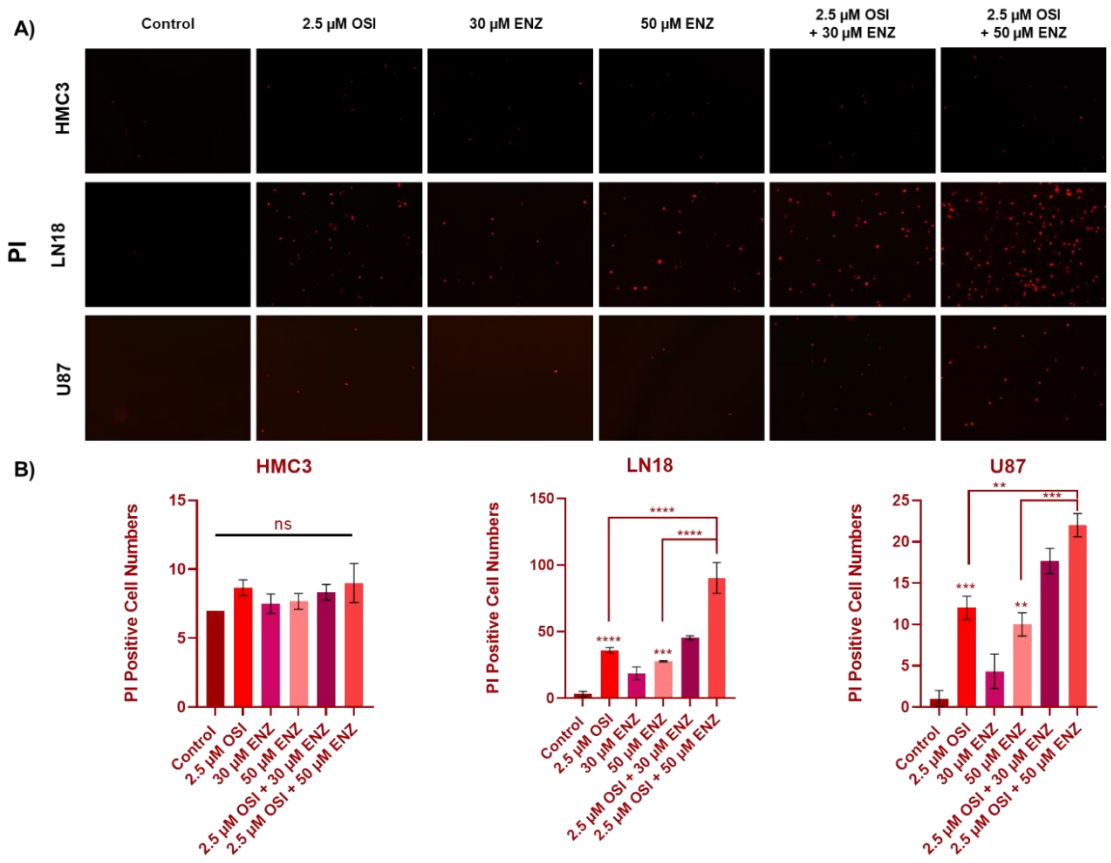


Figure 9: OSI concomitant ENZ usage gave rise to elevated dead cells via PI staining in LN18 and U87 cell lines. A-B. Using PI under the fluorescent microscope, non-viable cells were observed and the combination of OSI and ENZ augmented the number of dead cells while HMC3 was not disturbed by PI. At least three experiments were conducted. Representative pictures were taken at 5 x magnification. Scale bar: 200 μm. Each bar stands for the mean ±SD of 3 different experiments. Statistical significance: ns: no significant, **p<0.01, ***p<0.001, and ****p<0.0001.

3.5 DNA FRAGMENTATION WAS AUGMENTED IN LN18 AND U87 CELLS EXPOSED TO OSIMERTINIB AND ENZALUTAMIDE CO-TREATMENT

DAPI was used to reveal the difference between dead and live cells by detecting fragmented nuclei in cells. Even though DAPI also stains the nuclei of living cells, dead cells are proclivity to shine more due to the absorption potency of disruption of selective permeability of the cell. Under the fluorescence microscope, it divulged that HMC3 did not have significant DNA fragmentation compared to LN18 and U87 in OSI combined with ENZ for 24 h administration. Both monotherapy and combined

(2.5 µM OSI and 50 µM ENZ) treatments indicated elevated nuclear fragmentation by appearing as bright bluish dots in LN18 and U87 cell lines. For all cell lines, experiments were repeated at least 3 times (Figure 10 A-B).

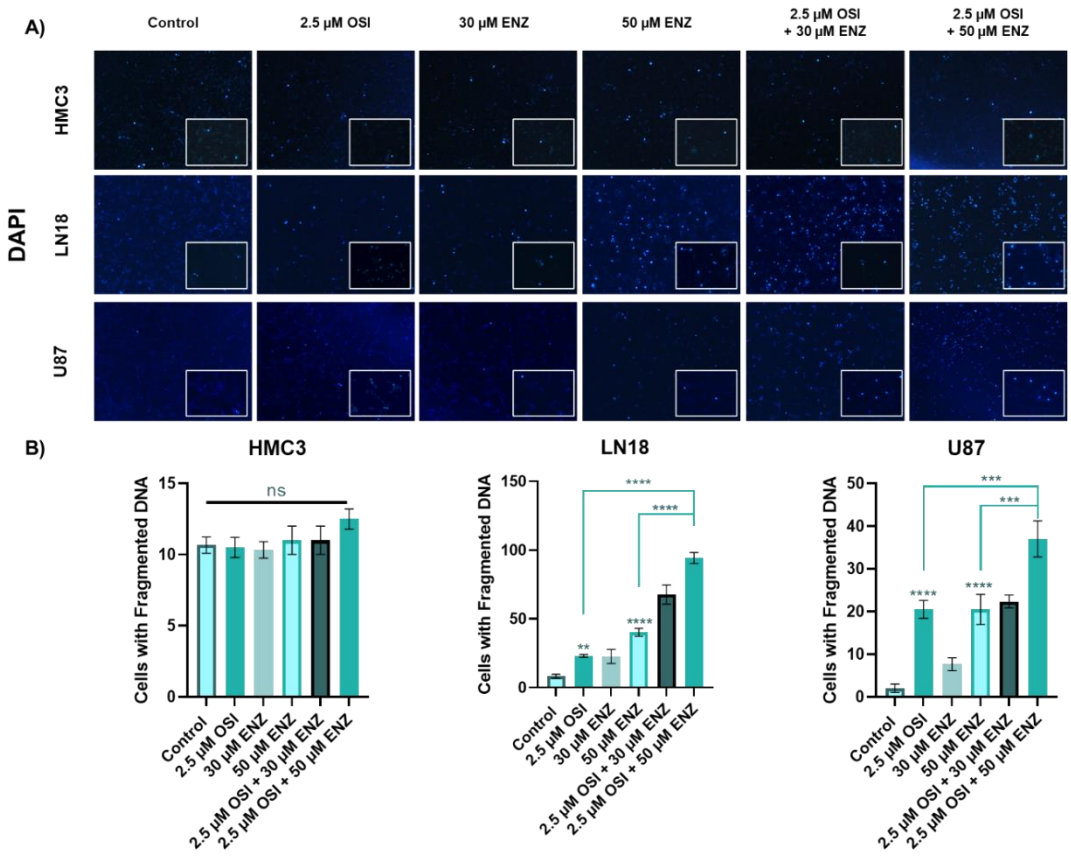


Figure 10: DAPI staining unmasked DNA fragmentation in GBM cells in response to OSI and/or ENZ, whereas it was not observed with any effect on microglia, HMC3. A-B. Alone or combined therapy of OSI and ENZ increased DNA fragmentation in LN18 and U87 via DAPI dye. In contrast, HMC3 did not have a detectable effect following OSI and/or ENZ treatment. Fluorescence images were acquired at 5 x and 20 x magnifications (ex/em: 359/461 nm). Scale bars: 200 and 50 µm. Values are represented as the mean ±SD. Statistical significance: ns: no significant, $^{**}p<0.01$, $^{***}p<0.001$, and $^{****}p<0.0001$.

3.6 THE COMBINATION OF OSIMERTINIB AND ENZALUTAMIDE ATTENUATED THE MITOCHONDRIAL MEMBRANE POTENTIAL IN LN18 AND U87 CELLS LINES

To uncover the live cells based on mitochondrial membrane potential ($\Delta\Psi_M$) all conditions (control, 2.5 µM OSI, 30 µM ENZ, 50 µM ENZ, 2.5 µM OSI + 30 µM

ENZ and 2.5 µM OSI + 50 µM ENZ) were dyed with $DiOC_6$ in HMC3, LN18 and U87 cells. In HMC3 cells, all conditions displayed the same vitality. However, in LN18 and U87 $DiOC_6$ demonstrated that combination treatment of 2.5 µM OSI and 50 µM ENZ attenuated the mitochondrial membrane potential. The intensity of cells stained with $DiOC_6$ was quantified by ImageJ software and graphs were generated via GraphPad Prism (Figure 11 A-B).

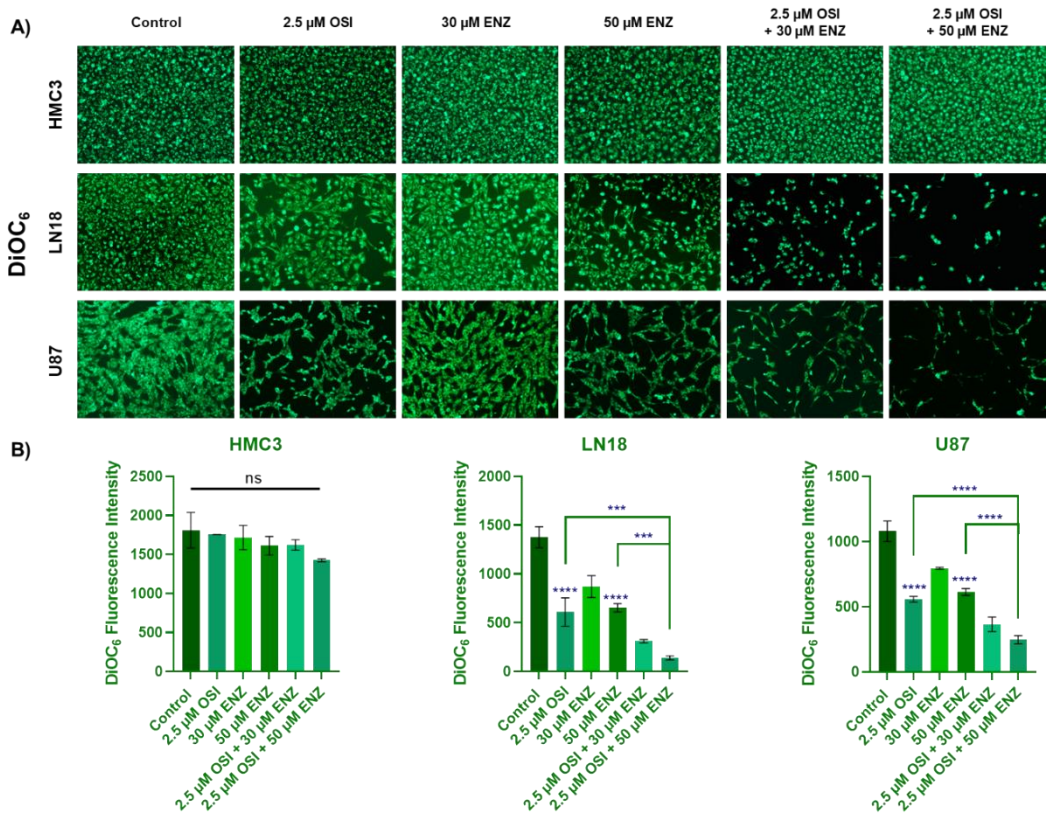


Figure 11: Mitochondrial membrane potential was reduced in LN18 and U87 in the co-treatment of OSI and ENZ for 24 h. A-B. Under the fluorescence microscope at 482/504 nm, HMC3 sustained their vividness among all conditions via $DiOC_6$ staining while mitochondrial membrane potential was decreased by alone and combined therapy in GBM cells. Images of live cells were captured at 10 x zoom. Scale bar: 100 µm. Results are represented as the mean ±SD. Statistical significance: ns, ***p<0.001, and ****p<0.0001.

3.7 THE ABILITY OF COLONY FORMATION OF LN18 AND U87 CELLS WAS DECLINED BY COMBINATION OF OSIMERTINIB AND ENZALUTAMIDE

As a further step, the 2D colony formation potential was conducted with the optimized dosages of the previous experiments. Unlike MTT and Trypan blue exclusion assays, it was also wanted to check long-term survival potency from a single cell whether it expands into a colony. In this experiment, LN18 and U87 were administered as follows in a dose-dependent manner for 24 h: control, 2.5 µM OSI, 30 µM ENZ, 50 µM ENZ, 2.5 µM OSI + 30 µM ENZ and 2.5 µM OSI + 50 µM ENZ. Crystal violet staining revealed that alone treatments (2.5 µM OSI and 50 µM ENZ) and their combination declined the colony potential. The colony areas were gauged by ImageJ and experiments were performed with at least 3 repeats (Figure 12 A-B).

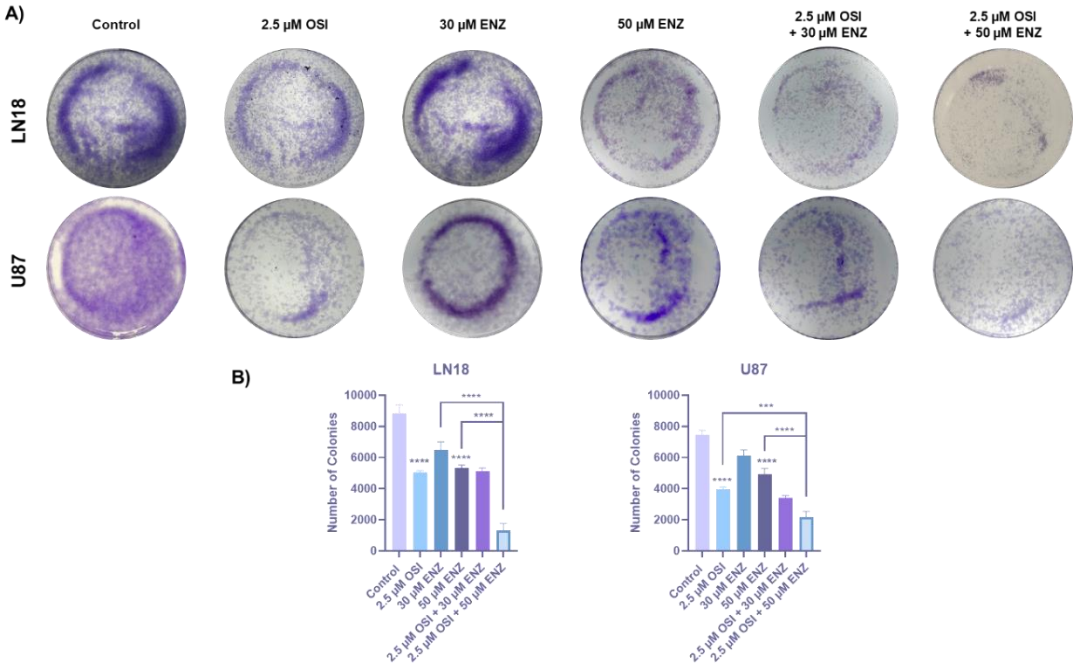


Figure 12: The 2D colony capacity of GBM cells was diminished in the combination of OSI and ENZ. A-B. Colony formation assay was conducted in LN18 and U87 cell lines. 2.5 µM OSI combined with 50 µM ENZ led to impaired ability of 2D colony formation. The results were assessed with a one-way analysis of variance (ANOVA) and plotted using GraphPad Prism. Error bars represent ±SD. Statistical significance: ***p<0.001, and ****p<0.0001.

3.8 3D COLONY FORMATION POTENCY OF LN18 AND U87 WERE HALTED BY THE COMBINATION OF OSIMERTINIB AND ENZALUTAMIDE IN GLIOBLASTOMA CELLS

In addition to the 2D colony formation assay, the 3D version of colony formation was also checked to observe disruption/recovery of spheroid formation of the GBM cells without adhering to any surface by hanging drop method. Drawing upon the hanging drop method was a dose- and time-dependent (24, 48 and 72 h) manner assay for LN18 and U87 cells. Both GBM cell lines showed that 2.5 µM OSI, 50 µM ENZ and their combination successfully disrupted the spheroid formation for 24 hours of treatment. As of 48 h treatment, GBM cells underwent a recovery stage even though the rate of recovery was slow in both alone (2.5 µM OSI and 50 µM ENZ) and the combination treatment. Diameters of spheroids were measured by the ImageJ software, and the values were converted into graphs by GraphPad Prism (Figure 13 A-D).

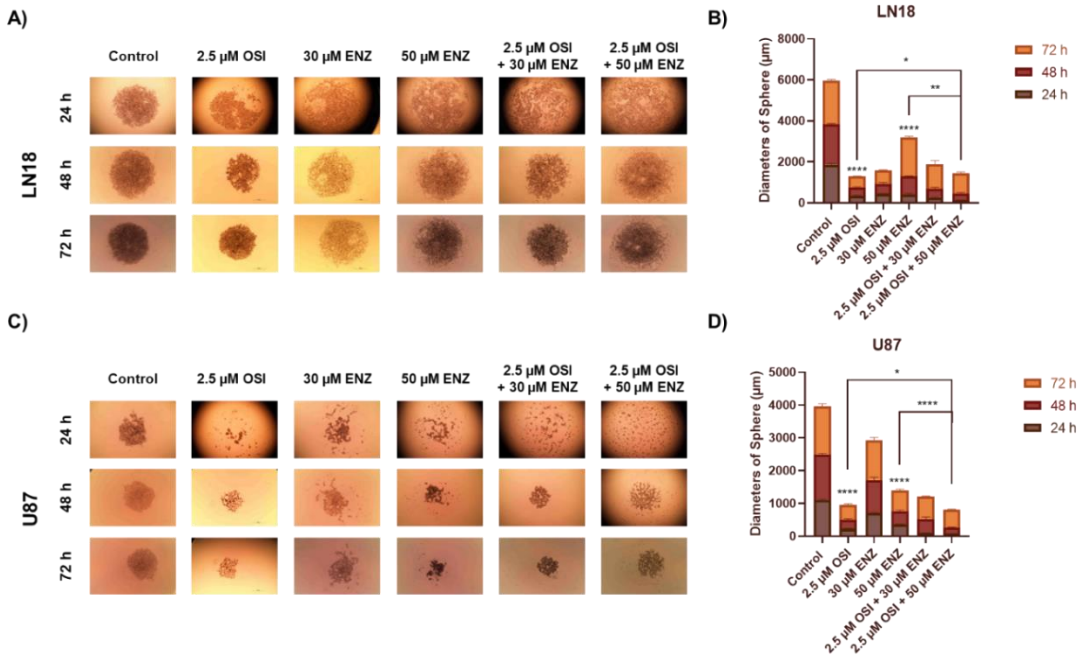
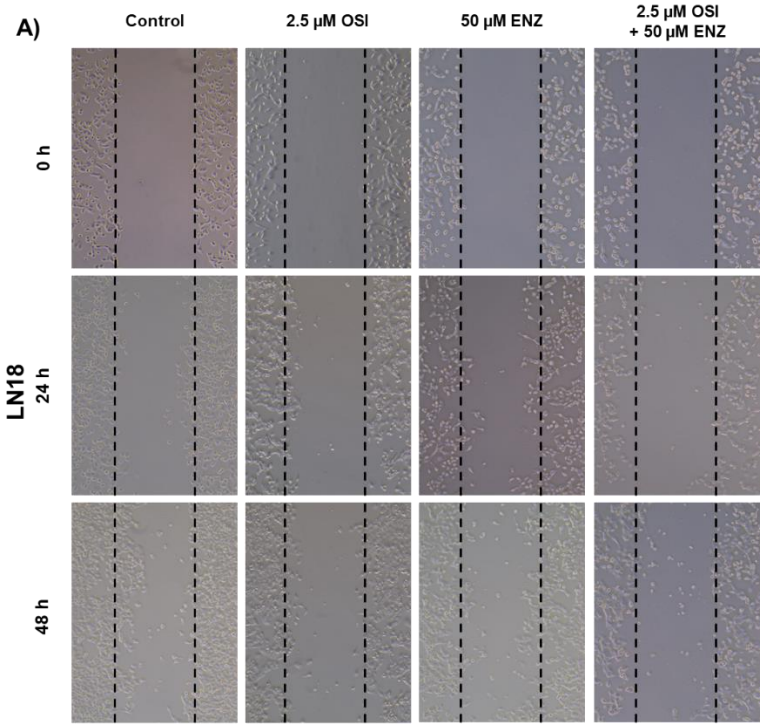


Figure 13: Hanging drop assay unveiled that co-treatment with OSI and ENZ disrupted the spheroid formation and delayed subsequent recovery in 3D cell culture. **A-D.** Using OSI and ENZ in LN18 and U87 cells gave rise to impede the 3D colony formation for 24 h and after that the recovery was decelerated. The results were evaluated with two-way ANOVA. Images were captured at 4 x zoom under the inverted light microscope. Scale bar: 500 µm. Results are represented as the mean ±SD. Statistical significance: *p<0.05, **p<0.01 and ****p<0.0001.

3.9 THE RATE OF WOUND CLOSURE WAS SLOWED DOWN VIA OSIMERTINIB COMBINED WITH ENZALUTAMIDE IN LN18 AND U87 CELLS

To observe the filling of the gap over time in a confluent cell monolayer whether the therapy obstructs or increases the cell motility, the scratch was done with a 1 mL pipette tip. After scratching, the 0 h of the conditions (control, 2.5 µM OSI, 50 µM ENZ and 2.5 µM OSI and 50 µM ENZ) were shot in LN18 and U87 cells. The conditions were pictured as time-lapses to see wound closure under the inverted light microscope. It shows that in both cell lines, 24 hours of treatment successfully worked and hindered the wound closure in the combination of OSI and ENZ compared to the version of 0 h of treatment. After 24 hours, wound closure gradually progressed at a slow rate by the help of the administration of the drugs. Control cells have a rapid rate of wound closure compared to GBM cells administered by the drug treatments. Wound closure at every time-point was evaluated by the ImageJ wound healing tool and graphs were drawn by those calculated areas in GraphPad Prism (Figure 14 A-C).



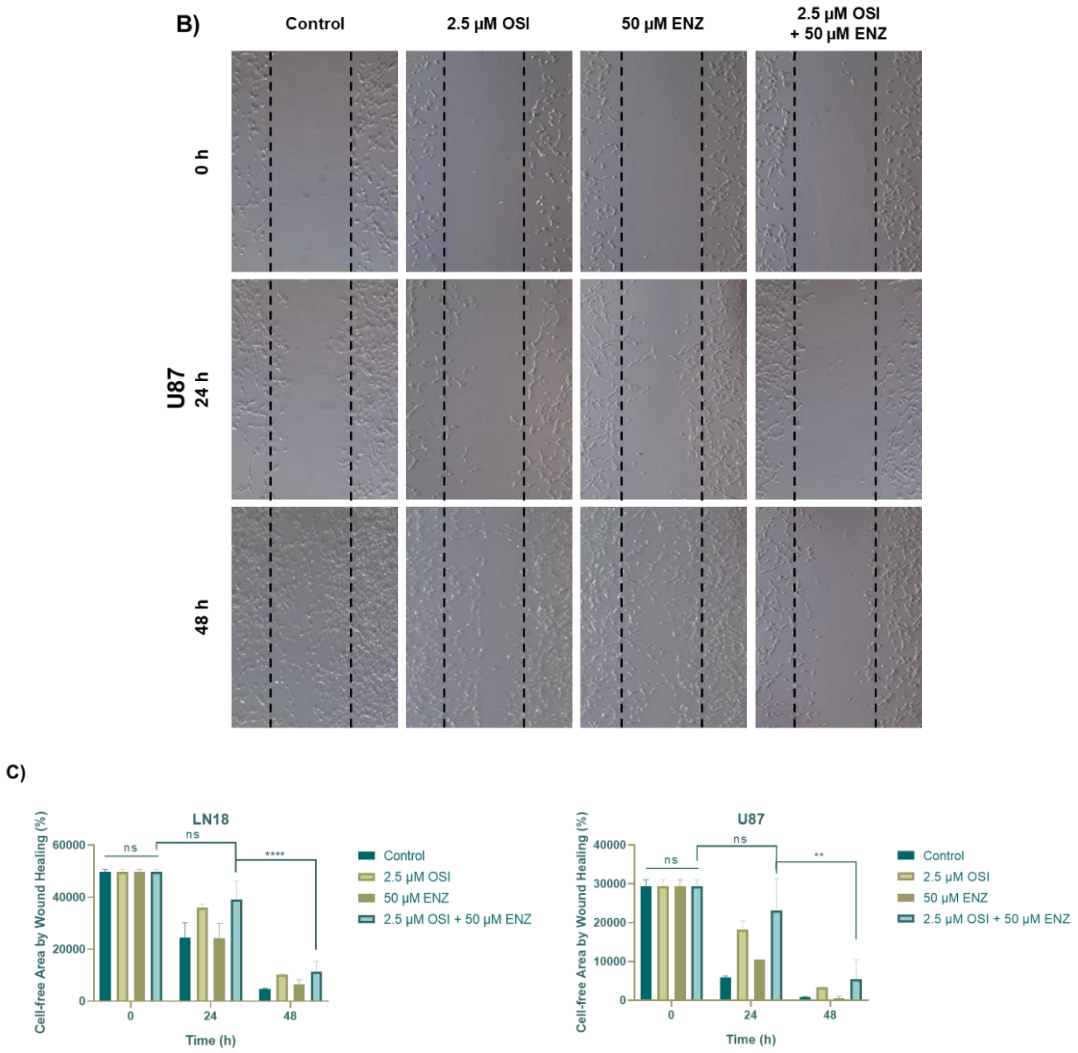


Figure 14: The progression of wound healing declined in LN18 and U87 using OSI and ENZ for 24 hours. A-C. OSI combined with ENZ slowed down the rate of wound closure in GBM cell lines in a time-dependent manner by scratch assay. Data was measured with two-way ANOVA. The photos were taken with 5 x magnification with the inverted light microscope. Scale bar: 200 µm. Every bar presents the mean ±SD of triplicates. Statistical significance: ns: no significant, $**p<0.01$ and $****p<0.0001$.

3.10 THE APOPTOTIC CELL POPULATION WAS INCREASED BY OSIMERTINIB CONCURRENT USAGE WITH ENZALUTAMIDE IN LN18 AND U87 CELL LINES

Flow cytometer was performed to assess the subG1 population, indicative of programmed cell death, as well as cell cycle phases in LN18 and U87 cell lines. The results displayed that both monotherapy and combination treatment with 2.5 µM OSI and 50 µM ENZ gradually elevated SubG1 phase for 24 h treatment. The combined

therapy has the highest proportion of SubG1-phase affected cells. No statistically significant differences were detected among the other cell cycle phase distributions. Graph was plotted with at least triplicates using two-way ANOVA (Figure 15 A-B).

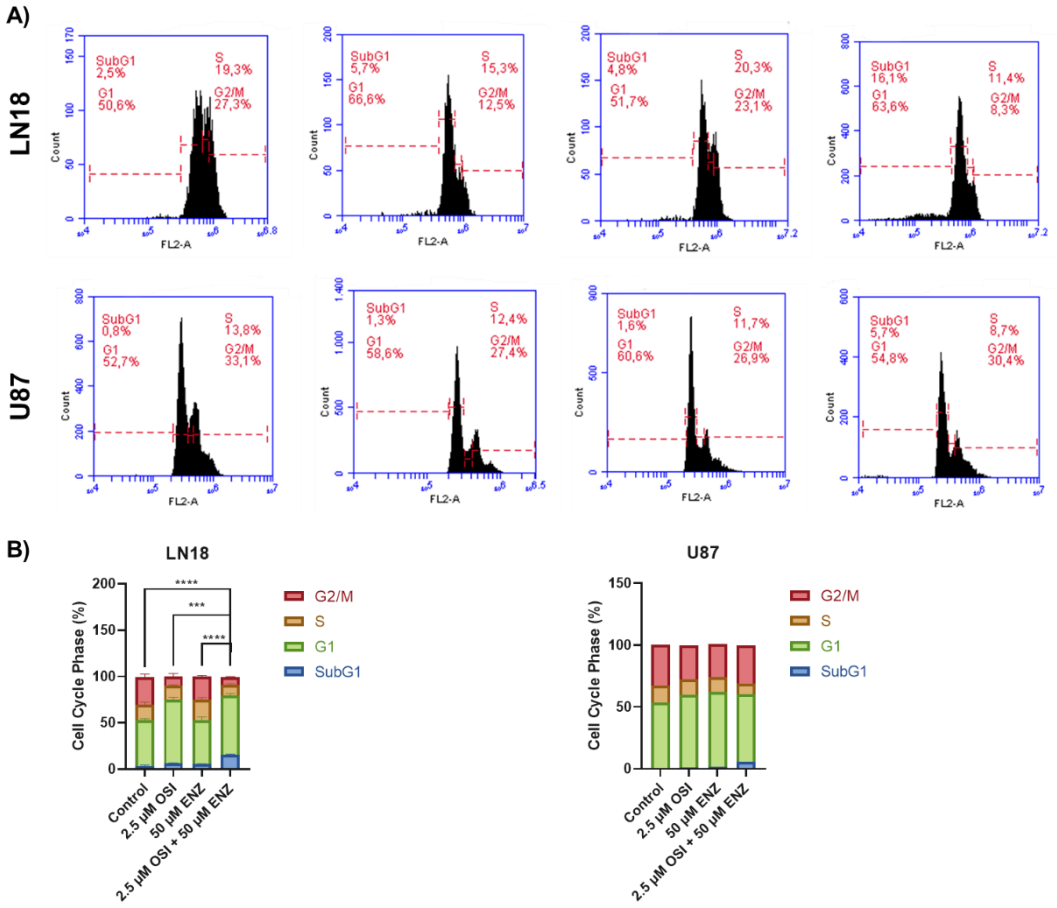


Figure 15: Apoptotic subG1 accumulation was increased via the combination of OSI and ENZ in LN18 and U87 cells. A. Flow cytometer was conducted to investigate cell cycle phases, including G1, S, G2/M and subG1 in LN18 and U87 cell lines. **B.** The graph showed that subG1 was elevated in monotherapy and the combination of 2.5 µM OSI and 50 µM ENZ in LN18 and U87 cell lines. Error bars represent ±SD. Statistical significance: ***p<0.001, and ****p<0.0001.

3.11 EGFR SIGNALING DOWNSTREAM TARGETS WERE AFFECTED BY THE COMBINED TREATMENT OF OSIMERTINIB AND ENZALUTAMIDE IN LN18 AND U87

To investigate the effects of monotherapy and combination of OSI and ENZ in EGFR signaling pathway if EGFR is blocked or not via OSI, western blotting was done in

LN18 and U87 cell lines. Expressions of p-AKT and p-ERK 1/2 (Thr202/Tyr204) were diminished by the help of 2.5 µM of OSI combined with 50 µM of ENZ after 24 h treatment while expressions of AKT and ERK 1/2 were not altered in LN18 and U87 cell lines. GAPDH was tackled as housekeeping marker and showed same expression in every condition in GBM cells (Figure 16).

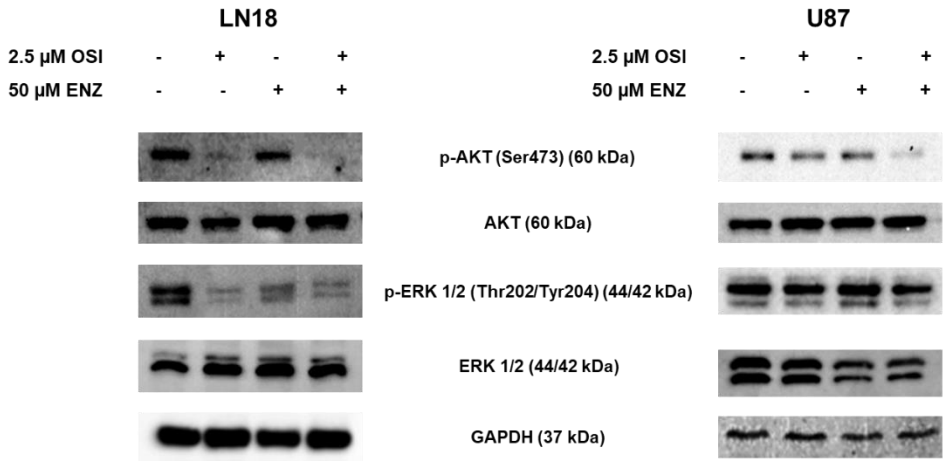


Figure 16: EGFR-related markers were deciphered after administration of OSI and ENZ in LN18 and U87. After 24 h treatment of OSI and/or ENZ, EGFR-associated proteins, p-AKT (Ser473), AKT, p-ERK 1/2 (Thr202/Tyr204) and ERK 1/2 were checked. GAPDH was utilized as a loading control.

3.12 AR SIGNALING PARTNERS WERE EVALUATED IN THE PRESENCE OF OSIMERTINIB AND ENZALUTAMIDE IN GLIOBLASTOMA CELLS

To evaluate the impact of monotherapy of ENZ and combination of ENZ and OSI in GBM cell lines through AR signaling pathway, western blotting was performed in tris-glycine gel. After administration of 2.5 µM OSI and 50 µM ENZ for 24 h showed that expression of p-AR (Ser380) was reduced in LN18 while expression of AR remained same in every condition in both GBM cell lines. However, PSMA expressions were elevated in the presence of OSI combined with ENZ in both cell lines. β-actin was utilized as a housekeeping marker and exhibited similar expression level in every condition in LN18 and U87 cell lines (Figure 17).

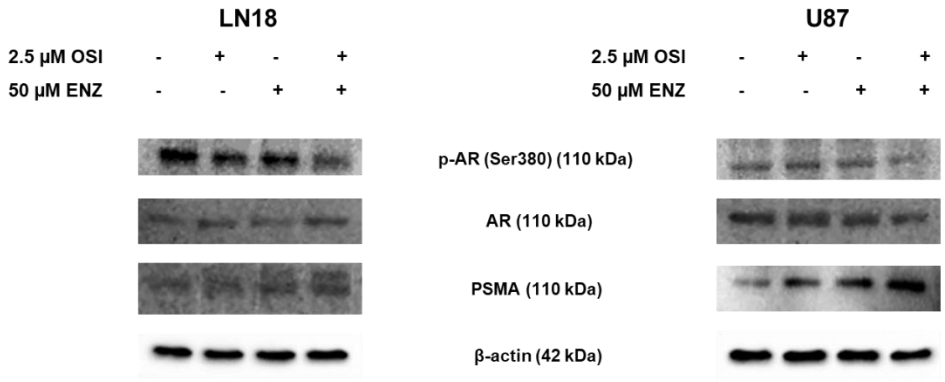


Figure 17: The expression of AR pathway-related markers with OSI, ENZ and its combination were deciphered in LN18 and U87 cell lines. Expression alterations of p-AR (Ser380), AR and PSMA were evaluated via OSI and/or ENZ in GBM cells. β-actin was utilized as a housekeeping marker.

3.13 THE CELL CYCLE WAS ARRESTED UTILIZING OSIMERTINIB AND ENZALUTAMIDE IN LN18 AND U87 CELLS

The impact of OSI and ENZ on cell cycles was investigated with immunoblotting methods. The results showed that expression of cyclin D1 was declined via 2.5 μM OSI and 50 μM in LN18 and U87 cells. Cyclin E2 expression was elevated in the combination of 2.5 μM OSI and 50 μM ENZ in LN18 while decreased in U87 cell line. As a loading control, β-actin was used, and similar expressions were observed in both GBM cells (Figure 18).

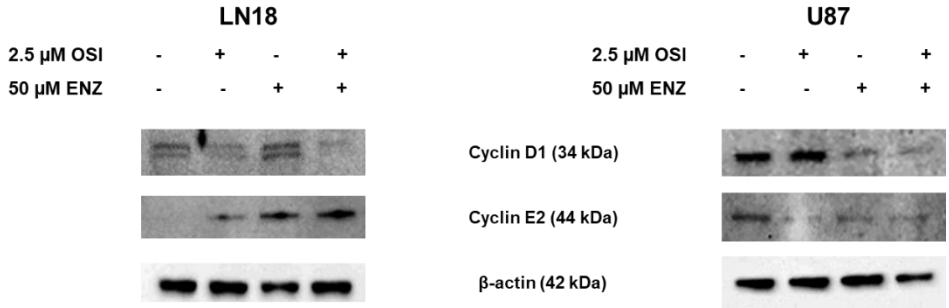


Figure 18: The cell cycle was arrested in OSI combined with ENZ in LN18 and U87 cells. Expression of Cyclin D1 was reduced via 2.5 μM OSI and 50 μM ENZ in GBM cells. Expression of cyclin E2 was enhanced in 2.5 μM OSI with 50 μM ENZ in LN18 but reduced in U87 cell line. β-actin was utilized as a loading control.

3.14 EPITHELIAL-MESENCHYMAL TRANSITION MARKERS WERE CHECKED AFTER ADMINISTRATION OF MONOTHERAPY OR COMBINATION OF OSIMERTINIB AND ENZALUTAMIDE

To interpret EMT state of the cells after exposure to OSI, ENZ and combination of OSI and ENZ, EMT-associated markers were checked by immunoblotting method. In both cell lines, N-cadherin expression was successfully reduced using combination of 2.5 µM OSI and 50 µM ENZ after 24 h treatment. Expression of E-cadherin was increased in the combined treatment of OSI and ENZ in LN18, while E-cadherin expression remained stable in U87 after the treatment in all conditions. GAPDH was used as loading control, and its expression remained constant in every condition (Figure 19).

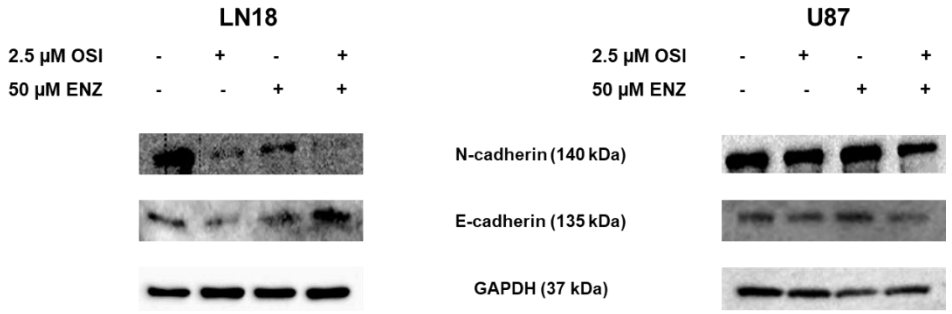


Figure 19: Epithelial- and mesenchymal-associated markers were investigated in LN18 and U87 in OSI combined with ENZ. Expression alterations of N-cadherin and E-cadherin were inspected within the 2.5 µM OSI, 50 µM ENZ and its combination GAPDH was used as loading control.

3.15 APOPTOTIC PROTEIN EXPRESSIONS WERE ALTERED AFTER OSIMERTINIB AND ENZALUTAMIDE COMBINED TREATMENT

Western blotting was done to check impacts of dual targeting of EGFR and AR with OSI and ENZ treatment on apoptosis. Pro-apoptotic and anti-apoptotic proteins were checked. OSI combined with ENZ treatment showed reduction in pro-caspase 3, pro-caspase-9, PARP and Bcl-x_L expressions in LN18 and U87. Expressions of cleaved caspase-3 and cleaved PARP were enhanced in both GBM cell lines after administration of 2.5 µM OSI and 50 µM ENZ. GAPDH was tackled as a housekeeping and kept its expression at the same level in every condition (Figure 20).

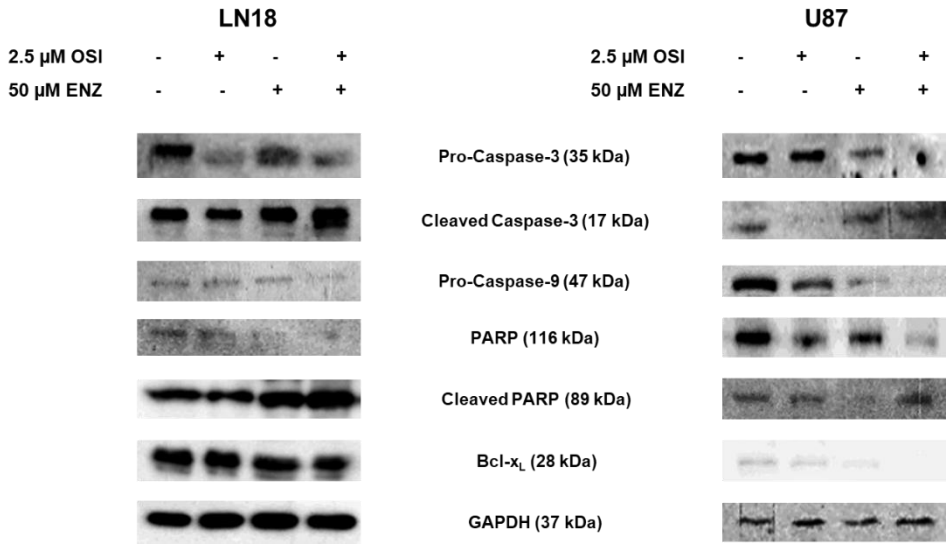


Figure 20: The combination of OSI and ENZ elevated pro-apoptotic biomarkers while declined anti-apoptotic proteins in GBM cells. Expression level of caspase 3, caspase 9 and PARP were detected as their full and cleaved versions. As anti-apoptotic expression level, Bcl-x_L, was evaluated. Housekeeping marker was GAPDH.

4. DISCUSSION

GBM is one of the most persistent cancer types and represents a fatal primary brain tumor in adults that arises without warning, usually appearing with new onset seizures or a few days of progressive focal weakness and headache (Maher & Bachoo, 2025; Muhammad et al., 2025). However, MR findings demonstrate a large mass that has likely been present for months to years (Maher & Bachoo, 2025). GBM's stealth-like behavior hides the apparent trait of this brain tumor: that it invades normal brain diffusely across long distances without damage to neuronal circuits early in the disease course at a time that may have been treated (Maher & Bachoo, 2025). GBM is the most prevalent tumor among brain and other CNS, accounting for 14.2% of all tumors and 50.9% of all aggressive tumor types. Genetic alterations affecting neuroglial stem or precursor cells could be the cause of GBM, and its incidence rate increases with age. This aggressive malignant brain tumor is a challenging disease due to its anatomical constraints, the biological sophistication of the tumor and the low functional status of affected individuals (Muhammad et al., 2025). This formidable brain tumor shows roughly OS at 12-15 months due to poor prognosis and rapid progression (S. Singh et al., 2025). Despite surgery, chemotherapy, radiation and new chemical agents, GBM, grade IV subtype, has limited OS because of TME, heterogeneity, coexistence with differentiated tumor cells and glioma stem-like cells (Maher & Bachoo, 2025; S. Singh et al., 2025). GBM is defined as short periods of steady disease post-treatment followed by inevitable recurrent brain tumor (Maher & Bachoo, 2025). GBM is driven by key oncogenic drivers and molecular alterations such as TERTp mutations, chromosomal anomalies, PDGFR, PI3K-AKT-mTOR and EGFR pathways, which are significant for tumorigenesis, invasion and resistance to conventional therapeutic strategies. Notably, in contrast to IDH-wt GBM, IDH-mutant ones exhibit better clinical outcomes (S. Singh et al., 2025).

TMZ remains the only approved chemotherapeutic agent for GBM, whereas BVZ, CCNU, intravenous BCNU and carmustine wafer implants are utilized for managing recurrent GBM and mitigating symptoms. TMZ is an orally taken drug that leads to mismatch repair in DNA by methylation at the O^6 position of guanine (Fisher & Adamson, 2021). Even though TMZ constitutes the standard of care, unfortunately,

half of the GBM individuals acquire resistance to TMZ due to MGMT enzyme activity. This chemoresistance is considered the primary reason for short median OS in GBM patients (Jezierzański et al., 2024). Consequently, novel treatment strategies are required to find alternative molecular targets beyond those affected by TMZ.

Overexpression of EGFR is observed in more than 50% of GBM cases, and downstream targets of EGFR mediates cell survival, proliferation, invasion and migration. Constitutive activation of EGFR brings about uncontrollable cell growth. Several EGFR variants have been detected in GBM, including EGFRvIII, EGFRvII, EGFRvIV, EGFRx and missense mutations. The most common variant, which has been associated with GBM, is EGFRvIII. This variant influences ECD of EGFR with a deletion of exons 2-7, giving rise to persistent activation of downstream targets (Ezzati et al., 2024). Although EGFRvIII is persistently active in GBM with a low kinase activity, EGFRvIII is co-expressed with wt EGFR to maintain cell proliferation and survival. EGFRvIII is a cancer-specific mutation, making it an attractive therapeutic target for treatment approaches such as reducing cell survival and inducing apoptosis (H. Xu et al., 2017). Drug repositioning is one of the most preferred treatment options instead of developing a chemical agent whose pharmacological evaluation will take many years. In contrast to 1st- and 2nd-generation EGFR TKIs, 3rd-generation EGFR inhibitors are considered better suited for GBM treatment because of their specificity, safer dosing profiles and elevated BBB penetration in GBM (Feng et al., 2025). Among 3rd-generation EGFR TKIs, OSI is regarded as one of the most promising therapeutic interventions for GBM due to its lipophilicity, low TPSA, specific target to EGFRvIII and its capacity to cross the BBB (Dong et al., 2018). Even though OSI is recommended for EGFR-positive tumors, EGFRvIII has low kinase activity, and its activity is sufficient to elevate cell survival and growth, also triggering wt EGFR together (Wee & Wang, 2017; An et al., 2018). Moreover, it also found that OSI suppressed the proliferation of EGFR-negative GBM cells and PDX models through MAPK-interacting kinases (MNK 1/2), which are downstream of the MAPK pathway to regulate the synthesis of protein. These findings suggest that OSI could be a multitarget kinase inhibitor due to its capability of inhibiting EGFR, ALK, FGFR1 and FAK as well as MNK 1/2 (C. Chen et al., 2021). Lately, multitarget kinase inhibitors are increasingly recommended in GBM treatment to target EGFR,

consolidating the relevance of OSI in this context (Denisova et al., 2022). Although OSI resistance has been reported in NSCLC, there remains a strong interest in combining OSI with the chemical agent that overcomes OSI resistance and targets multiple pathways to inhibit cell proliferation and tumor growth (Romaniello et al., 2025).

AR is a nuclear receptor that binds to DHT and testosterone for activation in a ligand-dependent manner to translocate to the nucleus, where it regulates processes, including cell proliferation, apoptosis, metastasis, cell cycle and DNA damage repair (Michmerhuizen et al., 2020; Zalcman et al., 2021; Fariña-Jerónimo et al., 2024). Furthermore, AR can be activated in a ligand-independent manner through ERK, mTOR and PI3K-AKT pathways (Recchia et al., 2009; Kolyvas et al., 2022). AR antagonist is one of the treatment options that target and hamper AR signaling in the cancer field (Helsen et al., 2014). Compared with 1st-generation AR antagonists, 2nd-generation AR antagonists are recommended due to fully blocking the AR function and promoting apoptosis (Rice et al., 2019; Campodonico et al., 2024; Danielli et al., 2025). Among 2nd-generation AR antagonists, ENZ has the most capacity to cross the BBB, which is a potential candidate for GBM therapies. Recently, it's been known that upregulation of AR is found in GBM, with the levels of expression correlating positively with tumor grade (Fariña-Jerónimo et al., 2024). Mainly, AR is activated in a ligand-independent manner in GBM owing to low levels of androgen in the brain (Zalcman et al., 2021; Fariña-Jerónimo et al., 2024). Usage of ENZ offers blocking growth and triggering apoptosis (Bolek et al., 2024). As ENZ has favorable pharmacological properties for penetration of the BBB, such as not being a substrate of P-gp, being lipophilic, low TPSA and optimal MW, ENZ is proposed to be utilized in GBM treatment (Dhillon et al., 2024; Rifaldi et al., 2025). It's shown that administration of ENZ reduced cell proliferation, promoted apoptosis and cell cycle arrest (Zalcman et al., 2018; N. Zhao et al., 2021; Chang et al., 2022).

The combination of ENZ with afatinib, a 2nd-generation EGFR TKI, has been previously shown to have a direct interaction between EGFR and AR, producing additive effects for the U87 cell line and synergistic effects for T98G and A172 cell lines; however, there was no further step on apoptosis, EMT or cell cycle (Zalcman et al., 2021). Additionally, low doses of ENZ are recommended to minimize the risk of

seizure even though the rate of incidence is below 1% (Campodonico et al., 2024). In GBM, AR functions through both ligand-dependent and -independent manners, especially through EGF ligand and MAPK pathway (Recchia et al., 2009; Kolyvas et al., 2022). We hypothesized that targeting multiple signaling pathways might provide an improved GBM treatment option due to its heterogeneity and challenges associated with BBB penetration. In addition to GBM cell lines, since GBM is a heterogeneous cancer, we also worked with microglia, the HMC3 cell line, to check if this drug combination only targets cancer cells or not. The current literature lacks studies investigating the combined impacts of ENZ and 3rd-generation EGFR TKIs in GBM, regarding their effect on the cell cycle, EMT and apoptosis. Therefore, this is the first study to assess dual targeting of EGFR and AR utilizing the administration of OSI and ENZ to examine their impact on cell cycle, EMT and apoptosis in GBM.

Our initial objective was to check the impacts of OSI and/or ENZ in LN18 and U87 cell lines, with HMC3 cell line, in a dose- and time-dependent manner. The results of the cell viability assay revealed that the combination of 2.5 µM OSI and 50 µM ENZ diminished the cell viability for 24 h treatment in both GBM cells, whereas HMC3 was not affected by any toxicity at any time points. The reason why a 24 h treatment interval was chosen is that only at that time point, both monotherapy and combined therapy showed statistical significance in LN18 and U87 cells. Our results are consistent with the combination of ENZ and afatinib, showing a reduction in cell viability in A172, U87 and T98G cell lines (Zalcman et al., 2021). Additional studies have published that the combination of Lapatinib and ENZ synergistically declined cell viability in LNCaP cell line (Shiota et al., 2015). Jovanović et al., study found that co-culturing of NSCLC and fibroblasts demonstrated that OSI targeted cancerous cells but not healthy ones (Jovanović Stojanov et al., 2023). Likewise, RWPE-1 cells were not affected by the cytotoxicity from ENZ combined with miR26a, while CRPC ones were influenced (Y. Wang et al., 2024). Moreover, ENZ reduced cell viability in MCF-7, MDA-MB-468 and MDA-MB-231 cells but had no influence on MCF-10A cells (Choupani et al., 2022). After we found a significant reduction in cell viability in GBM cells, we further assessed whether this combined therapy has additive or synergistic effects. To plot the graphs using SynergyFinder, multiple concentrations of OSI and ENZ were administered to LN18 and U87. The metadata demonstrated that ZIP,

Loewe, HAS, and Bliss scores are greater than 10, indicating synergistic effects in both GBM cell lines (Rodríguez-Vázquez et al., 2023). This observed synergistic effect is consistent with results for T98 and A172 cell lines with the combination of ENZ and afatinib (Zalcman et al., 2021). In addition, the combination of gefitinib and anastrozole, which hampers the estrogen receptor, has a synergistic effect on NSCLC (Shen et al., 2012). To validate MTT data, an ATP-based ELISA assay, which is an indicator of viability because it is an energy currency for all living entities, was conducted (Hammes et al., 2010). The results indicated that after 24 h treatment of 2.5 µM OSI in combination with 50 µM ENZ, the levels of ATP were gradually declined in LN18 and U87 cell lines. This result aligns with the combination of OSI and gedatolisib in GBM95 and T98G (de São José et al., 2024). To investigate cytotoxicity in a dose- and time-dependent manner, a survival assay was performed in HMC3, LN18 and U87 cell lines. In the HMC3 cell line, there was no cytotoxic response at any time point, and cells continued to proliferate. In contrast, the combination of 2.5 µM OSI and 50 µM ENZ demonstrated cytotoxicity following 24 h of treatment in LN18 and U87 cells. Even though at 48 h and 72 h this combination entered the partial recovery phase, the cells had a slow growth speed compared to other conditions. These results are consistent with the findings by Booth et al., who revealed increased cell death with trypan blue at 24 h combination treatment with OSI and GZ17-6.02 (Booth et al., 2021). Under the fluorescence microscope, dead cells, nuclear fragmentation and mitochondrial membrane potential were examined by PI, DAPI and $DiOC_6$ staining, respectively. PI staining showed that dead cells were increased in the combination of 2.5 µM OSI and 50 µM ENZ in LN18 and U87 cells, whereas HMC3 cells remained unaffected. In DAPI staining, elevated nuclear fragmentation was observed in 2.5 µM OSI combined with 50 µM ENZ in LN18 and U87, while DAPI did not influence HMC3 cells. In PC9/G cells, a similar output has been reported that the administration of gefitinib and resveratrol induced nuclear fragmentation (Zhu et al., 2015). $DiOC_6$ staining successfully declined the mitochondrial membrane potential, meaning a reduction in cell viability, via 2.5 µM OSI and 50 µM ENZ in GBM cells, whereas HMC3 was not affected by drug administration. Supporting these findings, nano delivery of ENZ and miR26a led to a reduction in mitochondrial membrane potential via $DiOC_6$ staining, while an increase in dead cells and nuclear

fragmentation with PI and DAPI dyes, respectively in CRPC mouse models (Y. Wang et al., 2024). The clonogenic capacity of the treatment of OSI and ENZ was evaluated. In LN18 and U87 cell lines, we found that colony formation capacity was diminished upon treatment with 2.5 μM OSI and 50 μM ENZ. The previous study showed that the synergistic effect of ENZ and perifosine decreased the number of colonies in LNCaP and C42B prostate cell lines (J. Hu et al., 2024). Another study also displayed that the combination of fulvestrant and AUY922 reduced the colony-forming rates in MCF-7 and T47D cell lines (Bai et al., 2017). In addition to the colony formation assay, the impact of 3D spheroid formation with OSI and ENZ was assessed in GBM cells in a dose- and time-dependent manner. The results revealed that at 24 h, the spheroid formation capacity was reduced by utilizing 2.5 μM OSI and 50 μM ENZ. At 48 h and 72 h, the GBM cells tried to undergo recovery for spheroid formation, but at a very slow rate. This is consistent with monotherapy of OSI, which led to decreased spheroid formation in LN18, U87, LN229 and SF539 (L. Hu et al., 2023). In addition, ENZ monotherapy reduced the potency of spheroids in C42B cell lines (Choi et al., 2021). After using 30 μM ENZ in many experiments to show this dosage is not statistically significant to inhibit cell proliferation, we merely continued 50 μM ENZ for subsequent experiments. A wound healing assay was performed to examine the capacity of cell migration after administration of 2.5 μM OSI and 50 μM ENZ in LN18 and U87 cells. After scratching the plate, at 24 h, the migration was effectively ceased under the combination of OSI and ENZ. At 48 h, although there was a minor recovery, migration remained impaired compared to controls and monotherapies in both GBM cell lines. These findings corroborate previous observations with the combination of OSI and gedatolisib that reduced the migration in GBM95 and T98G cells (de São José et al., 2024). To delve into cell cycle phases, a flow cytometer was used. In LN18 and U87 cell lines, the subG1 phase, an apoptosis indicator, was enhanced in the combination of 2.5 μM OSI and 50 μM ENZ. With respect to literature, the combined ENZ and lapatinib treatment showed an increased subG1 phase in LNCaP cells (Shiota et al., 2015). To check downstream targets of EGFR following monotherapy of OSI and combination treatment with OSI and ENZ in GBM cells, western blotting was performed. The expressions of p-AKT and p-ERK 1/2 revealed reduction via 2.5 μM OSI combined with 50 μM ENZ in LN18 and U87 cell lines. This result is relevant to

the monotherapy of OSI in the HCC827 cells (J. Xu et al., 2018). Also, OSI reduced the expressions of p-AKT and p-ERK 1/2 in LN229 and U87 cell lines (L. Hu et al., 2023). In C42 cells, ENZ declined the expression of p-AKT and p-ERK 1/2 (Zhang et al., 2019). To evaluate the AR signaling pathway, the protein expression levels of PSMA and p-AR were checked. 2.5 μM OSI combined with 50 μM ENZ showed that the level of PSMA expression was increased in LN18 and U87 cell lines, while p-AR expression declined in LN18. Usage of afatinib in U87 cells also demonstrated a reduction in p-AR expression, which is consistent with our findings (Zalcman et al., 2021). Moreover, one study showed that usage of ENZ augmented the expression of PSMA in 22Rv1, LNCaP and C4-2 cell lines (Staniszewska et al., 2021). To evaluate the cell cycle arrest, expression of cyclin D1 was assessed following monotherapy and combined therapy of 2.5 μM OSI and 50 μM ENZ. It showed that expression of cyclin D1 was diminished in the combined treatment in LN18 and U87 cells. This result is supported by earlier findings displaying decreased cyclin D1 expression by monotherapy of OSI in U87 and LN229 in a time- and dose-dependent manner (L. Hu et al., 2023). Administration of ENZ demonstrated that the expression level of cyclin D1 was reduced in both T24 and T24 gemcitabine-resistant bladder cancer cells (Kameyama et al., 2017). Cyclin E2 expression was elevated in LN18 cells, whereas it was diminished in U87 cell line following treatment with 2.5 μM OSI combination with 50 μM ENZ. Beyond its physiological roles in embryogenesis and wound healing, EMT is also a key phenomenon in cancer to initiate metastasis and invasion (Guarino, 2025). EMT markers were checked in LN18 and U87 cell lines using the western blotting method. In LN18 and U87 cell lines, the combined therapy of OSI and ENZ reduced expression of N-cadherin, a mesenchymal marker, while expression of E-cadherin was increased in the LN18 cells and remained unchanged in the U87 cell line. The observed decrease in N-cadherin expression level is consistent with results from the combination of ENZ and miR99b in LNCaP, C42B, 22Rv1 and MDA PCa 2b cell lines (Waseem & Wang, 2024). Moreover, OSI monotherapy enhanced the expression of E-cadherin and declined the expression of N-cadherin in the HCC827 cell line (J. Xu et al., 2018). There are two reasons that explain why GBM cell lines showed different regulations of E-cadherin: partial EMT instead of full EMT and highly low E-cadherin expression, contributing to increased MAPK signaling (Lewis-Tuffin et al.,

2010; Yamamoto et al., 2017). It is well established that in GBM, especially Bcl-x_L anti-apoptotic protein expression level is markedly increased, which is related to EGFRvIII, while levels of pro-apoptotic proteins are reduced (Malone et al., 2025). Even though the results of PI staining and flow cytometry are pioneer indicators of apoptosis, these methods do not directly confirm apoptosis but might lead the way for programmed cell death. Therefore, it was desired to examine the impacts of this combined treatment in LN18 and U87 through apoptosis more definitively via the western blotting technique. The western blotting results exhibited that the expressions of cleaved caspase-3 and PARP were elevated, whilst the expressions of full form caspase-3, caspase-9 and PARP were reduced, as well as Bcl-x_L expression level with the combination of 2.5 μM OSI and 50 μM ENZ for 24 h treatment in LN18 and U87 cell lines. The combined therapy of Lapatinib and ENZ induced programmed cell death in LNCaP cells (Shiota et al., 2015).

In conclusion, our study revealed that the combined therapy with OSI and ENZ shed light on the therapeutic approach for GBM without damage in non-cancerous cells in TME. This study elucidated the mechanisms underlying EGFR and AR. In addition, it has been revealed that the impacts of dual targeting of EGFR and AR via EGFR inhibitor and AR antagonist include inducing cell cycle arrest, reversing EMT and inducing apoptosis. As a future perspective, distinguishing between partial EMT and full EMT might provide deeper insights into how dual targeting modulates EMT. Additionally, further investigation is needed to reveal interaction between apoptosis and EMT.

5. REFERENCES

Aggarwal, V., Montoya, C. A., Donnenberg, V. S., & Sant, S. (2021). Interplay between tumor microenvironment and partial EMT as the driver of tumor progression. *IScience*, *24*(2), 102113. https://doi.org/10.1016/j.isci.2021.102113

An, Z., Aksoy, O., Zheng, T., Fan, Q.-W., & Weiss, W. A. (2018). Epidermal growth factor receptor and EGFRvIII in glioblastoma: signaling pathways and targeted therapies. *Oncogene*, *37*(12), 1561–1575. https://doi.org/10.1038/s41388-017-0045-7

Andrews Wright, N. M., & Goss, G. D. (2019). Third-generation epidermal growth factor receptor tyrosine kinase inhibitors for the treatment of non-small cell lung cancer. *Translational Lung Cancer Research*, *8*(S3), S247–S264. https://doi.org/10.21037/tlcr.2019.06.01

Arcella, A., Limanaqi, F., Ferese, R., Biagioni, F., Oliva, M. A., Storto, M., Fanelli, M., Gambardella, S., & Fornai, F. (2020). Dissecting Molecular Features of Gliomas: Genetic Loci and Validated Biomarkers. *International Journal of Molecular Sciences*, *21*(2), 685. https://doi.org/10.3390/ijms21020685

Armstrong, A. J., Szmulewitz, R. Z., Petrylak, D. P., Holzbeierlein, J., Villers, A., Azad, A., Alcaraz, A., Alekseev, B., Iguchi, T., Shore, N. D., Rosbrook, B., Sugg, J., Baron, B., Chen, L., & Stenzl, A. (2019). ARCHES: A Randomized, Phase III Study of Androgen Deprivation Therapy With Enzalutamide or Placebo in Men With Metastatic Hormone-Sensitive Prostate Cancer. *Journal of Clinical Oncology*, *37*(32), 2974–2986. https://doi.org/10.1200/JCO.19.00799

Attwa, M. W., Abdelhameed, A. S., & Kadi, A. A. (2025). An ultra-fast validated green UPLC-MS/MS method for the quantification of osimertinib in human liver microsomes: Screening for ADME parameters and in vitro metabolic stability. *Acta Chromatographica*. https://doi.org/10.1556/1326.2024.01300

Ayati, A., Moghimi, S., Salarinejad, S., Safavi, M., Pouramiri, B., & Foroumadi, A. (2020). A review on progression of epidermal growth factor receptor (EGFR) inhibitors as an efficient approach in cancer targeted therapy. *Bioorganic Chemistry*, *99*, 103811. https://doi.org/10.1016/j.bioorg.2020.103811

Bae, S. H., Park, M.-J., Lee, M. M., Kim, T. M., Lee, S.-H., Cho, S. Y., Kim, Y.-H., Kim, Y. J., Park, C.-K., & Kim, C.-Y. (2014). Toxicity profile of temozolomide in the treatment of 300 malignant glioma patients in Korea. *Journal of Korean Medical Science*, *29*(7), 980–984. https://doi.org/10.3346/jkms.2014.29.7.980

Bai, J., Zhou, G., Qiu, Y., Hu, Y., Liu, J., Zhao, J., Zhang, S., & Zhang, J. (2017). HSP90 inhibitor AUY922 can reverse Fulvestrant induced feedback reaction in

human breast cancer cells. *Cancer Science*, *108*(6), 1177–1184. https://doi.org/10.1111/cas.13238

Barberán, S., & Cebrià, F. (2019). The role of the EGFR signaling pathway in stem cell differentiation during planarian regeneration and homeostasis. *Seminars in Cell & Developmental Biology*, *87*, 45–57. https://doi.org/10.1016/j.semcdb.2018.05.011

Batra, J. S., Pienta, K. J., Pomper, M. G., Gorin, M. A., & Rowe, S. P. (2019). Can the interplay between androgen signaling and PSMA expression be leveraged for theranostic applications? *Translational Andrology and Urology*, *8*(S3), S263–S264. https://doi.org/10.21037/tau.2019.03.13

Beer, T. M., Armstrong, A. J., Rathkopf, D. E., Loriot, Y., Sternberg, C. N., Higano, C. S., Iversen, P., Bhattacharya, S., Carles, J., Chowdhury, S., Davis, I. D., de Bono, J. S., Evans, C. P., Fizazi, K., Joshua, A. M., Kim, C.-S., Kimura, G., Mainwaring, P., Mansbach, H., … Tombal, B. (2014). Enzalutamide in Metastatic Prostate Cancer before Chemotherapy. *New England Journal of Medicine*, *371*(5), 424–433. https://doi.org/10.1056/NEJMoa1405095

Bellettato, C. M., & Scarpa, M. (2018). Possible strategies to cross the blood-brain barrier. *Italian Journal of Pediatrics*, *44*(Suppl 2), 131. https://doi.org/10.1186/s13052-018-0563-0

Bolek, H., Yazgan, S. C., Yekedüz, E., Kaymakcalan, M. D., McKay, R. R., Gillessen, S., & Ürün, Y. (2024). Androgen receptor pathway inhibitors and drug–drug interactions in prostate cancer. *ESMO Open*, *9*(11), 103736. https://doi.org/10.1016/j.esmoop.2024.103736

Booth, L., West, C., Moore, R. P., Von Hoff, D., & Dent, P. (2021). GZ17-6.02 and Pemetrexed Interact to Kill Osimertinib-Resistant NSCLC Cells That Express Mutant ERBB1 Proteins. *Frontiers in Oncology*, *11*. https://doi.org/10.3389/fonc.2021.711043

Campodonico, F., Foppiani, L., Campodonico, V., & Introini, C. (2024). Practical implications of androgen receptor inhibitors for prostate cancer treatment. *Exploration of Targeted Anti-Tumor Therapy*, *5*(3), 543–550. https://doi.org/10.37349/etat.2024.00234

Chagoya, G., Kwatra, S. G., Nanni, C. W., Roberts, C. M., Phillips, S. M., Nullmeyergh, S., Gilmore, S. P., Spasojevic, I., Corcoran, D. L., Young, C. C., Ballman, K. V, Ramakrishna, R., Cross, D. A., Markert, J. M., Lim, M., Gilbert, M. R., Lesser, G. J., & Kwatra, M. M. (2020). Efficacy of osimertinib against EGFRvIII+ glioblastoma. In *Oncotarget* (Vol. 11, Issue 22). www.oncotarget.com

Chang, C.-Y., Chen, J.-T., Chen, T.-H., & Chen, R.-M. (2022). Enzalutamide Induces Apoptotic Insults to Human Drug-Resistant and -Sensitive Glioblastoma Cells via an Intrinsic Bax-Mitochondrion-Cytochrome C Caspase

Cascade Activation Pathway. *Molecules*, *27*(19), 6666. https://doi.org/10.3390/molecules27196666

Chen, C., Cheng, C., Wu, H., Wang, Z., Wang, L., Jiang, Z., Wang, A., Hu, C., Dong, Y., Niu, W., Qi, S., Qi, Z., Liu, J., Wang, W., Niu, C., & Liu, Q. (2021). Osimertinib successfully combats EGFR-negative glioblastoma cells by inhibiting the MAPK pathway. *Acta Pharmacologica Sinica*, *42*(1), 108–114. https://doi.org/10.1038/s41401-020-0418-2

Chen, Q.-H., Munoz, E., & Ashong, D. (2024). Insight into Recent Advances in Degrading Androgen Receptor for Castration-Resistant Prostate Cancer. *Cancers*, *16*(3). https://doi.org/10.3390/cancers16030663

Cheng, Z., Cui, H., Wang, Y., Yang, J., Lin, C., Shi, X., Zou, Y., Chen, J., Jia, X., & Su, L. (2024). The advance of the third-generation EGFR-TKI in the treatment of non-small cell lung cancer (Review). *Oncology Reports*, *51*(1). https://doi.org/10.3892/or.2023.8675

Choi, J. D., Kim, T. J., Jeong, B. C., Jeon, H. G., Jeon, S. S., Kang, M. Y., Yeom, S. Y., & Seo, S. Il. (2021). ISL1 promotes enzalutamide resistance in castration-resistant prostate cancer (CRPC) through epithelial to mesenchymal transition (EMT). *Scientific Reports*, *11*(1), 21984. https://doi.org/10.1038/s41598-021-01003-0

Choupani, E., Madjd, Z., Saraygord-Afshari, N., Kiani, J., & Hosseini, A. (2022). Combination of androgen receptor inhibitor enzalutamide with the CDK4/6 inhibitor ribociclib in triple negative breast cancer cells. *PloS One*, *17*(12), e0279522. https://doi.org/10.1371/journal.pone.0279522

Colclough, N., Chen, K., Johnström, P., Strittmatter, N., Yan, Y., Wrigley, G. L., Schou, M., Goodwin, R., Varnäs, K., Adua, S. J., Zhao, M., Nguyen, D. X., Maglennon, G., Barton, P., Atkinson, J., Zhang, L., Janefeldt, A., Wilson, J., Smith, A., … Cross, D. A. E. (2021). Preclinical Comparison of the Blood–brain barrier Permeability of Osimertinib with Other EGFR TKIs. *Clinical Cancer Research*, *27*(1), 189–201. https://doi.org/10.1158/1078-0432.CCR-19-1871

Cote, D. J., Samanic, C. M., Smith, T. R., Wang, M., Smith-Warner, S. A., Stampfer, M. J., & Egan, K. M. (2021). Alcohol intake and risk of glioma: results from three prospective cohort studies. *European Journal of Epidemiology*, *36*(9), 965–974. https://doi.org/10.1007/s10654-021-00800-1

Cross, D. A. E., Ashton, S. E., Ghiorghiu, S., Eberlein, C., Nebhan, C. A., Spitzler, P. J., Orme, J. P., Finlay, M. R. V., Ward, R. A., Mellor, M. J., Hughes, G., Rahi, A., Jacobs, V. N., Brewer, M. R., Ichihara, E., Sun, J., Jin, H., Ballard, P., Al-Kadhimi, K., … Pao, W. (2014). AZD9291, an Irreversible EGFR TKI, Overcomes T790M-Mediated Resistance to EGFR Inhibitors in Lung Cancer.

Cancer Discovery, *4*(9), 1046–1061. https://doi.org/10.1158/2159-8290.CD-14-0337

Czarnywojtek, A., Borowska, M., Dyrka, K., Van Gool, S., Sawicka-Gutaj, N., Moskal, J., Kościński, J., Graczyk, P., Hałas, T., Lewandowska, A. M., Czepczyński, R., & Ruchała, M. (2023). Glioblastoma Multiforme: The Latest Diagnostics and Treatment Techniques. *Pharmacology*, *108*(5), 423–431. https://doi.org/10.1159/000531319

D'Alessio, A., Proietti, G., Sica, G., & Scicchitano, B. M. (2019). Pathological and Molecular Features of Glioblastoma and Its Peritumoral Tissue. *Cancers*, *11*(4), 469. https://doi.org/10.3390/cancers11040469

Danielli, L., Tassinari, E., Marchetti, A., Rosellini, M., Mollica, V., Cheng, L., & Massari, F. (2025). Current androgen receptor antagonists under investigation for resistant prostate cancer: progress and challenges. *Expert Review of Anticancer Therapy*, *25*(5), 457–470. https://doi.org/10.1080/14737140.2025.2481141

Davey, R. A., & Grossmann, M. (2016). Androgen Receptor Structure, Function and Biology: From Bench to Bedside. *The Clinical Biochemist. Reviews*, *37*(1), 3–15.

Davis, M. (2016). Glioblastoma: Overview of Disease and Treatment. *Clinical Journal of Oncology Nursing*, *20*(5), S2–S8. https://doi.org/10.1188/16.CJON.S1.2-8

de São José, V. S., Vieira, B. M., Neto, V. M., & Lima, L. M. (2024). Repurposing Osimertinib and Gedatolisib for Glioblastoma Treatment: Evidence of Synergistic Effects in an In Vitro Phenotypic Study. *Pharmaceuticals*, *17*(12), 1623. https://doi.org/10.3390/ph17121623

Denisova, O. V., Merisaari, J., Kaur, A., Yetukuri, L., Jumppanen, M., von Schantz-Fant, C., Ohlmeyer, M., Wennerberg, K., Aittokallio, T., Taipale, M., & Westermarck, J. (2022). Development of actionable targets of multi-kinase inhibitors (AToMI) screening platform to dissect kinase targets of staurosporines in glioblastoma cells. *Scientific Reports*, *12*(1), 13796. https://doi.org/10.1038/s41598-022-18118-7

Dewdney, B., Jenkins, M. R., Best, S. A., Freytag, S., Prasad, K., Holst, J., Endersby, R., & Johns, T. G. (2023). From signalling pathways to targeted therapies: unravelling glioblastoma's secrets and harnessing two decades of progress. *Signal Transduction and Targeted Therapy*, *8*(1), 400. https://doi.org/10.1038/s41392-023-01637-8

Dhillon, S., Antolin, A. A., & Jones, A. M. (2024). *The Interplay Between Molecular Architecture, Pharmacology, and Suspected Adverse Drug Reactions Associated with Non-Steroidal Androgen Antagonists in The United Kingdom*. https://doi.org/10.1101/2024.07.09.24309949

Doğanlar, O., Doğanlar, Z. B., Kurtdere, A. K., Chasan, T., & Ok, E. S. (2020). Chronic exposure of human glioblastoma tumors to low concentrations of a pesticide mixture induced multidrug resistance against chemotherapy agents. *Ecotoxicology and Environmental Safety*, *202*, 110940. https://doi.org/10.1016/j.ecoenv.2020.110940

Dong, S.-T., Li, Y., Yang, H.-T., Wu, Y., Li, Y.-J., Ding, C.-Y., Meng, L., Dong, Z.-J., & Zhang, Y. (2018). An Accurate and Effective Method for Measuring Osimertinib by UPLC-TOF-MS and Its Pharmacokinetic Study in Rats. *Molecules*, *23*(11), 2894. https://doi.org/10.3390/molecules23112894

Dongre, A., & Weinberg, R. A. (2019). New insights into the mechanisms of epithelial–mesenchymal transition and implications for cancer. *Nature Reviews Molecular Cell Biology*, *20*(2), 69–84. https://doi.org/10.1038/s41580-018-0080-4

Eskander, G., Abdelhamid, S. G., Wahdan, S. A., & Radwan, S. M. (2025). Insights on the crosstalk among different cell death mechanisms. *Cell Death Discovery*, *11*(1), 56. https://doi.org/10.1038/s41420-025-02328-9

Ezzati, S., Salib, S., Balasubramaniam, M., & Aboud, O. (2024). Epidermal Growth Factor Receptor Inhibitors in Glioblastoma: Current Status and Future Possibilities. *International Journal of Molecular Sciences*, *25*(4), 2316. https://doi.org/10.3390/ijms25042316

Fariña-Jerónimo, H., Martín-Ramírez, R., González-Fernández, R., Medina, L., de Vera, A., Martín-Vasallo, P., & Plata-Bello, J. (2024). Androgen deficiency is associated with a better prognosis in glioblastoma. *European Journal of Medical Research*, *29*(1), 57. https://doi.org/10.1186/s40001-024-01648-3

Feng, S., Liu, H., Yun, C., Zhu, W., & Pan, Y. (2025). Application of EGFR-TKIs in brain tumors, a breakthrough in future? *Journal of Translational Medicine*, *23*(1), 449. https://doi.org/10.1186/s12967-025-06448-9

Ferlay J., Ervik M., Lam F., Laversanne M., Colombet M., Mery L., Piñeros M., Znaor A., Soerjomataram I., & Bray F. (2024). *Global Cancer Observatory: Cancer Today. Lyon, France: International Agency for Research on Cancer.* https://gco.iarc.who.int/today

Fisher, J. P., & Adamson, D. C. (2021). Current FDA-Approved Therapies for High-Grade Malignant Gliomas. *Biomedicines*, *9*(3). https://doi.org/10.3390/biomedicines9030324

Frumento, D., Grossi, G., Falesiedi, M., Musumeci, F., Carbone, A., & Schenone, S. (2024). Small Molecule Tyrosine Kinase Inhibitors (TKIs) for Glioblastoma Treatment. *International Journal of Molecular Sciences*, *25*(3), 1398. https://doi.org/10.3390/ijms25031398

Ganguly, D., Sims, M., Cai, C., Fan, M., & Pfeffer, L. M. (2018). Chromatin Remodeling Factor BRG1 Regulates Stemness and Chemosensitivity of Glioma Initiating Cells. *Stem Cells*, *36*(12), 1804–1815. https://doi.org/10.1002/stem.2909

Gao, J., Xiong, A., Liu, J., Li, X., Wang, J., Zhang, L., Liu, Y., Xiong, Y., Li, G., & He, X. (2024). PANoptosis: bridging apoptosis, pyroptosis, and necroptosis in cancer progression and treatment. *Cancer Gene Therapy*, *31*(7), 970–983. https://doi.org/10.1038/s41417-024-00765-9

Gatto, N. M., Ogata, P., & Lytle, B. (2021). Farming, Pesticides, and Brain Cancer: A 20-Year Updated Systematic Literature Review and Meta-Analysis. *Cancers*, *13*(17). https://doi.org/10.3390/cancers13174477

Gibbons, J. A., Ouatas, T., Krauwinkel, W., Ohtsu, Y., van der Walt, J.-S., Beddo, V., de Vries, M., & Mordenti, J. (2015). Clinical Pharmacokinetic Studies of Enzalutamide. *Clinical Pharmacokinetics*, *54*(10), 1043–1055. https://doi.org/10.1007/s40262-015-0271-5

Gomez, G. G., Wykosky, J., Zanca, C., Furnari, F. B., & Cavenee, W. K. (2013). Therapeutic resistance in cancer: microRNA regulation of EGFR signaling networks. *Cancer Biology & Medicine*, *10*(4), 192–205. https://doi.org/10.7497/j.issn.2095-3941.2013.04.003

Grande, E., Harvey, R. D., You, B., Batlle, J. F., Galbraith, H., Sarantopoulos, J., Ramalingam, S. S., Mann, H., So, K., Johnson, M., & Vishwanathan, K. (2019). Pharmacokinetic Study of Osimertinib in Cancer Patients with Mild or Moderate Hepatic Impairment. *The Journal of Pharmacology and Experimental Therapeutics*, *369*(2), 291–299. https://doi.org/10.1124/jpet.118.255919

Gregory, C. W., Fei, X., Ponguta, L. A., He, B., Bill, H. M., French, F. S., & Wilson, E. M. (2004). Epidermal Growth Factor Increases Coactivation of the Androgen Receptor in Recurrent Prostate Cancer. *Journal of Biological Chemistry*, *279*(8), 7119–7130. https://doi.org/10.1074/jbc.M307649200

Grochans, S., Cybulska, A. M., Simińska, D., Korbecki, J., Kojder, K., Chlubek, D., & Baranowska-Bosiacka, I. (2022). Epidemiology of Glioblastoma Multiforme–Literature Review. *Cancers*, *14*(10), 2412. https://doi.org/10.3390/cancers14102412

Guarino, M. (2025). EMT: from embryogenesis, through cancer progression, to the development of carcinosarcoma. *Differentiation*, *146*, 100903. https://doi.org/10.1016/j.diff.2025.100903

Gudenkauf, L. M., Gray, S., Gonzalez, B. D., Sachdeva, A., & Autio, K. (2024). Balancing Hormone Therapy: Mitigating Adverse Effects of Androgen-Deprivation Therapy and Exploring Alternatives in Prostate Cancer Management. *American Society of Clinical Oncology Educational Book*, *44*(3). https://doi.org/10.1200/EDBK_433126

Hammes, F., Goldschmidt, F., Vital, M., Wang, Y., & Egli, T. (2010). Measurement and interpretation of microbial adenosine tri-phosphate (ATP) in aquatic environments. *Water Research*, *44*(13), 3915–3923. https://doi.org/10.1016/j.watres.2010.04.015

Han, M., Kakar, M., Li, W., Iqbal, I., Hu, X., Liu, Y., Tang, Q., Sun, L., Shakir, Y., & Liu, T. (2024). Targeting MDM2-p53 interaction in Glioblastoma: Transcriptomic analysis and Peptide-Based inhibition strategy. *Bioorganic Chemistry*, *150*, 107620. https://doi.org/10.1016/j.bioorg.2024.107620

Hanif, F., Muzaffar, K., Perveen, K., Malhi, S. M., & Simjee, S. U. (2017). Glioblastoma Multiforme: A Review of its Epidemiology and Pathogenesis through Clinical Presentation and Treatment. *Asian Pacific Journal of Cancer Prevention : APJCP*, *18*(1), 3–9. https://doi.org/10.22034/APJCP.2017.18.1.3

He, J., Huang, Z., Han, L., Gong, Y., & Xie, C. (2021). Mechanisms and management of 3rd-generation EGFR-TKI resistance in advanced non-small cell lung cancer (Review). *International Journal of Oncology*, *59*(5). https://doi.org/10.3892/ijo.2021.5270

Hegi, M. E., Diserens, A.-C., Gorlia, T., Hamou, M.-F., de Tribolet, N., Weller, M., Kros, J. M., Hainfellner, J. A., Mason, W., Mariani, L., Bromberg, J. E. C., Hau, P., Mirimanoff, R. O., Cairncross, J. G., Janzer, R. C., & Stupp, R. (2005). MGMT Gene Silencing and Benefit from Temozolomide in Glioblastoma. *New England Journal of Medicine*, *352*(10), 997–1003. https://doi.org/10.1056/NEJMoa043331

Helsen, C., Van den Broeck, T., Voet, A., Prekovic, S., Van Poppel, H., Joniau, S., & Claessens, F. (2014). Androgen receptor antagonists for prostate cancer therapy. *Endocrine-Related Cancer*, *21*(4), T105–T118. https://doi.org/10.1530/ERC-13-0545

HSIEH, T.-F., CHEN, C.-C., MA, W.-L., CHUANG, W.-M., HUNG, X.-F., TSAI, Y.-R., LIN, M.-H. A., ZHANG, Q., ZHANG, C., CHANG, C., & SHYR, C.-R. (2013). Epidermal growth factor enhances androgen receptor-mediated bladder cancer progression and invasion via potentiation of AR transactivation. *Oncology Reports*, *30*(6), 2917–2922. https://doi.org/10.3892/or.2013.2792

Hu, J., Zhang, J., Han, B., Qu, Y., Zhang, Q., Yu, Z., Zhang, L., Han, J., Liu, H., Gao, L., Feng, T., Dou, B., Chen, W., & Sun, F. (2024). PLXNA1 confers enzalutamide resistance in prostate cancer via AKT signaling pathway. *Neoplasia (New York, N.Y.)*, *57*, 101047. https://doi.org/10.1016/j.neo.2024.101047

Hu, J., Zhao, Q., Kong, L.-Y., Wang, J., Yan, J., Xia, X., Jia, Z., Heimberger, A. B., & Li, S. (2021). Regulation of tumor immune suppression and cancer cell survival by CXCL1/2 elevation in glioblastoma multiforme. *Science Advances*, *7*(5). https://doi.org/10.1126/sciadv.abc2511

Hu, L., Shi, J., Shen, D., Zhai, X., Liang, D., Wang, J., Xie, C., Xia, Z., Cui, J., Liu, F., Du, S., Meng, S., & Piao, H. (2023). Osimertinib induces paraptosis and TRIP13 confers resistance in glioblastoma cells. *Cell Death Discovery*, *9*(1), 333. https://doi.org/10.1038/s41420-023-01632-6

Hu, Y., Sun, H., Owens, R. T., Wu, J., Chen, Y. Q., Berquin, I. M., Perry, D., O'Flaherty, J. T., & Edwards, I. J. (2009). Decorin Suppresses Prostate Tumor Growth through Inhibition of Epidermal Growth Factor and Androgen Receptor Pathways. *Neoplasia*, *11*(10), 1042–1053. https://doi.org/10.1593/neo.09760

Huang, F., Li, K., Shevach, J. W., & Wang, Q. (2025). Emerging therapies to overcome antiandrogen resistance and beyond in lethal prostate cancer. *Journal of the National Cancer Center*. https://doi.org/10.1016/j.jncc.2025.04.004

Huang, J., Lin, B., & Li, B. (2022). Anti-Androgen Receptor Therapies in Prostate Cancer: A Brief Update and Perspective. *Frontiers in Oncology*, *12*, 865350. https://doi.org/10.3389/fonc.2022.865350

Huang, Y.-F., Chiao, M.-T., Hsiao, T.-H., Zhan, Y.-X., Chen, T.-Y., Lee, C.-H., Liu, S.-Y., Liao, C.-H., Cheng, W.-Y., Yen, C.-M., Lai, C.-M., Chen, J.-P., Shen, C.-C., & Yang, M.-Y. (2024). Genetic mutation patterns among glioblastoma patients in the Taiwanese population – insights from a single institution retrospective study. *Cancer Gene Therapy*, *31*(6), 894–903. https://doi.org/10.1038/s41417-024-00746-y

Iancu, G., Serban, D., Badiu, C. D., Tanasescu, C., Tudosie, M. S., Tudor, C., Costea, D. O., Zgura, A., Iancu, R., & Vasile, D. (2022). Tyrosine kinase inhibitors in breast cancer (Review). *Experimental and Therapeutic Medicine*, *23*(2), 114. https://doi.org/10.3892/etm.2021.11037

IZUMI, K., ZHENG, Y., LI, Y., ZAENGLE, J., & MIYAMOTO, H. (2012). Epidermal growth factor induces bladder cancer cell proliferation through activation of the androgen receptor. *International Journal of Oncology*, *41*(5), 1587–1592. https://doi.org/10.3892/ijo.2012.1593

Jezierzański, M., Nafalska, N., Stopyra, M., Furgoł, T., Miciak, M., Kabut, J., & Gisterek-Grocholska, I. (2024). Temozolomide (TMZ) in the Treatment of Glioblastoma Multiforme—A Literature Review and Clinical Outcomes. *Current Oncology*, *31*(7), 3994–4002. https://doi.org/10.3390/curroncol31070296

JIAPAER, S., FURUTA, T., TANAKA, S., KITABAYASHI, T., & NAKADA, M. (2018). Potential Strategies Overcoming the Temozolomide Resistance for Glioblastoma. *Neurologia Medico-Chirurgica*, *58*(10), 405–421. https://doi.org/10.2176/nmc.ra.2018-0141

Jovanović Stojanov, S., Podolski-Renic, A., Dinić, J., Dragoj, M., Jovanović, M., Stepanović, A., Lupšić, E., Bajović, R., Glumac, S., Marić, D., Ercegovac, M., & Pešić, M. (2023). 69P Osimertinib is selective against NSCLC cells and

modulates the multidrug-resistant phenotype in patient-derived cell cultures and co-cultures of NSCLC cells and fibroblasts. *ESMO Open*, *8*(1), 100927. https://doi.org/10.1016/j.esmoop.2023.100927

Jovčevska, I. (2018). Genetic secrets of long-term glioblastoma survivors. *Bosnian Journal of Basic Medical Sciences*. https://doi.org/10.17305/bjbms.2018.3717

Kalkavan, H., & Green, D. R. (2018). MOMP, cell suicide as a BCL-2 family business. *Cell Death & Differentiation*, *25*(1), 46–55. https://doi.org/10.1038/cdd.2017.179

Kameyama, K., Horie, K., Mizutani, K., Kato, T., Fujita, Y., Kawakami, K., Kojima, T., Miyazaki, T., Deguchi, T., & Ito, M. (2017). Enzalutamide inhibits proliferation of gemcitabine-resistant bladder cancer cells with increased androgen receptor expression. *International Journal of Oncology*, *50*(1), 75–84. https://doi.org/10.3892/ijo.2016.3781

Kast, R. E., Halatsch, M.-E., & Rosell, R. (2021). OPALS: A New Osimertinib Adjunctive Treatment of Lung Adenocarcinoma or Glioblastoma Using Five Repurposed Drugs. *Cells*, *10*(5), 1148. https://doi.org/10.3390/cells10051148

Kennedy, S. P., Hastings, J. F., Han, J. Z. R., & Croucher, D. R. (2016). The Under-Appreciated Promiscuity of the Epidermal Growth Factor Receptor Family. *Frontiers in Cell and Developmental Biology*, *4*. https://doi.org/10.3389/fcell.2016.00088

Khabibov, M., Garifullin, A., Boumber, Y., Khaddour, K., Fernandez, M., Khamitov, F., Khalikova, L., Kuznetsova, N., Kit, O., & Kharin, L. (2022). Signaling pathways and therapeutic approaches in glioblastoma multiforme (Review). *International Journal of Oncology*, *60*(6), 69. https://doi.org/10.3892/ijo.2022.5359

Khandwala, K., Mubarak, F., & Minhas, K. (2021). The many faces of glioblastoma: Pictorial review of atypical imaging features. *The Neuroradiology Journal*, *34*(1), 33–41. https://doi.org/10.1177/1971400920965970

Kolyvas, E. A., Caldas, C., Kelly, K., & Ahmad, S. S. (2022). Androgen receptor function and targeted therapeutics across breast cancer subtypes. *Breast Cancer Research*, *24*(1), 79. https://doi.org/10.1186/s13058-022-01574-4

Kralj, S., Jukič, M., & Bren, U. (2023). Molecular Filters in Medicinal Chemistry. *Encyclopedia*, *3*(2), 501–511. https://doi.org/10.3390/encyclopedia3020035

Lan, Z., Li, X., & Zhang, X. (2024). Glioblastoma: An Update in Pathology, Molecular Mechanisms and Biomarkers. *International Journal of Molecular Sciences*, *25*(5), 3040. https://doi.org/10.3390/ijms25053040

Lee, D. H., Ryu, H.-W., Won, H.-R., & Kwon, S. H. (2017). Advances in epigenetic glioblastoma therapy. *Oncotarget*, *8*(11), 18577–18589. https://doi.org/10.18632/oncotarget.14612

Lemmon, M. A., & Schlessinger, J. (2010). Cell Signaling by Receptor Tyrosine Kinases. *Cell*, *141*(7), 1117–1134. https://doi.org/10.1016/j.cell.2010.06.011

Lewis-Tuffin, L. J., Rodriguez, F., Giannini, C., Scheithauer, B., Necela, B. M., Sarkaria, J. N., & Anastasiadis, P. Z. (2010). Misregulated E-Cadherin Expression Associated with an Aggressive Brain Tumor Phenotype. *PLoS ONE*, *5*(10), e13665. https://doi.org/10.1371/journal.pone.0013665

Li, J., Feng, L., & Lu, Y. (2022). Glioblastoma multiforme: Diagnosis, treatment, and invasion. *Journal of Biomedical Research*, *37*(1), 47–58. https://doi.org/10.7555/JBR.36.20220156

Li, P., Chen, J., & Miyamoto, H. (2017). Androgen Receptor Signaling in Bladder Cancer. *Cancers*, *9*(2), 20. https://doi.org/10.3390/cancers9020020

Liu, A., Hou, C., Chen, H., Zong, X., & Zong, P. (2016). Genetics and Epigenetics of Glioblastoma: Applications and Overall Incidence of IDH1 Mutation. *Frontiers in Oncology*, *6*. https://doi.org/10.3389/fonc.2016.00016

Liu, X., Chen, X., Shi, L., Shan, Q., Cao, Q., Yue, C., Li, H., Li, S., Wang, J., Gao, S., Niu, M., & Yu, R. (2019). The third-generation EGFR inhibitor AZD9291 overcomes primary resistance by continuously blocking ERK signaling in glioblastoma. *Journal of Experimental & Clinical Cancer Research*, *38*(1), 219. https://doi.org/10.1186/s13046-019-1235-7

Lu, V. M., O'Connor, K. P., Shah, A. H., Eichberg, D. G., Luther, E. M., Komotar, R. J., & Ivan, M. E. (2020). The prognostic significance of CDKN2A homozygous deletion in IDH-mutant lower-grade glioma and glioblastoma: a systematic review of the contemporary literature. *Journal of Neuro-Oncology*, *148*(2), 221–229. https://doi.org/10.1007/s11060-020-03528-2

Maher, E. A., & Bachoo, R. M. (2025). Glioblastoma. In *Rosenberg's Molecular and Genetic Basis of Neurological and Psychiatric Disease* (pp. 215–227). Elsevier. https://doi.org/10.1016/B978-0-443-19176-3.00047-9

Malone, K., LaCasse, E., & Beug, S. T. (2025). Cell death in glioblastoma and the central nervous system. *Cellular Oncology*, *48*(2), 313–349. https://doi.org/10.1007/s13402-024-01007-8

Mao, X., Xue, X., Wang, L., Lin, W., & Zhang, X. (2022). Deep learning identified glioblastoma subtypes based on internal genomic expression ranks. *BMC Cancer*, *22*(1), 86. https://doi.org/10.1186/s12885-022-09191-2

McConnell, D. D., Carr, S. B., & Litofsky, N. S. (2019). Potential effects of nicotine on glioblastoma and chemoradiotherapy: a review. *Expert Review of Neurotherapeutics*, *19*(6), 545–555. https://doi.org/10.1080/14737175.2019.1617701

Michmerhuizen, A. R., Spratt, D. E., Pierce, L. J., & Speers, C. W. (2020). ARe we there yet? Understanding androgen receptor signaling in breast cancer. *Npj Breast Cancer*, *6*(1), 47. https://doi.org/10.1038/s41523-020-00190-9

Mondal, A., Saha, S., Ghosh, A., Lathia, J. D., & Sarma, J. Das. (2025). Connexin43 functions as a non-canonical phenotypic stability factor in promoting hybrid Epithelial/Mesenchymal phenotype in glioblastoma cells. *Translational Oncology*, *59*, 102463. https://doi.org/10.1016/j.tranon.2025.102463

Muhammad, S., Maridevaru, M. C., Roy, S., Chen, D., Zeng, W., Sun, L., Zhang, Y., & Guo, B. (2025). Piezodynamic Therapy: Unleashing Mechanical Energy and Featuristic Next Generation Therapeutic Paradigms for Glioblastoma. *ACS Nano*, *19*(37), 33008–33058. https://doi.org/10.1021/acsnano.5c11629

Mustafa, M., Ahmad, R., Tantry, I. Q., Ahmad, W., Siddiqui, S., Alam, M., Abbas, K., Moinuddin, Hassan, Md. I., Habib, S., & Islam, S. (2024). Apoptosis: A Comprehensive Overview of Signaling Pathways, Morphological Changes, and Physiological Significance and Therapeutic Implications. *Cells*, *13*(22), 1838. https://doi.org/10.3390/cells13221838

Nakada, M., Kita, D., Watanabe, T., Hayashi, Y., Teng, L., Pyko, I. V., & Hamada, J.-I. (2011). Aberrant Signaling Pathways in Glioma. *Cancers*, *3*(3), 3242–3278. https://doi.org/10.3390/cancers3033242

Ohgaki, H., & Kleihues, P. (2013). The Definition of Primary and Secondary Glioblastoma. *Clinical Cancer Research*, *19*(4), 764–772. https://doi.org/10.1158/1078-0432.CCR-12-3002

Olympios, N., Gilard, V., Marguet, F., Clatot, F., Di Fiore, F., & Fontanilles, M. (2021). TERT Promoter Alterations in Glioblastoma: A Systematic Review. *Cancers*, *13*(5). https://doi.org/10.3390/cancers13051147

Oronsky, B., Reid, T. R., Oronsky, A., Sandhu, N., & Knox, S. J. (2021). A Review of Newly Diagnosed Glioblastoma. *Frontiers in Oncology*, *10*. https://doi.org/10.3389/fonc.2020.574012

Ortiz, R., Perazzoli, G., Cabeza, L., Jiménez-Luna, C., Luque, R., Prados, J., & Melguizo, C. (2021). Temozolomide: An Updated Overview of Resistance Mechanisms, Nanotechnology Advances and Clinical Applications. *Current Neuropharmacology*, *19*(4), 513–537. https://doi.org/10.2174/1570159X18666200626204005

Ostrom, Q. T., Francis, S. S., & Barnholtz-Sloan, J. S. (2021). Epidemiology of Brain and Other CNS Tumors. *Current Neurology and Neuroscience Reports*, *21*(12), 68. https://doi.org/10.1007/s11910-021-01152-9

Pan, P. C., & Magge, R. S. (2020). Mechanisms of EGFR Resistance in Glioblastoma. *International Journal of Molecular Sciences*, *21*(22), 8471. https://doi.org/10.3390/ijms21228471

Park, W., Wei, S., Kim, B.-S., Kim, B., Bae, S.-J., Chae, Y. C., Ryu, D., & Ha, K.-T. (2023). Diversity and complexity of cell death: a historical review. *Experimental & Molecular Medicine*, *55*(8), 1573–1594. https://doi.org/10.1038/s12276-023-01078-x

Patel, N. P., Lyon, K. A., & Huang, J. H. (2019). The effect of race on the prognosis of the glioblastoma patient: a brief review. *Neurological Research*, *41*(11), 967–971. https://doi.org/10.1080/01616412.2019.1638018

Pearson, J. R. D., & Regad, T. (2017). Targeting cellular pathways in glioblastoma multiforme. *Signal Transduction and Targeted Therapy*, *2*(1), 17040. https://doi.org/10.1038/sigtrans.2017.40

Pellot Ortiz, K. I., Rechberger, J. S., Nonnenbroich, L. F., Daniels, D. J., & Sarkaria, J. N. (2023). MDM2 Inhibition in the Treatment of Glioblastoma: From Concept to Clinical Investigation. *Biomedicines*, *11*(7). https://doi.org/10.3390/biomedicines11071879

Petrylak, D. P., McKean, M., Lang, J. M., Gao, X., Dreicer, R., Geynisman, D. M., Stewart, T. F., Gandhi, M., Appleman, L. J., Dorff, T. B., Chatta, G. S., Tutrone, R., De La Cerda, J., Berghorn, E., Gong, J., Yu, T., Dominy, E., Chan, E., & Shore, N. D. (2024). ARV-766, a proteolysis targeting chimera (PROTAC) androgen receptor (AR) degrader, in metastatic castration-resistant prostate cancer (mCRPC): Initial results of a phase 1/2 study. *Journal of Clinical Oncology*, *42*(16_suppl), 5011–5011. https://doi.org/10.1200/JCO.2024.42.16_suppl.5011

Phillips, H. S., Kharbanda, S., Chen, R., Forrest, W. F., Soriano, R. H., Wu, T. D., Misra, A., Nigro, J. M., Colman, H., Soroceanu, L., Williams, P. M., Modrusan, Z., Feuerstein, B. G., & Aldape, K. (2006). Molecular subclasses of high-grade glioma predict prognosis, delineate a pattern of disease progression, and resemble stages in neurogenesis. *Cancer Cell*, *9*(3), 157–173. https://doi.org/10.1016/j.ccr.2006.02.019

Rabah, N., Ait Mohand, F.-E., & Kravchenko-Balasha, N. (2023). Understanding Glioblastoma Signaling, Heterogeneity, Invasiveness, and Drug Delivery Barriers. *International Journal of Molecular Sciences*, *24*(18), 14256. https://doi.org/10.3390/ijms241814256

Recchia, A. G., Musti, A. M., Lanzino, M., Panno, M. L., Turano, E., Zumpano, R., Belfiore, A., Andò, S., & Maggiolini, M. (2009). A cross-talk between the androgen receptor and the epidermal growth factor receptor leads to p38MAPK-dependent activation of mTOR and cyclinD1 expression in prostate and lung cancer cells. *The International Journal of Biochemistry & Cell Biology*, *41*(3), 603–614. https://doi.org/10.1016/j.biocel.2008.07.004

Rice, M. A., Malhotra, S. V., & Stoyanova, T. (2019). Second-Generation Antiandrogens: From Discovery to Standard of Care in Castration Resistant

Prostate Cancer. *Frontiers in Oncology*, *9*. https://doi.org/10.3389/fonc.2019.00801

Rifaldi, F., Tortorella, A., Sporeni, S., Lanzetta, I., Figini, S., Naspro, R. L. J., Lancia, A., Montagna, B., Secondino, S., Pedrazzoli, P., & Chiellino, S. (2025). Novel androgen receptor inhibitors in prostate cancer: What do we know so far? *Critical Reviews in Oncology/Hematology*, *215*, 104857. https://doi.org/10.1016/j.critrevonc.2025.104857

Rodríguez-Vázquez, G. O., Diaz-Quiñones, A. O., Chorna, N., Salgado-Villanueva, I. K., Tang, J., Ortiz, W. I. S., & Maldonado, H. M. (2023). Synergistic interactions of cytarabine-adavosertib in leukemic cell lines proliferation and metabolomic endpoints. *Biomedicine & Pharmacotherapy*, *166*, 115352. https://doi.org/10.1016/j.biopha.2023.115352

Romani, M., Pistillo, M. P., & Banelli, B. (2018). Epigenetic Targeting of Glioblastoma. *Frontiers in Oncology*, *8*, 448. https://doi.org/10.3389/fonc.2018.00448

Romaniello, D., Morselli, A., & Marrocco, I. (2025). Strategies to Overcome Resistance to Osimertinib in EGFR-Mutated Lung Cancer. *International Journal of Molecular Sciences*, *26*(7), 2957. https://doi.org/10.3390/ijms26072957

Sallinen, S.-L., konen, T., Haapasalo, H., & Schleutker, J. (2005). CHEK2 mutations in primary glioblastomas. *Journal of Neuro-Oncology*, *74*(1), 93–95. https://doi.org/10.1007/s11060-005-5953-7

Scher, H. I., Fizazi, K., Saad, F., Taplin, M.-E., Sternberg, C. N., Miller, K., de Wit, R., Mulders, P., Chi, K. N., Shore, N. D., Armstrong, A. J., Flaig, T. W., Fléchon, A., Mainwaring, P., Fleming, M., Hainsworth, J. D., Hirmand, M., Selby, B., Seely, L., & de Bono, J. S. (2012). Increased Survival with Enzalutamide in Prostate Cancer after Chemotherapy. *New England Journal of Medicine*, *367*(13), 1187–1197. https://doi.org/10.1056/NEJMoa1207506

Sheikh, S., Sturzu, A., Nägele, T., Ernemann, U., & Heckl, S. (2021). Effect of Different Alcoholic Beverages on Human Glioblastoma Cell Lines. *Current Nutrition & Food Science*, *17*(8), 850–857. https://doi.org/10.2174/1573401317666210618124223

Shen, L., Li, Z., Shen, S., Niu, X., Yu, Y., Li, Z., Liao, M., Chen, Z., & Lu, S. (2012). The synergistic effect of EGFR tyrosine kinase inhibitor gefitinib in combination with aromatase inhibitor anastrozole in non-small cell lung cancer cell lines. *Lung Cancer*, *78*(3), 193–200. https://doi.org/10.1016/j.lungcan.2012.08.012

Shiota, M., Bishop, J. L., Takeuchi, A., Nip, K. M., Cordonnier, T., Beraldi, E., Kuruma, H., Gleave, M. E., & Zoubeidi, A. (2015). Inhibition of the HER2-YB1-AR axis with Lapatinib synergistically enhances Enzalutamide anti-tumor

efficacy in castration resistant prostate cancer. *Oncotarget*, *6*(11), 9086–9098. https://doi.org/10.18632/oncotarget.3602

Simińska, D., Korbecki, J., Kojder, K., Jeżewski, D., Tarnowski, M., Tomasiak, P., Piotrowska, K., Masztalewicz, M., Kolasa, A., Chlubek, D., & Baranowska-Bosiacka, I. (2022). Androgen Receptor Expression in the Various Regions of Resected Glioblastoma Multiforme Tumors and in an In Vitro Model. *International Journal of Molecular Sciences*, *23*(21), 13004. https://doi.org/10.3390/ijms232113004

Singh, N., Miner, A., Hennis, L., & Mittal, S. (2020). Mechanisms of temozolomide resistance in glioblastoma - a comprehensive review. *Cancer Drug Resistance*. https://doi.org/10.20517/cdr.2020.79

Singh, S., Dey, D., Barik, D., Mohapatra, I., Kim, S., Sharma, M., Prasad, S., Wang, P., Singh, A., & Singh, G. (2025). Glioblastoma at the crossroads: current understanding and future therapeutic horizons. *Signal Transduction and Targeted Therapy*, *10*(1), 213. https://doi.org/10.1038/s41392-025-02299-4

Smith, C. J., Perfetti, T. A., Chokshi, C., Venugopal, C., Ashford, J. W., & Singh, S. K. (2024). Risk factors for glioblastoma are shared by other brain tumor types. *Human & Experimental Toxicology*, *43*. https://doi.org/10.1177/09603271241241796

Sommer, U., Siciliano, T., Ebersbach, C., Beier, A.-M. K., Stope, M. B., Jöhrens, K., Baretton, G. B., Borkowetz, A., Thomas, C., & Erb, H. H. H. (2022). Impact of Androgen Receptor Activity on Prostate-Specific Membrane Antigen Expression in Prostate Cancer Cells. *International Journal of Molecular Sciences*, *23*(3), 1046. https://doi.org/10.3390/ijms23031046

Staniszewska, M., Fragoso Costa, P., Eiber, M., Klose, J. M., Wosniack, J., Reis, H., Szarvas, T., Hadaschik, B., Lückerath, K., Herrmann, K., Fendler, W. P., & Iking, J. (2021). Enzalutamide Enhances PSMA Expression of PSMA-Low Prostate Cancer. *International Journal of Molecular Sciences*, *22*(14), 7431. https://doi.org/10.3390/ijms22147431

Sternberg, C. N., Fizazi, K., Saad, F., Shore, N. D., De Giorgi, U., Penson, D. F., Ferreira, U., Efstathiou, E., Madziarska, K., Kolinsky, M. P., Cubero, D. I. G., Noerby, B., Zohren, F., Lin, X., Modelska, K., Sugg, J., Steinberg, J., & Hussain, M. (2020). Enzalutamide and Survival in Nonmetastatic, Castration-Resistant Prostate Cancer. *New England Journal of Medicine*, *382*(23), 2197–2206. https://doi.org/10.1056/NEJMoa2003892

Sudhesh Dev, S., Zainal Abidin, S. A., Farghadani, R., Othman, I., & Naidu, R. (2021). Receptor Tyrosine Kinases and Their Signaling Pathways as Therapeutic Targets of Curcumin in Cancer. *Frontiers in Pharmacology*, *12*. https://doi.org/10.3389/fphar.2021.772510

Tamimi, A. F., & Juweid, M. (2017). Epidemiology and Outcome of Glioblastoma. In *Glioblastoma* (pp. 143–153). Codon Publications. https://doi.org/10.15586/codon.glioblastoma.2017.ch8

Tilak, M., Holborn, J., New, L. A., Lalonde, J., & Jones, N. (2021). Receptor Tyrosine Kinase Signaling and Targeting in Glioblastoma Multiforme. *International Journal of Molecular Sciences*, *22*(4), 1831. https://doi.org/10.3390/ijms22041831

Uribe, M. L., Marrocco, I., & Yarden, Y. (2021). EGFR in Cancer: Signaling Mechanisms, Drugs, and Acquired Resistance. *Cancers*, *13*(11), 2748. https://doi.org/10.3390/cancers13112748

Valdés-Rives, S. A., Casique-Aguirre, D., Germán-Castelán, L., Velasco-Velázquez, M. A., & González-Arenas, A. (2017). Apoptotic Signaling Pathways in Glioblastoma and Therapeutic Implications. *BioMed Research International*, *2017*, 1–12. https://doi.org/10.1155/2017/7403747

Varrone, A., Varnäs, K., Jucaite, A., Cselényi, Z., Johnström, P., Schou, M., Vazquez-Romero, A., Moein, M. M., Halldin, C., Brown, A. P., Vishwanathan, K., & Farde, L. (2020). A PET study in healthy subjects of brain exposure of 11C-labelled osimertinib - A drug intended for treatment of brain metastases in non-small cell lung cancer. *Journal of Cerebral Blood Flow and Metabolism : Official Journal of the International Society of Cerebral Blood Flow and Metabolism*, *40*(4), 799–807. https://doi.org/10.1177/0271678X19843776

Verhaak, R. G. W. (2016). Moving the needle: Optimizing classification for glioma. *Science Translational Medicine*, *8*(350). https://doi.org/10.1126/scitranslmed.aah4740

Verhaak, R. G. W., Hoadley, K. A., Purdom, E., Wang, V., Qi, Y., Wilkerson, M. D., Miller, C. R., Ding, L., Golub, T., Mesirov, J. P., Alexe, G., Lawrence, M., O'Kelly, M., Tamayo, P., Weir, B. A., Gabriel, S., Winckler, W., Gupta, S., Jakkula, L., … Hayes, D. N. (2010). Integrated Genomic Analysis Identifies Clinically Relevant Subtypes of Glioblastoma Characterized by Abnormalities in PDGFRA, IDH1, EGFR, and NF1. *Cancer Cell*, *17*(1), 98–110. https://doi.org/10.1016/j.ccr.2009.12.020

Vitale, I., Pietrocola, F., Guilbaud, E., Aaronson, S. A., Abrams, J. M., Adam, D., Agostini, M., Agostinis, P., Alnemri, E. S., Altucci, L., Amelio, I., Andrews, D. W., Aqeilan, R. I., Arama, E., Baehrecke, E. H., Balachandran, S., Bano, D., Barlev, N. A., Bartek, J., … Galluzzi, L. (2023). Apoptotic cell death in disease—Current understanding of the NCCD 2023. *Cell Death & Differentiation*, *30*(5), 1097–1154. https://doi.org/10.1038/s41418-023-01153-w

Wang, Q., Hu, B., Hu, X., Kim, H., Squatrito, M., Scarpace, L., deCarvalho, A. C., Lyu, S., Li, P., Li, Y., Barthel, F., Cho, H. J., Lin, Y.-H., Satani, N., Martinez-Ledesma, E., Zheng, S., Chang, E., Sauvé, C.-E. G., Olar, A., … Verhaak, R. G.

W. (2017). Tumor Evolution of Glioma-Intrinsic Gene Expression Subtypes Associates with Immunological Changes in the Microenvironment. *Cancer Cell*, *32*(1), 42-56.e6. https://doi.org/10.1016/j.ccell.2017.06.003

Wang, Y., Chen, J., Gong, L., Wang, Y., Siltari, A., Lou, Y.-R., Murtola, T. J., Gao, S., & Gao, Y. (2024). MiR26a reverses enzalutamide resistance in a bone-tumor targeted system with an enhanced effect on bone metastatic CRPC. *Journal of Nanobiotechnology*, *22*(1), 145. https://doi.org/10.1186/s12951-024-02438-z

Waseem, M., & Wang, B.-D. (2024). Combination of miR-99b-5p and Enzalutamide or Abiraterone Synergizes the Suppression of EMT-Mediated Metastasis in Prostate Cancer. *Cancers*, *16*(10), 1933. https://doi.org/10.3390/cancers16101933

Wee, P., & Wang, Z. (2017). Epidermal Growth Factor Receptor Cell Proliferation Signaling Pathways. *Cancers*, *9*(5), 52. https://doi.org/10.3390/cancers9050052

Wu, Q., Berglund, A. E., & Etame, A. B. (2021). The Impact of Epigenetic Modifications on Adaptive Resistance Evolution in Glioblastoma. *International Journal of Molecular Sciences*, *22*(15), 8324. https://doi.org/10.3390/ijms22158324

Wu, W., Klockow, J. L., Zhang, M., Lafortune, F., Chang, E., Jin, L., Wu, Y., & Daldrup-Link, H. E. (2021). Glioblastoma multiforme (GBM): An overview of current therapies and mechanisms of resistance. *Pharmacological Research*, *171*, 105780. https://doi.org/10.1016/j.phrs.2021.105780

Xia, P. (2026). The significance of epithelial–mesenchymal transition (EMT) in the initiation, plasticity, and treatment of glioblastoma. *Genes & Diseases*, *13*(1), 101711. https://doi.org/10.1016/j.gendis.2025.101711

Xu, C., Hou, P., Li, X., Xiao, M., Zhang, Z., Li, Z., Xu, J., Liu, G., Tan, Y., & Fang, C. (2024). Comprehensive understanding of glioblastoma molecular phenotypes: classification, characteristics, and transition. *Cancer Biology & Medicine*, 1–19. https://doi.org/10.20892/j.issn.2095-3941.2023.0510

Xu, H., Zong, H., Ma, C., Ming, X., Shang, M., Li, K., He, X., Du, H., & Cao, L. (2017). Epidermal growth factor receptor in glioblastoma. *Oncology Letters*, *14*(1), 512–516. https://doi.org/10.3892/ol.2017.6221

Xu, J., Zhao, X., He, D., Wang, J., Li, W., Liu, Y., Ma, L., Jiang, M., Teng, Y., Wang, Z., Gu, M., Wu, J., Wang, Y., Yue, W., & Zhang, S. (2018). Loss of EGFR confers acquired resistance to AZD9291 in an EGFR-mutant non-small cell lung cancer cell line with an epithelial–mesenchymal transition phenotype. *Journal of Cancer Research and Clinical Oncology*, *144*(8), 1413–1422. https://doi.org/10.1007/s00432-018-2668-7

Yamamoto, M., Sakane, K., Tominaga, K., Gotoh, N., Niwa, T., Kikuchi, Y., Tada, K., Goshima, N., Semba, K., & Inoue, J. (2017). Intratumoral bidirectional

transitions between epithelial and mesenchymal cells in triple-negative breast cancer. *Cancer Science*, *108*(6), 1210–1222. https://doi.org/10.1111/cas.13246

Zalcman, N., Canello, T., Ovadia, H., Charbit, H., Zelikovitch, B., Mordechai, A., Fellig, Y., Rabani, S., Shahar, T., Lossos, A., & Lavon, I. (2018). Androgen receptor: a potential therapeutic target for glioblastoma. *Oncotarget*, *9*(28), 19980–19993. https://doi.org/10.18632/oncotarget.25007

Zalcman, N., Gutreiman, M., Shahar, T., Weller, M., & Lavon, I. (2021). Androgen Receptor Activation in Glioblastoma Can Be Achieved by Ligand-Independent Signaling through EGFR—A Potential Therapeutic Target. *International Journal of Molecular Sciences*, *22*(20), 10954. https://doi.org/10.3390/ijms222010954

Zhang, M., Sun, Y., Meng, J., Zhang, L., Liang, C., & Chang, C. (2019). Targeting AR-Beclin 1 complex-modulated growth factor signaling increases the antiandrogen Enzalutamide sensitivity to better suppress the castration-resistant prostate cancer growth. *Cancer Letters*, *442*, 483–490. https://doi.org/10.1016/j.canlet.2018.11.008

Zhao, N., Wang, F., Ahmed, S., Liu, K., Zhang, C., Cathcart, S. J., DiMaio, D. J., Punsoni, M., Guan, B., Zhou, P., Wang, S., Batra, S. K., Bronich, T., Hei, T. K., Lin, C., & Zhang, C. (2021). Androgen Receptor, Although Not a Specific Marker For, Is a Novel Target to Suppress Glioma Stem Cells as a Therapeutic Strategy for Glioblastoma. *Frontiers in Oncology*, *11*. https://doi.org/10.3389/fonc.2021.616625

Zhao, Y., Chen, Y., Liu, R., Liu, M., You, N., Zhao, K., Zhang, J., & Xu, B. (2024). Knockdown of ATRX enhances radiosensitivity in glioblastoma. *Chinese Neurosurgical Journal*, *10*(1), 19. https://doi.org/10.1186/s41016-024-00371-6

Zheng, Y., Izumi, K., Yao, J. L., & Miyamoto, H. (2011). Dihydrotestosterone upregulates the expression of epidermal growth factor receptor and ERBB2 in androgen receptor-positive bladder cancer cells. *Endocrine-Related Cancer*, *18*(4), 451–464. https://doi.org/10.1530/ERC-11-0010

Zhou, S., Huang, Y., Chen, Y., Liu, Y., Xie, L., You, Y., Tong, S., Xu, J., Jiang, G., Song, Q., Mei, N., Ma, F., Gao, X., Chen, H., & Chen, J. (2023). Reprogramming systemic and local immune function to empower immunotherapy against glioblastoma. *Nature Communications*, *14*(1), 435. https://doi.org/10.1038/s41467-023-35957-8

Zhou, Y., Jia, P., Fang, Y., Zhu, W., Gong, Y., Fan, T., & Yin, J. (2024). Comprehensive understanding of the adverse effects associated with temozolomide: a disproportionate analysis based on the FAERS database. *Frontiers in Pharmacology*, *15*. https://doi.org/10.3389/fphar.2024.1437436

Zhu, Y., He, W., Gao, X., Li, B., Mei, C., Xu, R., & Chen, H. (2015). Resveratrol overcomes gefitinib resistance by increasing the intracellular gefitinib

concentration and triggering apoptosis, autophagy and senescence in PC9/G NSCLC cells. *Scientific Reports*, *5*(1), 17730. https://doi.org/10.1038/srep17730

Zurth, C., Sandman, S., Trummel, D., Seidel, D., Nubbemeyer, R., & Gieschen, H. (2019). Higher blood–brain barrier penetration of [14C]apalutamide and [14C]enzalutamide compared to [14C]darolutamide in rats using whole-body autoradiography. *Journal of Clinical Oncology*, *37*(7_suppl), 156–156. https://doi.org/10.1200/JCO.2019.37.7_suppl.156

6. SUPPLEMENTARY

Supplementary Table 1. The recipe of MTT Reagent

MTT Reagent
0.1 g MTT
10 mL ddH_2O

Supplementary Table 2. The recipe of 4X BSA

4X BSA (4 mg/mL)
0.02 g BSA
0.09 g NaCl
Up to 10 mL with ddH_2O

Supplementary Table 3. The recipe of M-PER with protease and phosphatase inhibitor cocktails

M-PER +
5 mL of M-PER without protease and phosphatase inhibitor cocktail (Thermo Fisher)
200 µL of 25X protease inhibitor cocktail (Roche)
100 µL phosphatase inhibitor cocktail (Thermo Fisher)

Supplementary Table 4. 10% Sodium dodecyl sulfate (SDS) recipe

10% SDS
1 g SDS
10 mL ddH_2O

Supplementary Table 5. 10% Ammonium persulfate (APS) recipe

10% APS
1 g APS
10 mL ddH_2O

Supplementary Table 6. The recipe of 1.5 M Tris

1.5 M Tris (pH 8.8)
118.2 g Tris-HCl
Up to 500 mL ddH_2O

Supplementary Table 7. The recipe of 0.5 M Tris

0.5 M Tris (pH 6.8)
39.4 g Tris-HCl
Up to 500 mL ddH_2O

Supplementary Table 8. The recipe of 12% SDS-PAGE (Sodium dodecyl sulfate-polyacrylamide gel electrophoresis) in Merck System

	Merck System	
Gel Percentage	12% (Separating)	5% (Stacking)
ddH_2O	1.65 mL	1.02 mL
Acrylamide/Bisacrylamide 30% (37.5:1)	2 mL	0.255 mL
Tris	1.25 mL (1.5 M pH 8.8)	0.188 mL (0.5 M pH 6.8)
10% SDS	50 µL	15 µL
10% APS	33.4 µL	11.1 µL
TEMED	10 µL	2.5 µL
Total Volume	**5 mL**	**1.5 mL**

Supplementary Table 9. The recipe of 12% SDS-PAGE in Thermo Fisher System

	Thermo Fisher System	
Gel Percentage	12% (Separating)	5% (Stacking)
ddH_2O	2.3 mL	1.7 mL
Acrylamide/Bisacrylamide 30% (37.5:1)	2.8 mL	0.425 mL
Tris	1.75 mL (1.5 M pH 8.8)	0.313 mL (0.5 M pH 6.8)
10% SDS	70 µL	25 µL
10% APS	47 µL	18.5 µL
TEMED	14 µL	4.1 µL
Total Volume	**7 mL**	**2.5 mL**

Supplementary Table 10. The recipe of 10X Running Buffer

10X Running Buffer (pH 8.3)
30.3 g Tris-base
144 g Glycine
10 g SDS
Up to 1 L with ddH_2O

Supplementary Table 11. The recipe of 10X Transfer Buffer

10X Transfer Buffer (pH 8.3)
30.3 g Tris-base
144 g Glycine
Up to 1 L with ddH_2O

Supplementary Table 12. The recipe of 1X Transfer Buffer

1X Transfer Buffer
50 mL 10X Transfer buffer
100 mL methanol
350 mL ddH_2O

Supplementary Table 13. The recipe for 5% skim milk

5% Skim Milk
2.5 g skim milk powder
50 mL TBS-T

Supplementary Table 14. The recipe of Coomassie Brillant Blue G-250

Coomassie Brillant Blue G-250
0.4 g Coomassie G-250
90 mL methanol
20 mL acetic acid
Up to 200 mL with ddH_2O

Supplementary Table 15. The recipe of Destaining Solution

Destaining Solution
125 mL methanol
75 mL ddH_2O
25 mL acetic acid

Supplementary Table 16. The recipe of 10X TBS

10X TBS (pH 7.6)
24 g Tris
88 g NaCl
Up to 1 L with ddH_2O

Supplementary Table 17. The recipe of TBS-T

TBS-T
100 mL 10X TBS
1 mL Tween-20
900 mL ddH_2O

Supplementary Table 18. The p-Coumaric acid recipe

90 mM p-Coumaric Acid (store in the dark at +4°C)
0.148 g p-coumaric acid
10 mL absolute ethanol

Supplementary Table 19. The Luminol (3-aminopthalhydrazide) recipe

250 mM Luminol (store in the dark at -20°C)
0.44 g Luminol
10 mL DMSO

Supplementary Table 20. The recipe of 1 M Tris-HCl

1 M Tris-HCl (pH 8.5)
8.72 g Tris-base
4.42 g Tris-HCl
100 mL ddH_2O

Supplementary Table 21. The recipe of ECL

ECL			
Solution A		**Solution B**	
ddH_2O	4.5 mL	ddH_2O	4.5 mL
1 M Tris-HCl pH 8.5	0.5 mL	1 M Tris-HCl pH 8.5	0.5 mL
p-Coumaric acid	22.5 µL	H_2O_2 30%	3 µL
Luminol	50 µL		

Supplementary Table 22. The list of chemicals

Chemicals	Brand	Cat No.
0.25% Trypsin-EDTA (1X)	Gibco	25200-056
10X PBS	EcoTech	PBS10X-10
4X Laemmli	EcoTech	LSB-4X
Acetic acid	Bio-Rad	64-19-7
Acrylamide/Bis-acrylamide 30% (37.5:1)	EcoTech	AB3751100
AKT (rabbit)	St. John's Laboratory	STJ91550
Ammonium persulfate (APS)	Sigma-Aldrich	7727-54-0

AR (rabbit)	Cell Signaling Technology	D6F11
AZD 9291 (Osimertinib)	Cayman Chemical	16237
Bcl-xL (rabbit)	GeneTex	GTX637939
Bradford Reagent	Sigma-Aldrich	B6916
BSA	Sigma-Aldrich	A2153
Caspase 3 (rabbit)	Novus	NB100-56708SS
Caspase 9 (rabbit)	GeneTex	GTX112888
Colorcode prestained protein marker (10-180 kDa)	Abbkine	BMM3001
Coomassie Brillant Blue G-250	Merck	B2025-1EA
Crystal Violet (0.5%)	KimyaLab	V21166.100
Cyclin D1 (mouse)	GeneTex	GTX108624
Cyclin E2 (rabbit)	Cell Signaling Technology	4132
DAPI	Thermo Fisher	D1306
$DiOC_6$	Thermo Fisher	D273
DMEM, high glucose	Gibco	11965092
DMSO	Riedel-De-Haën	41640
E-cadherin (rabbit)	Cell Signaling Technology	3195T
ERK 1/2 (mouse)	St. John's Laboratory	STJ97534
Ethanol Absolute	Isolab	9200262500
Fetal Bovine Serum (FBS)	Gibco	A5256701
GAPDH (rabbit)	Boster	A00227-1
Glycine	Bio-Rad	1610717EDU
Halt™ Protease and Phosphatase Inhibitor Cocktail (100X)	Thermo Fisher	78440
HRP Conjugated AffiniPure Goat Anti-Rabbit IgG (H+L)	Boster	BA1054
HRP-conjugated secondary antibody (anti-mouse)	Cell Signaling Technology	7076
HRP-conjugated secondary antibody (anti-rabbit)	Cell Signaling Technology	7074
Human Adenosine triphosphate, ATP ELISA Kit	BT-Lab	E3132Hu
Hydrochloric acid 30%	KimyaLab	V00318.905
Hydrogen peroxide	TEKKİM	TK.0880220.01001
Luminol	Sigma-Aldrich	123072
MDV 3100 (Enzalutamide)	Cayman Chemical	11596
Methanol	Sigma-Aldrich	32213
M-PER	Thermo Fisher	78501
MTT Reagent	BioBasic	298-93-1

N-cadherin (rabbit)	Cell Signaling Technology	13116T
PageRuler™ Prestained Protein Ladder	Thermo Fisher	26617
p-AKT (Ser473) (rabbit)	Cell Signaling Technology	9271
p-Androgen Receptor (Ser380)	Santa Cruz	sc-377546
PARP (rabbit)	Cell Signaling Technology	9532
p-Coumaric acid	Sigma-Aldrich	501-984
Penicillin/Streptomycin Solution (10,000 U/mL)	Gibco	15140-122
p-ERK 1/2 (rabbit)	Cell Signaling Technology	9101
Propidium Iodide	Sigma-Aldrich	P4170
Protease Inhibitor Cocktail	Roche	4693116001
PSMA (rabbit)	Elabscience	D-AB-10276L
RNase A	EcoTech	EZRA1, EZRA 5
SDS	Scharlau	SD0010
Skim milk powder	BioShop	SKI400.250
Sodium chloride	Merck	1064041000
TEMED	Merck	110-18-9
Tris-base	Sigma-Aldrich	T1503
Tris-HCl	Scharlau	TR0425
Trypan blue (0.4% solution)	EcoTech	TRY-B100
Tween-20	Sigma-Aldrich	P1379
β-actin (rabbit)	Cell Signaling Technology	4970

Supplementary Table 23. The list of devices

Device	Brand
Axio Observer 5 Colibri 7	Carl Zeiss Microscopy
Azure 300 Chemiluminescent Western Blot Imager	Azure Biosystems
Biometra Fastblot	Analytic Jena
C6 Flow Cytometer	BD Accuri
Centrifuge 5418 R	Eppendorf
Centrifuge 5424 R	Eppendorf
Centrifuge Z 206 A	Hermle
CO_2 incubator (C150) (9040-0078)	BINDER
Digital Orbital Shaker (SKO180S)	DLAB
ECLIPSE TS100 (Inverted microscope)	Nikon
FLV1090 Mini Refrigerator	Flavel
Heat blocker	Thermo Fisher
Inverted Microscope (H600L)	Nikon

Invitrogen Mini Gel Tank	Thermo Fisher
Lab Benchtop Mini Centrifuge	ONiLAB Scientific
Laminar Flow Cabinet	Labconco
Milli Q Ultrapure Water Purification System	Merck
Mini vortex	Isolab
mPAGE Mini Gel Tank (MGT-4)	Merck
Multiskan FC 357 Microplate photometer	Thermo Fisher
MW151 MAX pH Meter	Milwaukee
Power Supply	VWR
PowerPac Basic Power Supply	Bio-Rad
Roller (MX-T6-S)	DLAB
Self-contained Ice Machine	Scotsman AF 80
Ultra-low Temperature Freezer	Haier
Vertical Laboratory Steam Sterilizers	Nuve
Water Bath VWB 18	VWR